The impact of patchiness on plant-flow interactions and consequences for seagrass habitat suitability: a multiscale study

A thesis submitted in fulfilment
of the requirements for the degree
of
Doctor of Philosophy
in
Earth Sciences
at
The University of Waikato
by

Tiago Dutra da Silva

THE UNIVERSITY OF
WAIKATO
Te Whare Wānanga o Waikato

2024

Abstract

Seagrasses are among the most productive marine ecosystems, providing essential ecological services. As ecosystem engineers, these flowering plants modify their environment through physical, chemical, and biological processes. A key physical mechanism involves stabilizing sediments by reducing near-bed flows, which result from the resistance created by plant stems. Flow attenuation increases sedimentation and reduces erosion of seabed, making seagrasses valuable for coastal protection in the face of climate change. Additional ecological services provided by seagrasses include improving water quality by cycling nutrients, providing habitat and feeding grounds for marine species, and sequestering carbon. However, the ability of seagrasses in providing these ecological services is strong influenced by the extent and spatial distribution of vegetation coverage. Patchiness in seagrass beds alters interactions between seagrass and water flow, with areas of varied flow resistance creating heterogeneous flow and turbulence conditions. This thesis assesses the impacts of patchiness, and in particular, the effect of gaps (bare sediment) in otherwise, continuous vegetation coverage, on plant-flow interactions through field measurements, numerical hydrodynamic modelling, and machine-learning classification methods. A multiscale approach is employed: First, a small-scale, field-based study explores the impacts of a bare patch on flow and turbulence, and the links with the spatial distribution of the surrounding seagrass. Second, a suite of numerical modelling simulations was undertaken to investigate the hydraulic interactions of multiple bare patches in a meadow-scale domain. Finally, estuary-scale species distribution models were developed based on topographic and sediment property variables to evaluate seagrass habitat suitability in a large tidal estuary, while also correlating habitat suitability with seagrass patchiness at a larger spatial scale.

The first chapter examines the effects of seagrass patchiness on plant-flow interactions. Data

on vegetation cover, bed elevation, and hydrodynamics were collected within and around a bare gap in the natural intertidal seagrass meadows of Tauranga Harbour, New Zealand. The small-scale, high-frequency measurements of flow and turbulence revealed faster flow speeds within bare gaps, and slower flow speeds above the surrounding seagrass, during the incoming flood phase of the tidal cycle. Although flow speeds were slower above the seagrass adjacent to the gap, turbulence, as characterised by the dissipation rate of turbulent kinetic energy, remained elevated above the vegetation These turbulence levels were dominated by down-deceleration events, which directed water and nutrient fluxes downward into the canopy, potentially explaining the presence of denser seagrass along the sides of the gap. We observed a spatial alignment between tidal flows and spatial distribution of seagrass: NDVI-derived maps of seagrass coverage demonstrated that the axis of seagrass continuity coincided with the dominant flow direction during flood tide at both the gap scale ($O(10^0)$m) and meadow scale ($O(10^2)$m), thus suggesting that small-scale plant-flow interactions are also strongly modulated by large-scale processes, such as tidal asymmetry. These findings suggest a feedback mechanism in which seagrass patchiness and spatial structure are shaped by flow transience, which then also influence ecological conditions associated with the survival and growth of the plants.

The work examining the impact of a single bare patch on plant-flow interactions was extended to investigate the collective impacts of multiple bare gaps at the meadow scale. This section used numerical modelling, focusing on unidirectional flows within emergent vegetation. Simulations with single gaps showed that horizontal flows were accelerated within the modelling domain, with the flow acceleration increasing up to a critical gap size. Beyond this critical size, further gap enlargement did not increase flow speeds. Paired-gaps simulations revealed that flow interactions occurred when the gaps were separated by distances less than or equal to two gap diameters, especially when aligned in the streamwise direction, where

wakes of accelerated flow interconnected, and flow changes were maximised. Minimal flow changes were observed for laterally aligned gaps. Hydrodynamic simulations involving multiple gaps assessed the effects of fragmentation, defined by the number and size of gaps, on flow at fixed levels of bare bed coverage. The results showed that the flow dynamics within aquatic canopies if also driven by spatial configuration of gaps, rather than bare bed coverage alone. Models with fewer, larger gaps caused greater flow acceleration within the idealised meadow than those with more numerous smaller gaps at the same coverage ratio. These effects were more pronounced at higher bare coverage levels, demonstrating that the arrangement of gaps is one of the driving factors in modifying flow and influencing ecosystem stressors linked to flow modification and habitat degradation.

Lastly, as feedback mechanisms are species- and system-specific, understanding the relationship between seagrass distribution and environmental factors across different systems is essential. To address this need, a regional-scale study was conducted to explore how topography and sediment composition determine the distribution and the habitat suitability of the temperate, shortleaf species *Zostera muelleri* in Tauranga Harbour, New Zealand. Using Random Forest species distribution models, the influences of twenty topographic and substrate variables on seagrass habitat suitability were assessed across a large (~240 km^2), predominantly intertidal (~60%) estuary. The models showed strong predictive performance as assessed by a mean area under the curve (AUC) of 0.84. Elevation emerged as the most significant factor (mean importance score = 0.29), followed by sediment composition (mean importance score = 0.17 to 0.22), while other topographic variables had a lesser impact (mean importance score < 0.17). Suitable habitats were predominantly located in sandy areas near mean sea level, within a narrow optimal elevation range. The study also revealed that broad-scale patchiness (minimum patch size = 0.1 ha) was significantly influenced by these environmental factors, with seagrass forming smaller, clustered patches in areas of lower habitat suitability, where

patches also exhibited a higher presence of bare gaps.

The combined findings of the three chapters highlight the controls of the spatial heterogeneity of aquatic vegetation, and in particular, the presence of gaps on the seagrass dynamics across scales. Understanding the links between spatial distributions and environmental drivers can be used to inform frameworks for targeted conservation and restoration of *Zostera muelleri*.

Acknowledgements

First and foremost, I would like to express my deepest gratitude to my partner, whose unwavering support and encouragement have been essential throughout this journey. Your patience and belief in me have been my greatest motivation.

I am incredibly grateful to my supervisors, Julia, Conrad, and Giovanni, for giving me the opportunity to pursue this research. Your guidance, expertise, and constructive feedback have been invaluable in shaping both this project and my development as a researcher.

To my mom and sister, your love and support have always been a constant source of strength. Thank you for believing in me and standing by my side, even from afar.

I would also like to extend my heartfelt thanks to my friends Romar, Heverton, Nery, Ana Ligia, Luciano, Glauco, Janete, and Timoh, among others. Your friendship and encouragement have been a vital part of this journey, and I am grateful to have you all in my life.

A special thanks to the Bay of Plenty Regional Council for providing the funding that made this research possible, and to the wonderful people of the Coastal Marine Group, as well as other colleagues and friends at the university, for their collaboration, insights, and camaraderie.

Finally, I am deeply appreciative of the many kind and welcoming people I have encountered throughout my time in New Zealand. Your warmth and hospitality have made this experience more meaningful.

Dedication

I would like to dedicate this thesis to the memory of all those who lost their lives during the COVID-19 pandemic and to their beloved ones. The pandemic has deeply affected many lives, and the hardships imposed extended across the globe. This research was no exception, as it was significantly impacted by the pandemic and the difficult times brought. The challenges of restricted fieldwork opportunities, working in isolation, being stranded overseas, and the uncertainty of the future during this period shaped much of the journey that led to the completion of this thesis. My heart goes out to all those who continue to carry the weight of this global tragedy.

Table of Contents

List of Figures

List of Tables

Chapter 1: Background and introduction

1.1 Seagrasses: significance and threats

Seagrasses are aquatic flowering plants that grow in the marine environment (Hartog & Kuo, 2006). Seagrass habitat occurs along the coasts of all continents (except the shores of Antarctica), covering about 0.1-0.2% of the global oceans (Hemminga & Duarte, 2000). These plants are highly productive ecosystems, which provide a plethora of ecological services such as carbon sequestration, sediment stabilization, habitat for marine species, and nutrient cycling (Duarte et al., 2013). However, globally seagrass loss has been widespread over the last few decades owing to causes such as nutrient enrichment of coastal waters (eutrophication), fishing, aquaculture, introduction of exotic species and pathogens, boating and anchoring, extreme climatic events such as heatwaves, and climate changes (Duarte, 2002; Short et al., 2011).

There are approximately 50-60 species of seagrasses worldwide (Ackerman, 2006), separated into tropical and temperate genera (Hemminga & Duarte, 2000). *Zostera muelleri* (Figure 1.1) is the only seagrass species in New Zealand and is also found in the coastal waters of Australia and Papua New Guinea. This species grows on silty and sandy tidal flats on coastal beaches and rocky reef platforms. In New Zealand, specific threats for the existence of *Zostera muelleri* include competition from invasive species, sedimentation, and eutrophication (Matheson & Schwarz, 2007).

Fragmentation of seagrass beds can occur due to various factors, both anthropogenic and natural. Anthropogenic activities, such as boating, anchoring, trawling, dredging, and coastal construction, can physically damage seagrass meadows, while natural processes, including physical disturbances from extreme climatic events and predation by large marine animals, also contribute to fragmentation (Abadie et al., 2015; Montefalcone et al., 2010; Swadling et al., 2023). Seagrass fragmentation often results in habitat patchiness, which can alter the spatial

structure of meadows, affecting the integrity and compromising the ecological function of these ecosystems (Boström et al., 2006). As seagrass meadows provide habitat for many marine organisms, fragmentation can impact faunal communities by influencing recruitment dynamics and altering the distribution of species such as estuarine-dependent fish, crabs, shrimps, and other epibenthic organisms (Hovel et al., 2002; Williams et al., 2016).

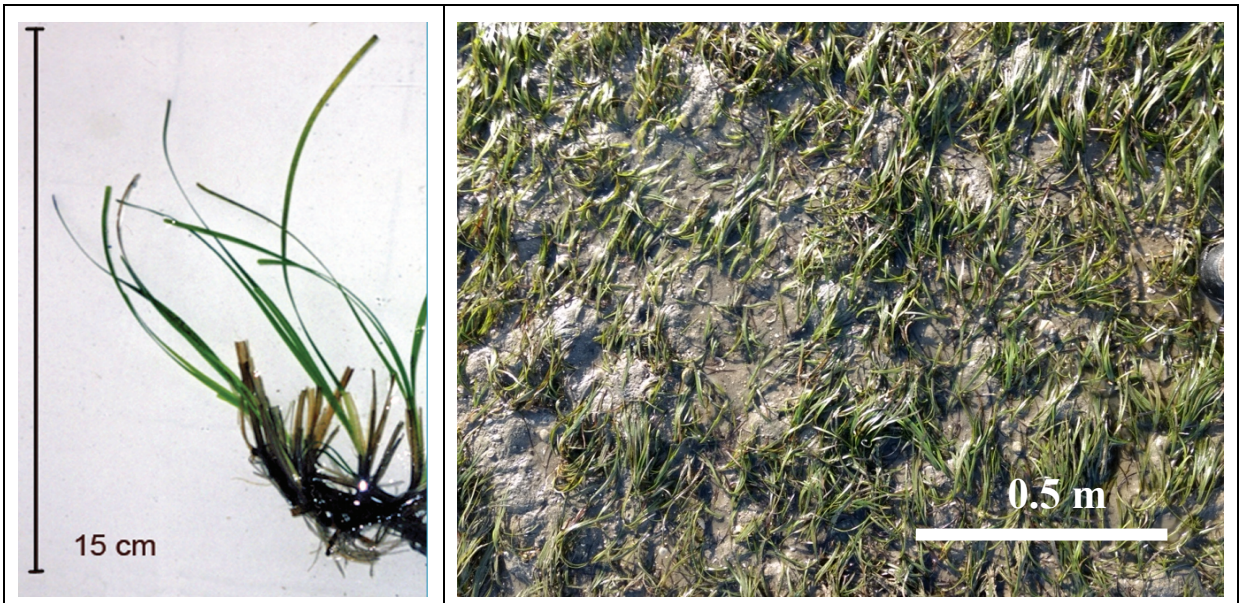

Figure 1.1: a) Typical New Zealand specimen of *Zostera muelleri* (extracted from: Matheson 2009) and b) In-situ close-up view of *Zostera muelleri* (Photo: Tiago Dutra da Silva).

1.2 Ecological and structural role of seagrasses

Seagrass beds are known as ecosystem engineers, given their ability to interact with and modify the surrounding environment. One key process is the reduction of flow speeds within the vegetation, which consequently enhances sedimentation and prevents resuspension of sediments (Jones et al., 1994; Madsen et al., 2001; Van Katwijk et al., 2010). Through this ability, seagrasses can shape coastal areas, often protecting coastal zones from physical hazards associated with extreme events such as storms and tsunamis. For this reason, seagrasses can have an important role in protecting coasts from the effects of a changing climate (Mullarney & Henderson, 2018; Ondiviela et al., 2014). By reducing current velocities, aquatic vegetation offers a sheltered habitat for a broad faunal assemblage, including fishes, crustaceans and

molluscs, providing nursery grounds for many commercially caught species (Ogden, 2006). Additionally, these organisms take advantage of the input of organic matter promoted by the reduction of flow velocities over the canopy. Organic matter trapped within seagrass bed sediments provides an abundant energy source, often forming the basis of complex food webs (Hemminga & Duarte, 2000; Ogden, 2006).

Other key ecological services seagrasses include organic carbon storage, nutrient cycling, and trophic transfers to adjacent habitats in tropical and temperate regions (Orth et al., 2006). Therefore, ecological dynamics in seagrass systems involve primary productivity, herbivory, benthic mineralization processes, burial, export, and import of particulate and dissolved matter, as well as nitrogen fixation (Hemminga & Duarte, 2000).

1.3 Plant-flow interactions and consequences for coastal morphodynamics

The ability of aquatic plants (including seagrasses) to reduce in-canopy flow is derived from the drag forces exerted by the vegetation on flow. The level of flow attenuation mostly depends on the level of plant submergence and canopy geometry. Emergent vegetation is equal to or taller than the water depth, while vegetation is submerged in scenarios where plant height is shorter than the water column (Mullarney & Henderson, 2018; Nepf, 2012a). In many hydrodynamic models based on the Reynolds Averaged Navier Stokes momentum equations (Nepf, 2012a), the drag exerted by vegetated canopies is often parametrised as an extra drag term ($C_d a h_v$), where C_d is an empirical drag coefficient (typically, $C_d \approx 1$), and a is the frontal area of the canopy per volume, defined as a ratio between the characteristic diameter or width (d) of individual stems or blades, and the squared average space between these elements, ΔS (i.e., $a = d/\Delta S^2$).

While emergent vegetation exerts drag on the entire water column, for the case of submerged seagrass, two different flow regimes exist for unidirectional flows. When vegetation is sparse

and does not promote enough drag to interact with flow, the vertical profiles of mean velocities form a rough boundary-layer. As vegetation density increases, a region of strong vertical shear is developed at the top of the canopy, generating turbulent eddies that propagate and penetrate downwards into the canopy (Nepf & Ghisalberti, 2008). The shear layer promotes the exchange of mass and momentum between vegetation and the overlying water column (Ghisalberti & Nepf, 2006). In very dense vegetation, a shielding effect is exerted by the canopy, and the width of the shear layer at the top of the canopy is smaller than the canopy height (Ghisalberti & Nepf, 2005; Nepf, 2012b).

In addition to the attenuation of unidirectional currents, vegetation canopies also exert influence on oscillatory flows within coastal systems. However, the reduction of wave velocities within seagrass meadows is smaller than reductions observed in unidirectional flows (Lowe et al., 2005; Luhar et al., 2010). Plant-wave interactions result in a reduction of wave energy reaching the shoreline (Forrester et al., 2024). The amount of dissipation depends on plant morphology, water depth, and wave height and steepness (Chen et al., 2007; Temmerman et al., 2023). Similar to unidirectional flows, the density of vegetation has been shown to enhance the ability of seagrass beds to attenuate wave height, with greater wave dissipation occurring in beds with higher biomass (Hansen & Reidenbach, 2013; Reidenbach & Thomas, 2018). Reduction in wave speeds can also increase wave steepness in certain conditions, such as shallow water and dense vegetation (Möller et al., 2014). Stem flexibility reduces the ability of aquatic vegetation to shelter the seabed from both unidirectional and orbital flows (Fonseca et al., 2019). Oscillatory velocities tilt and bend seagrass leaves in the direction of flow for much of the wave cycle (Bradley & Houser, 2009). Flexible vegetation exerts less drag on flow compared to equivalent rigid vegetation (Chapman et al., 2014; Mullarney & Henderson, 2018). In the moderately flexible species *Schoenoplectus americanus*, wave energy dissipation was 30% of that expected for an equivalent rigid plant (Riffe et al., 2011).

The trapping effect associated with flow deceleration in dense aquatic canopies reduces turbidity in the water and consequently improves light penetration through the water column. Settling of particulates also provides a source of essential minerals and thus, nutrient availability (Fonseca & Bell, 1998; Hemminga & Duarte, 2000). Slowing the water flow over the bed not only promotes sedimentation but also increases the threshold in which the trapped particles are mobilised, which in turn has the effect of stabilizing the marine bottom (Fonseca & Fisher, 1986; Lefebvre et al., 2010). Moreover, the root systems of seagrasses further stabilize sediments by decreasing sediment erodibility in coastal areas (Ganthy et al., 2015).

1.4 Plant-flow interactions in fragmented habitats

The majority of physical descriptions of interactions between aquatic plants and associated ecomorphological processes rely on continuous patches or meadows that are extensive enough to modify and interact with the mean flow. However, when otherwise continuous meadows or large patches become fragmented, these physical processes are disrupted (Colomer & Serra, 2021). In fact, patchiness is an inherent characteristic of vegetated ecosystems, with only a few regions exhibiting uniformity (Koch et al., 2006). Within these fragmented aquatic canopies, the flow modifications at the transitions between bare and vegetated areas or areas of different densities result in complex flow patterns (Gambi et al., 1990). As water flows across an isolated patch of submerged vegetation of finite width, the drag exerted by the vegetation diverts the flow around the sides and over the top of the canopy (Figure 1.2a and b). At these edges, vortices and recirculating eddies develop, leading to increased erosion at the front and lateral edges of the patch. In contrast, the wake behind the patch experiences reduced shear stress, creating a deposition zone in the streamwise direction (Hu et al., 2018; Meire et al., 2014). Conversely, when a single bare gap is present within a vegetated canopy, the absence of vegetation within the gap reduces drag, causing the flow to accelerate across this area (Figure 1.2b and c; Granata et al. 2001).

Previous studies have extensively explored the hydrodynamic processes resulted from interactions among vegetated patches. When two vegetation patches are laterally aligned relative to a unidirectional flow, the resulting interpatch interactions generate positive feedback that promotes lateral expansion and eventual merging of the patches (Meire et al., 2014). Other studies have identified positive feedback predominantly in the streamwise direction, leading to vegetation growth, which occurs primarily in the flow-parallel direction. The proximity of neighbouring patches along the stream creates positive feedback that enhances sediment deposition and promotes the expansion of vegetated landscapes (Yamasaki et al., 2019). The wakes of two circular patches separated by an along-stream and cross-stream distances equal or greater than 8 times the patch diameter have minimal interaction, resulting in flow and deposition patterns around each patch that resemble those of a single, isolated patch. In contrast, when the patches are closer, wake interaction occurs, leading to additional longitudinal deposition along the centreline between the patches, though this deposition occurs further downstream than that associated with each individual patch. At intermediate patch separation distances, the wake of the upstream patch is significantly shortened, while the wake of the downstream patch becomes elongated (de Lima et al., 2015).

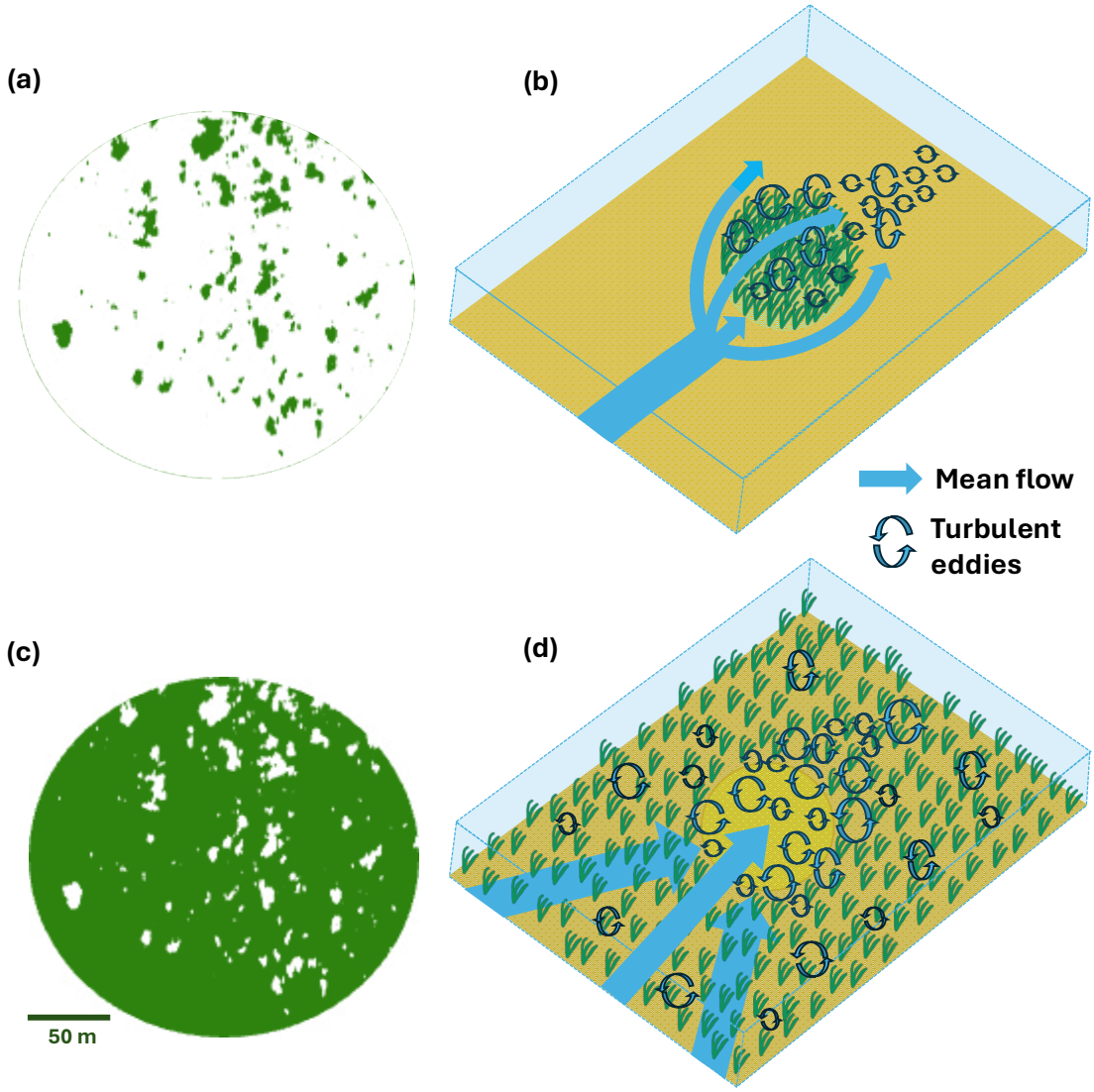

Figure 1.2: Conceptual representation of flow–patch interactions under different vegetation configurations. (a) Example of a fragmented seagrass meadow with sparse vegetation patches (green) embedded in a bare matrix (white); (b) Conceptual diagram showing how flow diverges around a vegetated patch and generates turbulent eddies in the wake zone; (c) Example of a dense seagrass meadow with a few large bare gaps (white) embedded within continuous vegetation (green); (d) Conceptual diagram illustrating how flow accelerates into bare gaps within a vegetated matrix, generating turbulence.

The impacts of gaps on flow and the vertical distribution and organization of turbulent motions within aquatic canopies under unidirectional flow have been primarily investigated through flume experiments using vegetation at varying levels of submergence. If a submerged canopy ($h_v < H$, where h_v is the canopy height and H the water depth) is interrupted by a gap, flow directions are altered, shear is produced with the consequent formation of a turbulent wake

downstream of the gap edge (Banerjee et al., 2013). The evolution of a turbulent wake (i.e., a region of chaotic, swirling flow downstream of the gap edge) will depend on the length of the gap. In the case of short gaps (L_{gap} /hv ≤ 1, where L_{gap} is the gap length), experiments have shown that skimming flow prevails. Flow passes over the gap without significantly extending downward into the gap, and the coherent turbulent vortices formed at the top of the vegetation remain confined to the upper layer on top of the canopy. For larger gap lengths (L_{gap} /h_v ≥ 2), the turbulence produced at the top and the edge of the upstream canopy reattaches to the bed at a downstream distance X_L, resulting in the formation of a vertical recirculation zone. Reattachment lengths vary from 4 ≤ L_{gap} /h_v ≤ 5 (Chung et al., 2021; Chung & Koseff, 2021; Hamed et al., 2020). Transversal gaps induce weaker changes in turbulence within emergent canopies compared to submerged ones. Rigid emergent stems attenuate momentum by dissipating turbulent energy during flow-canopy interactions. In these emergent canopies, mean velocity fields exhibit alterations upstream the gap at a distance up to five times the stem diameter, whereas turbulent kinetic energy and related metrics are affected over shorter distances, less than 3 times the stem diameter (Ranjan et al., 2022).

The interactions between gaps are less understood compared to those between vegetated patches. Multiple gaps within a canopy can alter flow dynamics in complex ways, potentially increasing turbulence and modifying the patterns of erosion and deposition. These effects can vary significantly depending on the size, shape, and spacing of the gaps, as well as the overall structure of the surrounding vegetation. While some studies suggest that gaps may enhance flow acceleration and turbulence, leading to increased erosion at the edges (Adhitya et al., 2014; Barcelona et al., 2021; Granata et al., 2001), the overall impact on landscape evolution and patch stability remains poorly quantified. Further research is needed to clarify how multiple gaps interact within a fragmented canopy and how these interactions influence broader hydrodynamic processes and habitat resilience.

1.5 Feedback processes in patchy aquatic landscapes

Understanding the factors that shape spatial structures in ecosystems, particularly in seagrass habitats, is a complex challenge in ecology. Spatial patterns in vegetated ecosystems often arise from scale-dependent feedback mechanisms, where positive and negative interactions occur across different spatial scales. Changes in spatial patterns, such as increase in patchiness can indicate escalating stress within vegetated ecosystems (Van Der Heide et al., 2007). Similar self-organised patterns have been observed in diverse ecosystems, including intertidal mudflats and marshes, where different configurations, such as gaps, labyrinths, and stripes, emerge due to interactions between vegetation and environmental factors like resource competition and hydrodynamic forces (Rietkerk & Van De Koppel, 2008).

In fragmented seagrass meadows, the reduced flow within patches contrasts with enhanced flow at the patch edges, potentially driving a shift from vegetated to unvegetated states (Vandenbruwaene et al., 2011). These scale-dependent feedback are influenced by factors such as current velocity, sediment transport, and water depth, all of which interact non-linearly with vegetation density (Van Wesenbeeck et al., 2008). Positive feedback occurs within vegetated patches, where reduced flow promotes sedimentation and nutrient accumulation, fostering vegetation growth (local facilitation, Figure 1.3). Conversely, negative feedback occurs in bare areas, where increased flow leads to erosion and reduced sedimentation, inhibiting colonization (broader inhibition). These sets of feedback emphasize the balance that determines seagrass habitat suitability, where fragmentation can either facilitate or disrupt the persistence of plants (Koch et al., 2006).

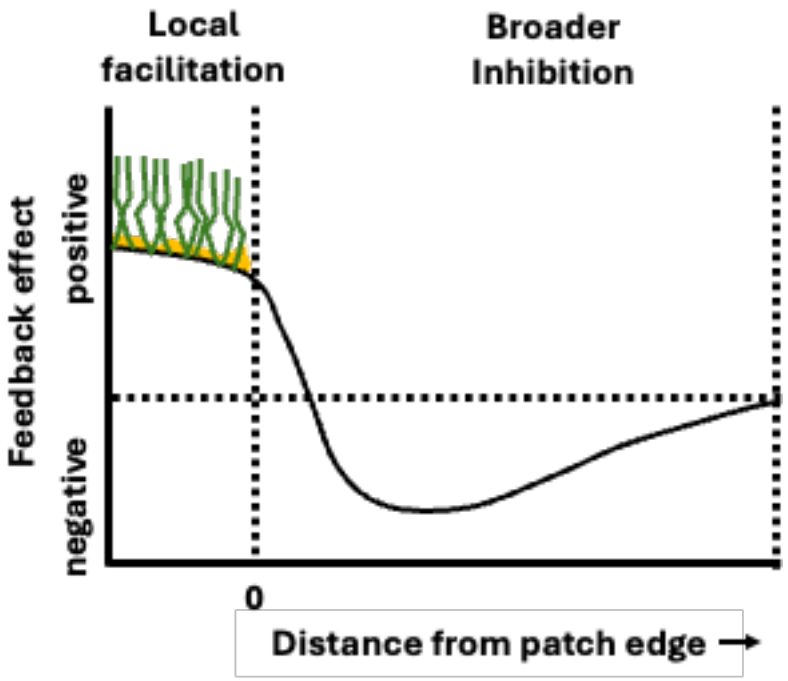

Figure 1.3: Schematic representation of expected feedback of the environment on vegetation growth relative to the distance of a vegetated patch. Dashed horizontal line represent zero feedback effect and the vertical dashed line represent the patch edge (adapted from Van Wesenbeeck et al. 2008).

Although the core mechanisms driving vegetation–flow feedbacks are similar across aquatic systems, the specific dynamics of these processes can vary according to the structural and functional traits of the species involved. While feedback mechanisms between vegetation and flow are well documented for some seagrass species, particularly those with low and flexible canopies, such mechanisms are not universally applicable across all aquatic vegetation types. The strength and spatial expression of hydrodynamic feedbacks vary significantly with species-specific biomorphological traits (Koehl, 2022a; Nikora, 2010). Emergent or rigid-stemmed species such as saltmarsh plants and mangroves exert greater drag, resulting in stronger flow attenuation within patches and steeper velocity gradients at patch edges (H. M. Nepf, 2012a). In contrast, submerged canopy-forming species often develop taller and denser meadows that influence drag, turbulence generation, light attenuation, and sediment retention. These structural differences affect the balance between positive and negative feedbacks: denser canopies may reduce sediment resuspension even under fragmented conditions, whereas more

flexible or sparsely vegetated systems are more susceptible to edge erosion, increasing the risk of further fragmentation (Infantes et al., 2012). Although many aquatic plants exhibit phenotypic plasticity by adjusting shoot density or canopy height in response to environmental cues, such responses are bounded by species-specific morphological constraints. Some species can adapt structurally, while others depend more heavily on clonal growth or seed dispersal for persistence (Santamaría, 2002).

1.6 Research questions

The overall goal of this thesis is to investigate the impact of patchiness on plant-flow interactions and the implications for seagrass habitat suitability. Through a multiscale approach, this research aims to understand how different spatial configurations of seagrass coverage influence hydrodynamics, and ultimately, the suitability of these environments for sustaining healthy seagrass meadows. In particular, we explore the following research questions:

1. What are the temporal and spatial variations in flow and turbulence within and surrounding bare gaps in shortleaf seagrass meadows, and how do these variations connect to the spatial distribution of seagrass?
2. How do bare gaps of varying sizes and different spatial configurations interact to collectively affect horizontal flow within meadows of emergent aquatic vegetation?
3. How effectively do topographic variables predict habitat suitability of shortleaf temperate seagrass, and what are the connections of these variables to patchiness patterns?

1.7 Approach used in this thesis

To address the research questions outlined earlier, this thesis adopts a multiscale and multi-methodological approach, integrating field measurements, numerical modelling, and data-

driven analysis across different spatial scales. The progression from patch-scale hydrodynamics to estuary-scale habitat modelling is illustrated in Figure 1.4.

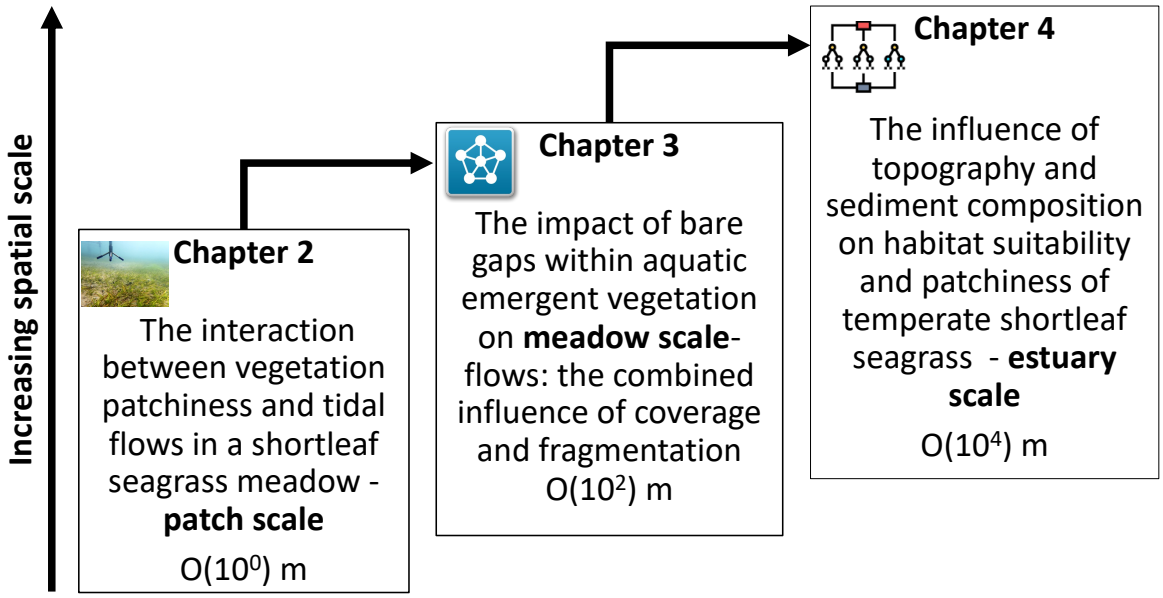

Figure 1.4: Schematic representation of the spatial scale progression addressed in this thesis.

Chapter 2 focuses on field-based measurements to assess flow and turbulence at a fine spatial scale in a natural environment, where flow conditions are more complex than in laboratory settings. Chapter 3 applies hydrodynamic models to systematically analyse the impact of bare gaps on horizontal flow and the dependence on fragmentation levels, at a meadow scale. Chapter 4 employs machine-learning models to investigate how topography and sediment composition influence the spatial distribution of suitable habitats for shortleaf temperate seagrass. While Chapter 3 presents an idealised study, Chapters 2 and 4 rely on data from a natural seagrass system in Tauranga Harbour, on the North Island of New Zealand (Figure 1.3a).

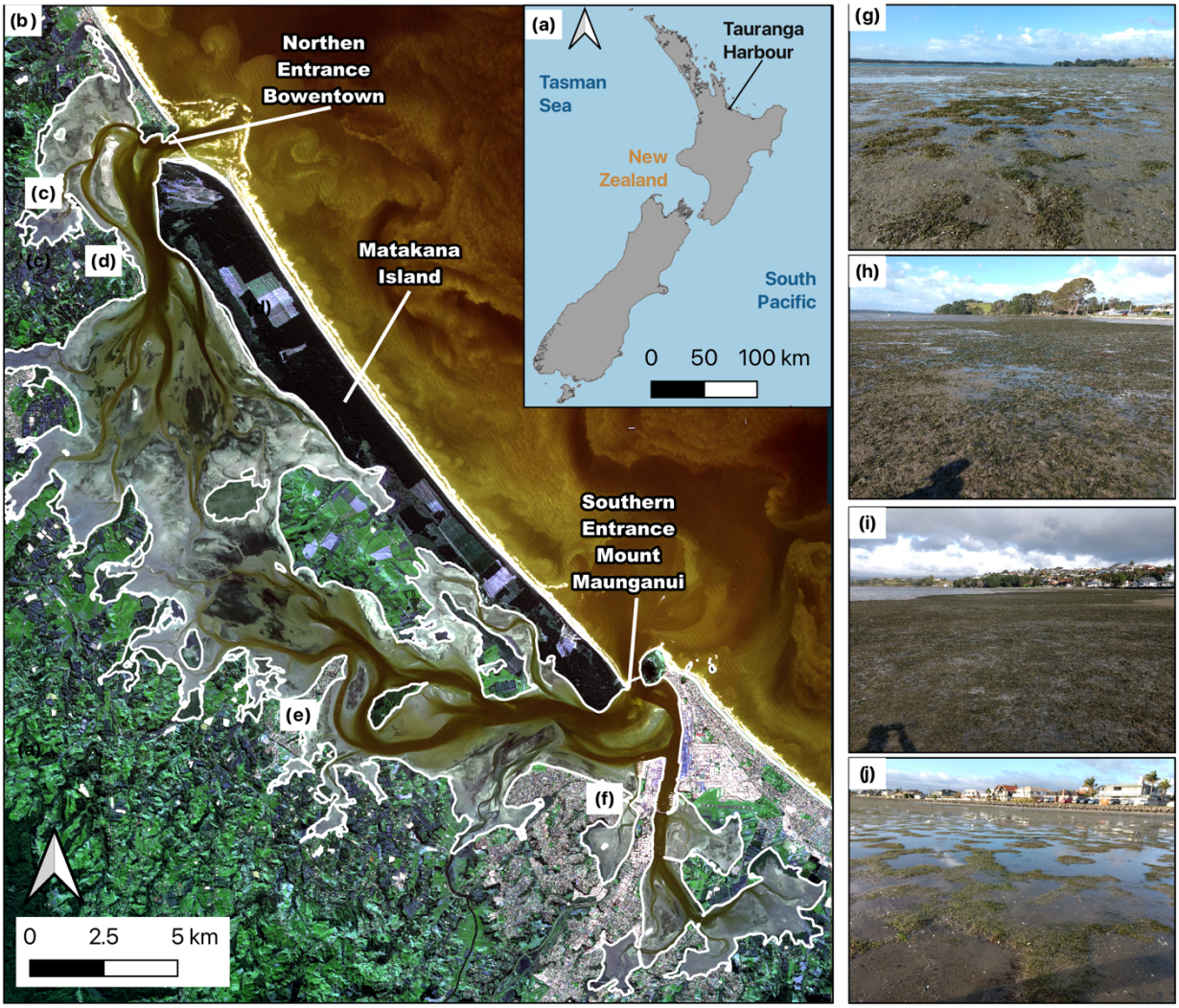

Figure 1.5: (a) Location of Tauranga Harbour on the North Island of New Zealand; (b) Sentinel-2 imagery of the entire estuary; (c-f) indicate the approximate locations corresponding to the photos in (g-j), representing examples of *Zostera muelleri* meadows in Tuapiro, Ongare, Omokoroa, and Otumoetai, respectively. (Photos in g-j: Tiago D. da Silva).

1.8 The field site: Tauranga Harbour

Covering approximately 240 km², Tauranga Harbour is a large, barrier-enclosed estuary with a microtidal, semidiurnal regime with tidal ranges of 1.62 m at spring tide and 1.24 m at neap tide (Heath, 1985). The estuary is shielded from the open sea by Matakana Island and two barrier tombolos: Bowentown at the northern entrance and Mount Maunganui at the southern entrance (Figure 1.3b). This system consists of two main basins, separated by extensive intertidal flats, with limited hydrodynamic exchange between them (Heath, 1976; Hume et al., 2007). The estuary is shallow, with water depths rarely exceeding 10 meters, and around 66% of the

seafloor area is composed of tidal flats (Inglis et al., 2006). The total catchment area spans approximately 1,300 km² and is predominantly used for horticulture and agriculture. The northern basin drains an area of 270 km² with an average inflow of 4.1 m³/s, equivalent to 0.1% of the tidal prism, while the southern basin covers 1,030 km² with an inflow of 30.5 m³/s, corresponding to 0.48% of the tidal prism (Park, 2016).

In 2021 approximately 25.8% of the entire harbour was colonised by *Zostera muelleri*, with most of the seagrass concentrated in the intertidal middle portion of the harbour. Seagrass coverage gradually decreases from subtidal to the shallower regions near the coastline and is denser in the Northen basin of the harbour (Shao et al., 2024). Seagrass coverage in the harbour experienced a substantial reduction of approximately 50%, declining from 2,237 ha in 1990 to 1,184 ha in 2019 (Ha et al., 2021), with some recent recovery reported (Shao et al., 2024).

1.9 Thesis outline

This thesis comprises three distinct studies, each developed with the aim of being published in international, peer-reviewed scientific journals. Each study addresses progressively larger spatial scales:

- Chapter 2 presents a field-based study where flow and turbulence measurements were conducted at a small spatial scale ($O(10^0 m)$) within and around a distinct bare gap in a shortleaf seagrass meadow in Tauranga Harbour, New Zealand. The variability of tidal flows at different locations was linked to the spatial distribution of seagrass at both the gap and meadow scales. This work was published in the journal *Limnology and Oceanography* in September 2024, with myself as the first author.
- Chapter 3 explores the impacts of multiple bare gaps on the hydrodynamics of vegetated within aquatic systems. Hydrodynamic models were used to simulate unidirectional flows within emergent vegetation, at a meadow scale ($O(10^2 m)$). The interactions of

accelerated flow associated with gaps of varying sizes at different levels of vegetation coverage were assessed using parameters that account for changes in the bulk horizontal flow within the model domain. This work has been submitted to the journal *Advances in Water Resources* with myself as the first author.

- Chapter 4 employs a machine-learning classifier to explore how topographic and sediment composition variables can predict the presence and absence of seagrass at the estuary scale (O(10^3m)), in Tauranga Harbour, New Zealand. The spatial predictions of seagrass based on these variables were interpreted as indicators of seagrass habitat suitability, making this study one of the first to use machine-learning to assess the specific physical environmental requirements for *Zostera muelleri*. The connections between habitat suitability for seagrass and seagrass patchiness were also evaluated. This study is intended for submission to the journal *Science of the Total Environment*, with myself as the lead author.
- Chapter 5 consolidates the key findings of this thesis and concludes with recommendations for future research.

Chapter 2: The interaction between vegetation patchiness and tidal flows in a shortleaf seagrass meadow

Contribution of authors

Chapter 2 replicates the paper titled “The interaction between vegetation patchiness and tidal flows in a shortleaf seagrass meadow” by Tiago D. da Silva, Julia C. Mullarney, Conrad A. Pilditch, and Giovanni Coco, published in *Limnology and Oceanography* (L&O) in 2024. Most of the text and figures are identical to the published version, except for relabelled figures, tables, and equation numbers, along with a few revisions, as suggested by the examiners of this thesis. In addition, I wrote MATLAB scripts to process and analyse the measured data, prepared all the figures for the manuscript, and contributed to both the initial and subsequent drafts. My co-authors, Julia C. Mullarney, Conrad A. Pilditch, and Giovanni Coco, provided fieldwork and editorial support, guidance, and valuable feedback throughout the drafting process and in response to reviewers during peer review.

Abstract

Seagrasses are critical coastal habitats that provide numerous ecosystem services. The inherent patchiness within meadows exerts a significant influence on the flow-vegetation interaction, which in turn, affects the array of services provided by these environments. We present field observations of vegetation distribution and hydrodynamic measurements within and surrounding an approximately 2-m diameter gap (bare sediment) in a fragmented seagrass meadow. We show that variability in mean flows and turbulence is correlated with meadow structure at small ($O(10^0$ m)) and large ($O(10^2$ m)) spatial scales. Our observations reveal that bare gaps within seagrass meadows lead to faster flows and lower bed elevations. Despite slower flow speeds above the dense seagrass adjacent to the gap, the rates of dissipation of turbulent energy above the vegetation are typically around an order of magnitude larger than above the bare bed. Associated with this enhanced dissipation of turbulent energy, we observed a dominance of down-deceleration events promoting fluid exchange and mixing and driving mass flux into the canopy. Analysis of directional variograms demonstrates that the major continuity axis within NDVI (normalised difference vegetation index) imagery (used as a proxy for vegetation biomass) coincides with the major axis of flow on both gap and meadow scales. Conversely, along the axis of minor flow variance, vegetation remains dense and exhibits greater uniformity. These findings indicate a feedback mechanism between seagrass meadow patchiness and spatial structure through flow modification, which may be beneficial for plant development.

2.1 Introduction

Seagrass meadows can shape coastal environments by altering flows and preventing sediment resuspension (Contti Neto et al., 2022; Lefebvre et al., 2010; Van Katwijk et al., 2010). Thus, these plants act as ecosystem engineers (Meysick et al., 2019), providing various benefits such as shoreline protection (Mullarney & Henderson, 2018; Ondiviela et al., 2014) and habitat provision (Orth et al., 2006). The services provided by seagrasses are influenced by their spatial heterogeneity (Burnett & Gaylord, 2022; Uhrin & Turner, 2018), which, in turn, is determined by factors such as light availability, nutrient levels and physical stress, including hydrodynamic forces resulted from the interaction between flow and vegetation (Duarte et al., 2006). Flow conditions within an optimal physiological range can enhance seagrass bed development by facilitating beneficial plant-flow interactions. In such cases water flow acts as a regulator, by thinning the diffusional boundary layer and promoting blade movement (Hurd, 2000), thereby enhancing nutrient uptake, photosynthesis, and overall productivity (Andrews et al., 2023; Koehl, 2022b; Vacchi et al., 2012). However, when flow speeds exceed species-specific thresholds, hydrodynamic forces can become a stressor. Severe flow conditions may physically damage shoots, inhibit seedling recruitment, and increase sediment resuspension, which reduces light availability and compromises photosynthesis (Adams et al., 2016; Fonseca et al., 2019; Schanz & Asmus, 2003). Therefore, although flow is critical to seagrass functioning, whether positive effects arise is dependent on hydrodynamic conditions remaining within a suitable range.

The inherent heterogeneity of vegetated canopies adds an additional layer of complexity to plant-flow interactions (Folkard, 2019). In contrast to more uniform meadows, fragmented meadows characterised by numerous edges experience changes in flow patterns and bed shear stress (Colomer & Serra, 2021), which affects suspended sediment concentrations (Carr et al., 2016; Peterson et al., 2004; Swadling et al., 2023). Such meadows are more vulnerable to wave

and current action, potentially leading to plant dislodgement and sediment redistribution (Lai et al., 2018; Montefalcone et al., 2010; Ramage & Schiel, 1999).

While studies have investigated hydrodynamics in vegetated patches (e.g., Bouma et al. 2007; Vandenbruwaene et al. 2011; de Lima et al. 2015), research on bare gaps within seagrass beds remains limited. Existing studies often utilize laboratory setups or simplified models (e.g., Hamed et al. 2020; Chung et al. 2021; Ranjan et al. 2022). Comprehensive field-based investigations in natural settings characterised by complex geometries and diverse flow conditions are lacking (Tinoco et al., 2020). Moreover, the mechanisms through which plant-flow interactions affect meadow organization are not yet completely understood (Folkard, 2019).

This field study examines the variability in near-bed hydrodynamics within and around a bare gap within aquatic vegetation and explores the possible implications arising from plant-flow-gap interactions. In particular, we assess how the changes in flow velocity across a tidal cycle are correlated with the spatial arrangement of vegetation in a monospecific intertidal shortleaf seagrass meadow. We captured concurrent flow and turbulence conditions over a short spatial scale ($O(10^0$ m)), in contrast to the few existing field-based studies, which undertook large-scale ($O(10^3$ m)) measurements from vegetated and bare regions of seagrass meadows, which were non-synoptic (e.g., Hansen and Reidenbach, 2017). The spatial and temporal variability in tidal currents within and adjacent to a bare gap was explored and contextualised by linking flows to seagrass distributions at both the small gap and larger meadow scales, using photogrammetric maps of vegetation.

2.2 Methods

2.2.1 Study site

Field observations were taken from the intertidal sandflats in Tauranga Harbour on the North Island of New Zealand (Figure 2.1a and b). With an area of 218 km^2, Tauranga Harbour is a micro-tidal (mean tidal range of 1.4 m), semi-enclosed water body protected by a barrier island and has only two connections with the open sea, at the north and the south of the estuary. The estuary is comprised of extensive intertidal sandflats which are often colonised by *Zostera muelleri*, a perennial, short-leaf seagrass species. In Tauranga Harbour the *Z. muelleri* forms monospecific and highly fragmented meadows, often resulting in a mosaic of low-tide exposed hummocks of seagrass and waterlogged bare hollows. The total coverage of seagrass in the estuary has declined by approximately 50% between 1990 and 2019 (Ha et al., 2021). This decline has been attributed to multiple interrelated factors, including increased sedimentation leading to reduced light availability, nutrient enrichment promoting algal overgrowth, and grazing pressure from black swans (Dos Santos et al., 2013; Flowers et al., 2024).

Our small-scale detailed measurements of flow were taken from a relatively isolated gap situated in the middle of the vegetated intertidal flats of Otumoetai, located in the southern basin of the harbour (Figure 2.1c and d). The series of flow and turbulence measurements were conducted from March 11th to March 13th, 2020, specifically chosen to coincide with spring tides. Each day, we measured flow velocities throughout one tidal cycle (referred to as tidal cycles 1 to 4). In addition, during low tide on these days, we performed bed elevation measurements and collected seagrass samples for biomass analysis. For a detailed timeline of the fieldwork undertaken, please refer to Appendix A, Table A.1.

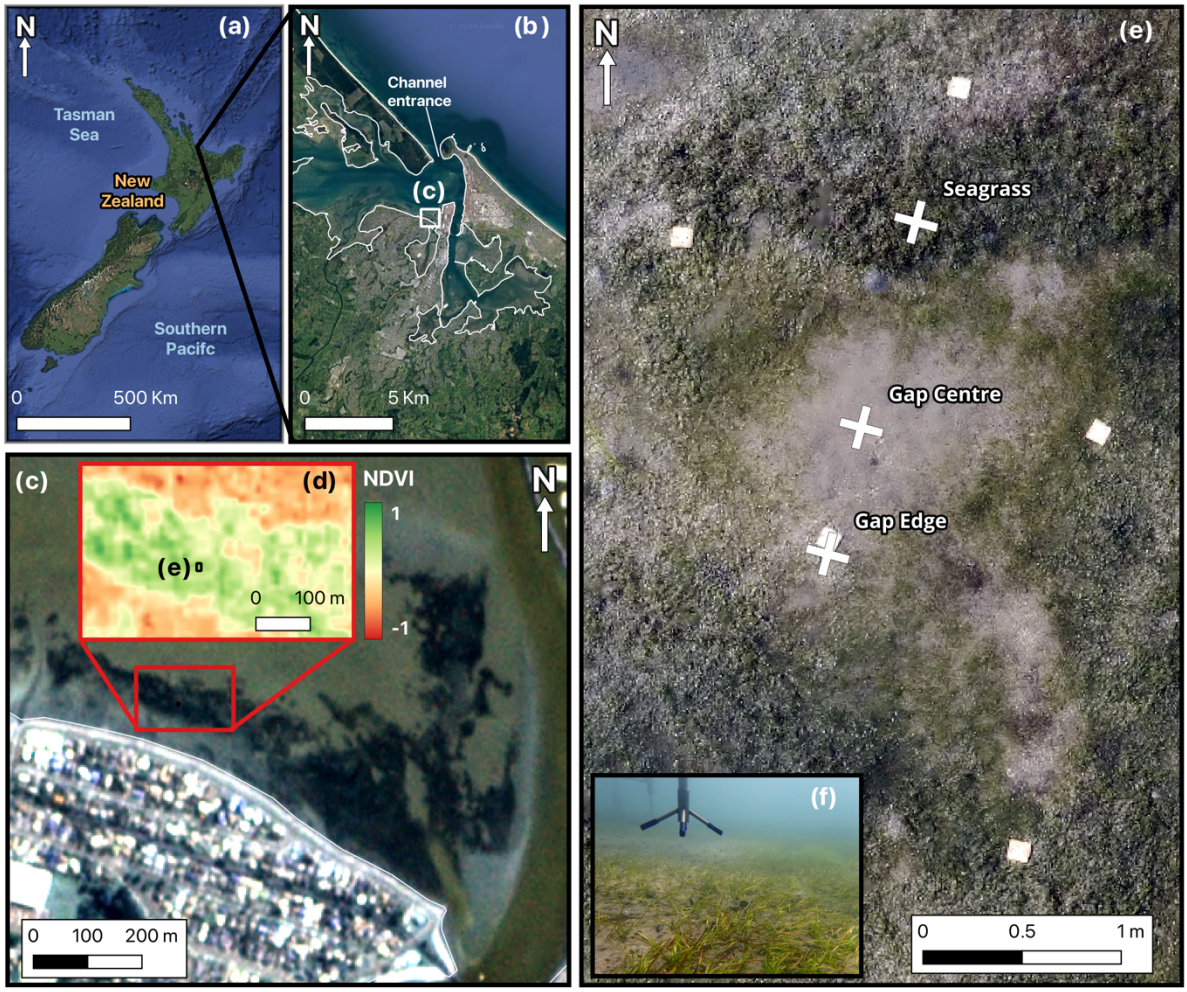

Figure 2.1: (a and b) Location of study-site at Otumoetai, in the southern basin of Tauranga Harbour, New Zealand; (c) PlanetScope imagery of the intertidal flats of Otumoetai; (d) NDVI (normalised difference vegetation index) composition of the area around the gap denoted by the black square; (e) Photogrammetric map of the study area indicating the fixed measurement positions (white crosses); (f) Vectrino Profiler ADV positioned at the Gap Edge. The white squares in (e) are targets used for reconstruction of the photomosaics.

2.2.2 Gap and meadow characterisation

We installed a geodetic benchmark at the study site and fixed a global positioning system (GPS) base station to provide correctional data to a real-time kinematic (RTK) mobile receiver. The GPS-RTK system yielded position data with sub-centimetre accuracy in both vertical and horizontal dimensions (mean ± SD of 8.06 ±0.56 × 10^{-3} and 7.44 ±0.5 × 10^{-3} m, respectively). A total of 216 bed elevation readings were manually performed at randomly distributed points across a 5 × 5 m area surrounding the gap. The orthometric bed heights referenced to the New Zealand Vertical Datum 2016 (NZVD16) were interpolated through an empirical Bayesian

kriging tool, resulting in a continuous topographical map of the gap with a resolution of 0.03 m.

A photogrammetric survey was carried out in the same area as the bed level survey, using a wide-angle mini camera and a mini NDVI (Normalised Difference Vegetation Index) camera mounted on a 3-m-long pole to create photographic ortho mosaics of the gap. Ground targets and the use of GPS-RTK equipment allowed the georectification of the imagery (Figure 2.1e). The resulting photomosaic has a spatial resolution of 0.008 m. The NDVI is widely used as a proxy of vegetation density and plant health, including seagrasses (Nurdin et al., 2022; Zoffoli et al., 2022). The index ranges between -1 and +1 and is calculated based on the ratio between the digital values of the red (R) and near infrared (NIR) bands (NDVI = (NIR - R) / (NIR + R)).

To evaluate the spatial organization of vegetation within the landscape scale we also used a level 1B multiband satellite imagery of PlanetScope from Planet Labs, through the Education and Research Program (https://www.planet.com/markets/education-and-research/). The imagery has a spatial resolution of 3 m and in addition to the Red, Green, and Blue spectral bands, the output includes a Near Infrared band. This combination allows the calculation of NDVI after conversion of Top-of-Atmosphere reflectance (TOA) to Surface Reflectance (SR) using the ACOLITE processor (Vanhellemont & Ruddick, 2018). We selected an image from March 30th, 2020 (21:35:33 UTC), the closest available image to the date of the hydrodynamics measurements captured at low tide when the intertidal flat was exposed. Considering the 17-d gap between the hydrodynamic measurements and the satellite imagery, it is unlikely that the spatial distribution of the seagrass would have changed significantly during this period. Hence, the image is representative of the vegetation conditions during our sampling period.

To assess the accuracy of PlanetScope imagery to characterise seagrass biomass through NDVI, we collected 26 seagrass samples from the surrounding experimental area and

performed a linear regression analysis on both above and below-ground biomass. The sampling locations and results of this analysis are given in the Appendix B In Addition, we conducted a comparison of our findings with the spatial arrangement of seagrass using aerial imagery with a spatial resolution of 0.1 meters, provided by Land Information New Zealand (LINZ, https://data.linz.govt.nz/). This image was acquired in January 2022. The free, open-source, geographic information system software QGIS was used for imagery processing.

2.2.3 Hydrodynamic measurements

We conducted a series of high-frequency concurrent velocity measurements at different points within and around the seagrass gap (Figure 2.1e). The data was collected using 3 profiling Acoustic Doppler Velocimeters (10 MHz Nortek Vectrino Profilers, VP - Figure 2.1f) sampling at 50 Hz, with a vertical resolution of 1 mm over a profile of 30 mm. Measurements were taken for 4 different tidal cycles in total. During the first two tidal cycles, instruments were deployed to capture a profile from 0.13 to 0.16 m above the bed, while during the last two tidal cycles the instruments measured profiles from 0.05 to 0.08 m above the bed.

At the study site the average seagrass leaf length is typically 0.06 ± 0.03 m (mean ±SE, n = 50; Crawshaw 2020), so all measurements avoided the interference of seagrass blades in the sampling volume of the instrument, noting that the effective height when vegetation is deflected by the tidal flow is smaller than the leaf length.

For tides 1 and 3, instruments were kept fixed at their locations throughout the entire tidal cycle: one of the instruments was deployed over the dense seagrass in the seaward edge of the gap (herein referred as seagrass, Figure 2.1e), the second instrument was fixed in the approximate centre of the gap over the bare bed (gap centre) and the third instrument was deployed over the sparse seagrass close the shoreward limit of the gap (gap edge). For tides 2 and 4, the outer instruments (seagrass and gap edge) were moved to collect data at different

locations within and around the gap, while the instrument in the centre of the gap remained in the same location throughout the measurements. For these tides, data were captured for between 10 and 20 min at each location (see Supporting Information, Appendix C). Water levels were obtained from pressure data collected at a sampling rate of 6 Hz at 0.17 m above the bed using a Conductivity-Temperature-Depth probe (RBR Concerto) co-located on the same frame as the profilers.

2.2.4 Data analysis

Vectrino Profiler velocity data were processed to remove low quality data (correlations < 50%). Spikes were removed by implementing a phase-space thresholding method (Goring & Nikora, 2002). Overall, the low correlation velocities and spikes accounted for 4.5% of the data and gaps were then filled using a spectral technique (Xu et al., 2002). After these steps, the velocities were rotated from beam coordinates into the direction of the axis of maximum variance, that is, the direction of the first principal component of the time series of the horizontal flow velocities. Thus, hereafter u, v and w denotes the components of instantaneous velocities relative to the major, minor, and vertical axis of flow, respectively. Tidal ellipses are shown in Figure 2.3. Time-averaged flow velocities and turbulence parameters were calculated for 10-min windows with 50% overlap.

In-situ observations during the experiment and a preliminary analysis of the pressure data indicated the presence of small-scale waves (significant wave height, H_S < 0.1 m) during the measurements. Therefore, a decomposition of velocity signal into wave and turbulent components was undertaken using the method described in Zhang et al. (2021). The decomposition was performed when within a given 10-min velocity data segment, the power spectrum densities (PSDs) related to waves were greater than 10% of the total energy contained across the full frequency range of the turbulent spectrum, as suggested by Hansen and Reidenbach (2013).

Turbulence was characterised by the dissipation rate of turbulent kinetic energy (ε, m^2/s^3), which was estimated using the structure function method as described by Wiles et al. (2006). A detailed description of the structure function method is provided in the Appendix D.

2.2.5 Spatial distribution of seagrass

To further investigate the links between flow transience and the spatial organization of the seagrass, we constructed maps of the directional semi-variograms of vegetation biomass (using NDVI as a proxy) and compared these maps with the major and minor principal components of tidal flow. The semi-variogram is a measure of spatial variability that quantifies the similarity (or dissimilarity) between pairs of data points as a function of their spatial separation distance (h). Isotropic semi-variograms encompass variance across all directions, while anisotropic directional semi-variograms focus on variance along specific orientations (α). This technique is particularly useful for understanding the spatial structure and patterns in geostatistical data (Wackernagel, 2003), including seagrasses (Ooi et al., 2014). An experimental directional semi-variogram $\hat{\gamma}(h, \alpha)$ is calculated as half of the mean-squared differences of NDVI values between all pairs of different data points separated by a distance (h) in the direction (α),

$$\hat{\gamma}(h, \alpha) = \frac{1}{2N} \sum_{i=1}^{N(h,\alpha)} [NDVI(L_i) - NDVI(L_i + h)]^2, \quad (2.1)$$

where $NDVI(L_i)$ is the NDVI value at the location L_i. The scale of spatial continuity of NDVI in a given direction can be characterised in the semi-variogram as the "range" (r), defined as the separation distance (h) in which γ ceases to grow further and reaches an asymptotic state of stability, commonly referred as the "sill". To identify the sill and the range, we fitted a theoretical spherical variogram model to the experimental semi-variograms.

The semi-variogram analysis was applied both to the NDVI imagery surveyed around the gap and the PlanetScope image at the meadow scale. The former imagery allowed the identification of spatial continuity at a smaller spatial scale with h ranging from 0.03 to 6.9 m, while the latter was used to extract the continuity at larger spatial scales from 3 to 180 m. We constructed experimental semi-variograms for the NDVI imagery in direction (α) intervals of 10°, subsequently combining them to derive variogram maps. The semi-variance values ($\hat{\gamma}(h, \alpha)$) were then plotted on a grid, creating a two-dimensional map that visualizes spatial continuity and variability of NDVI. The direction with the greatest (r) indicates the primary direction of spatial correlation or continuity in the distribution of seagrass. A continuity ellipse can then be constructed, whereby the major axis is the direction of maximum continuity with the length (r). The shape and orientation of the ellipse denote the distance beyond which spatial correlation becomes negligible. Together, the variogram map and continuity ellipse aid in understanding spatial structure, anisotropy, and scale of spatial correlation within the seagrass meadow.

2.3 Results

2.3.1 Morphological characterisation of the gap

Seagrass biomass (as expressed by the NDVI) and bed elevations in and around the gap are shown in Figure 2.2. The bare gap is asymmetrical and elongated towards the southeast with a long axis of ~2.6 m, and width of ~1.8 m in the perpendicular direction. The transition from the bare bed to fully vegetated sandflat is gradual, and seagrass is denser at the southwest and northeast edges of the gap, across the minor axis of the gap. In addition, bed levels within the bare area are lower with a maximum height difference from the deepest location at the gap centre to the bed level in the surrounding vegetation of around 0.05 m.

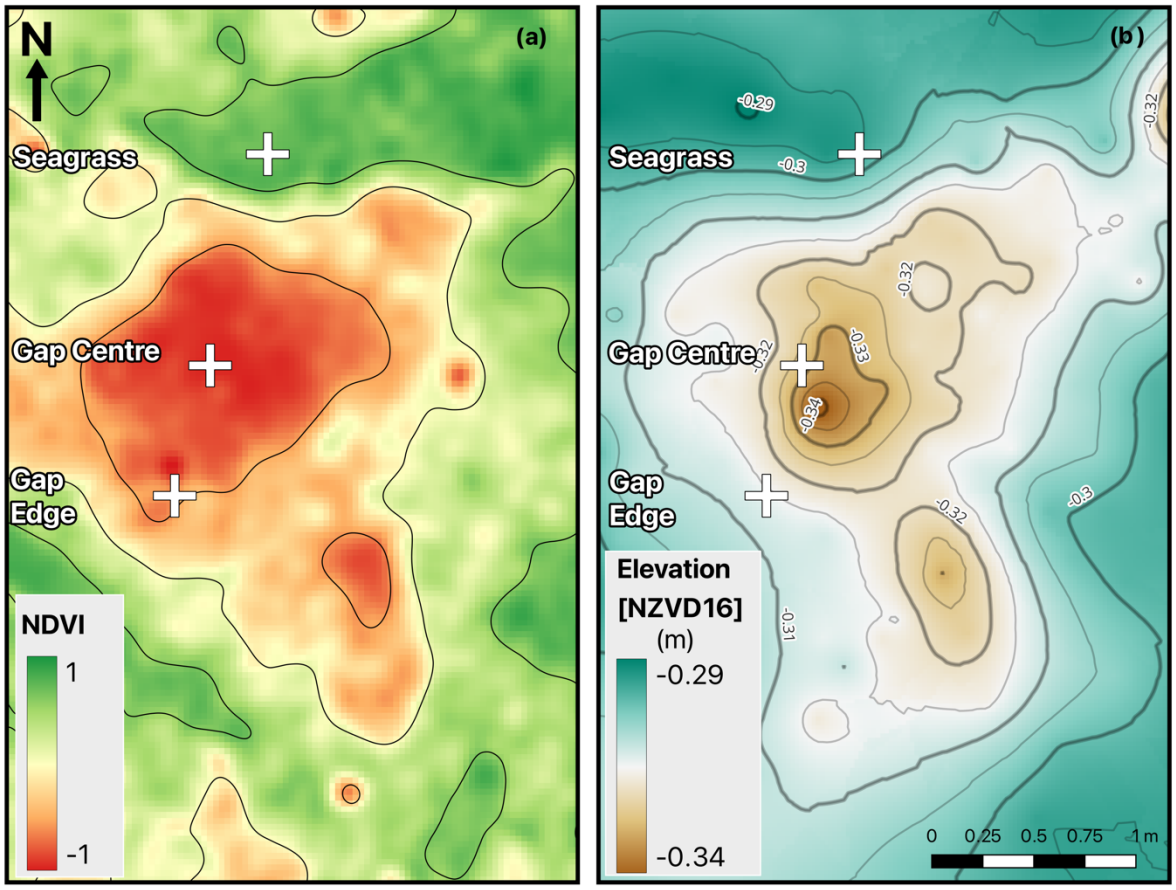

Figure 2.2: (a) Normalised difference vegetation index (NDVI) depicting the vegetation biomass and (b) bed levels within and around the gap, expressed as orthogonal heights, referenced to NZVD16 Vertical Datum. The crosses show the fixed measurement locations for velocity (Vectrino Profilers).

2.3.2 Relationship between tidal flow transience and gap morphology

For clarity, we report in the next two sections observations from the tidal cycle during which measurement locations remained fixed, when the instruments were deployed at the nearest vertical measured position to the bed (tidal cycle 3). Over the vertical velocity profile, we extracted the results at the point where noise-associated error were smallest (Thomas et al., 2017), which in our measurements corresponded to 0.067 m above the bed. Note that the presented results were found to be consistent across all tides, including those over which instrument locations were moved (see Appendix C, Figure C.2. for the additional time series).

To explore the links between flow conditions, vegetation distribution and bed topography, we plotted tidal ellipses, together with the vectors indicating the direction and magnitude of the

mean horizontal speeds during flood and ebb tidal stages, and the topographic contours (Figure 2.3). Flood and ebb tides were separated by the times of high and low water recorded by the pressor sensor. Tidal currents are faster during the incoming flood stage (southeast direction) while ebb currents are weaker, and flows are almost perpendicular to the flood direction, to the northeast direction. Figure 2.3 illustrates that the gap is elongated in the direction of the prevailing flow conditions, which are predominantly influenced by the flood currents.

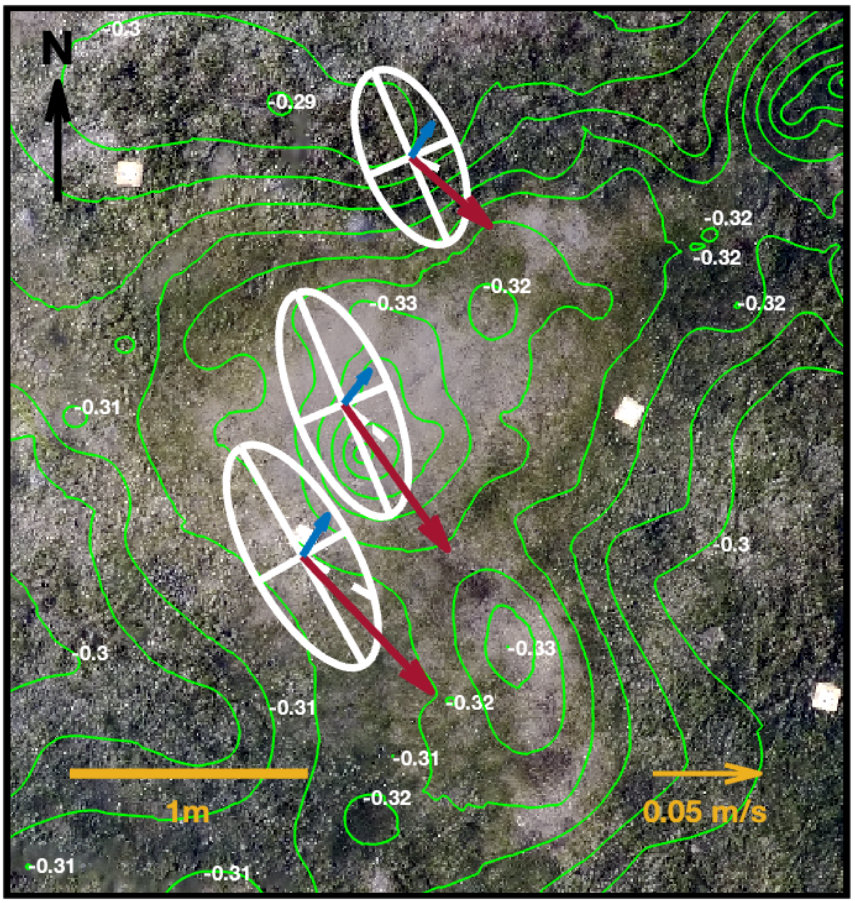

Figure 2.3: Gap morphology and flow patterns, illustrated by the photogrammetric 2D model of the gap and the topographic contours, overlapped by the tidal ellipses (white lines) and vectors of mean flow during flood (red arrows) and ebb tides (blue arrows).

We examined the variability of vegetation density as the flow approached and exited the gap. For each 10-min period, we defined an upstream and downstream 3-m transect based on the mean horizontal flow directions from the measurement location at the centre of the gap (Figure 2.4a). NDVI values at 0.1 m intervals along the transects were then extracted and used as a

proxy for vegetation density. These data shown in Figure 2.4b thus provide an indication of the upstream and downstream vegetation biomass encountered by the flow at a particular time.

Although upstream of the gap vegetation is overall less dense, there is a predominance of barren bed downstream from the gap centre, suggesting the influence of the stronger flood tidal currents along the direction of enhanced flood currents. In contrast to the sparse vegetation along the axis of intensified flood currents, seagrass is denser along the axis of the weaker ebb flow, especially downstream of the gap.

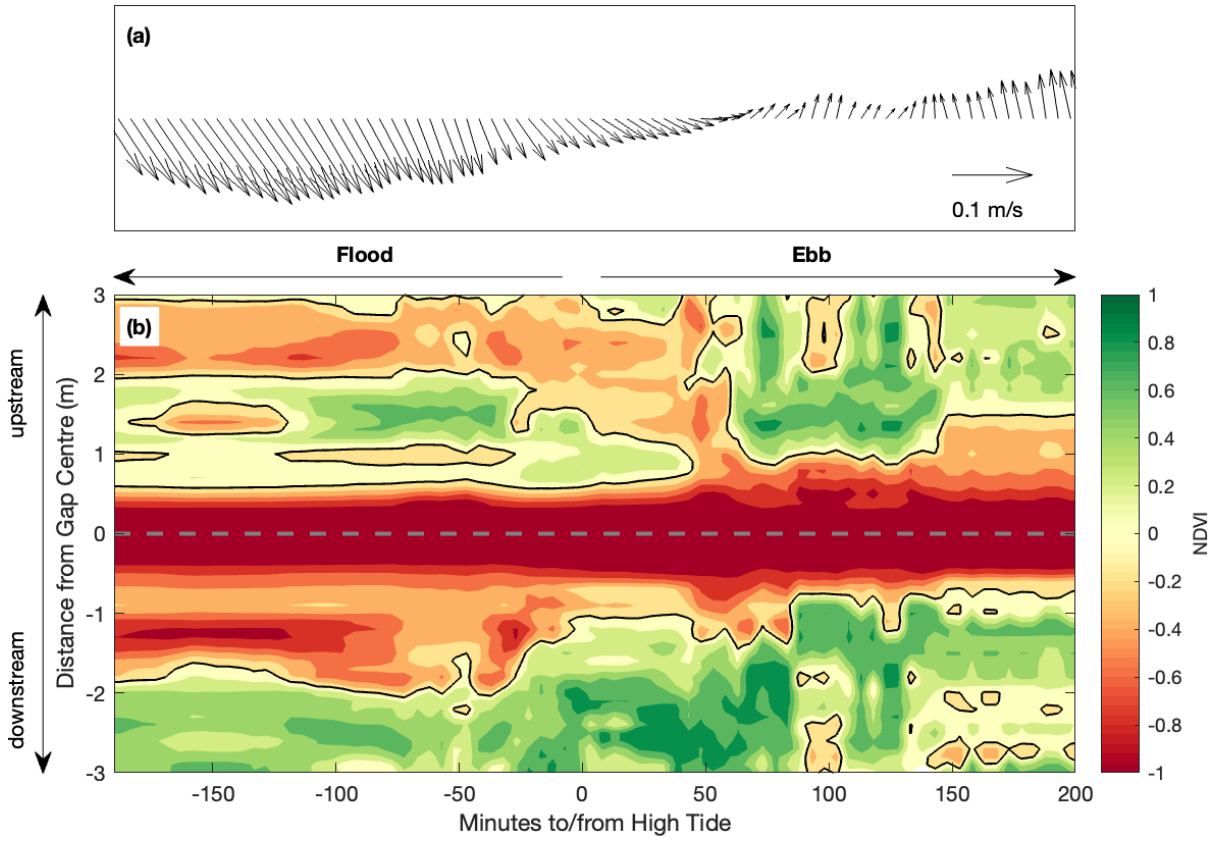

Figure 2.4: (a) Time-series of vectors of mean horizontal flow velocities, measured at the gap centre and calculated in 10-minute segments with 50% overlap; (b) NDVI values extracted over a 3 m transect projected upstream and downstream from the gap centre along the flow directions (green corresponds to higher vegetation density, while the red colours correspond to bare bed). The dashed grey line denotes the centre of the gap.

2.3.3 Spatial and temporal variability of currents and turbulence within and around the gap

Time series of the mean flow direction (a) and horizontal speed (b), and dissipation rates of turbulent kinetic energy (c) are shown in Figure 2.5, and a statistical summary of key

parameters is presented in Table 2.1. Note that the faster flood currents travel alongshore (perpendicular to the measurement transect), while the weaker ebb currents move in the cross-shore direction (parallel to the measurement transect (Figure 2.3a and b). Horizontal flow speeds are initially much stronger over the gap, both at the centre and the edge, than above the seagrass (up to approximately four times larger, 143 min before the high tide, Figure 2.5b), with slightly faster flow speeds in the centre of the gap than close to the edge. During the peak in the tidal currents within the gap, the flow speeds are 0.12 m s^{-1} at the gap centre and edge and 0.03 m s^{-1} above the seagrass. At approximately 42 min before high tide, there is a slight rotation in the flow, with a change towards the northeast direction (Figure 2.5a), while speeds from the three locations remain similar. For the remainder of the tidal cycle (from 60 min before high tide), both flow speeds and directions are similar between the three sites.

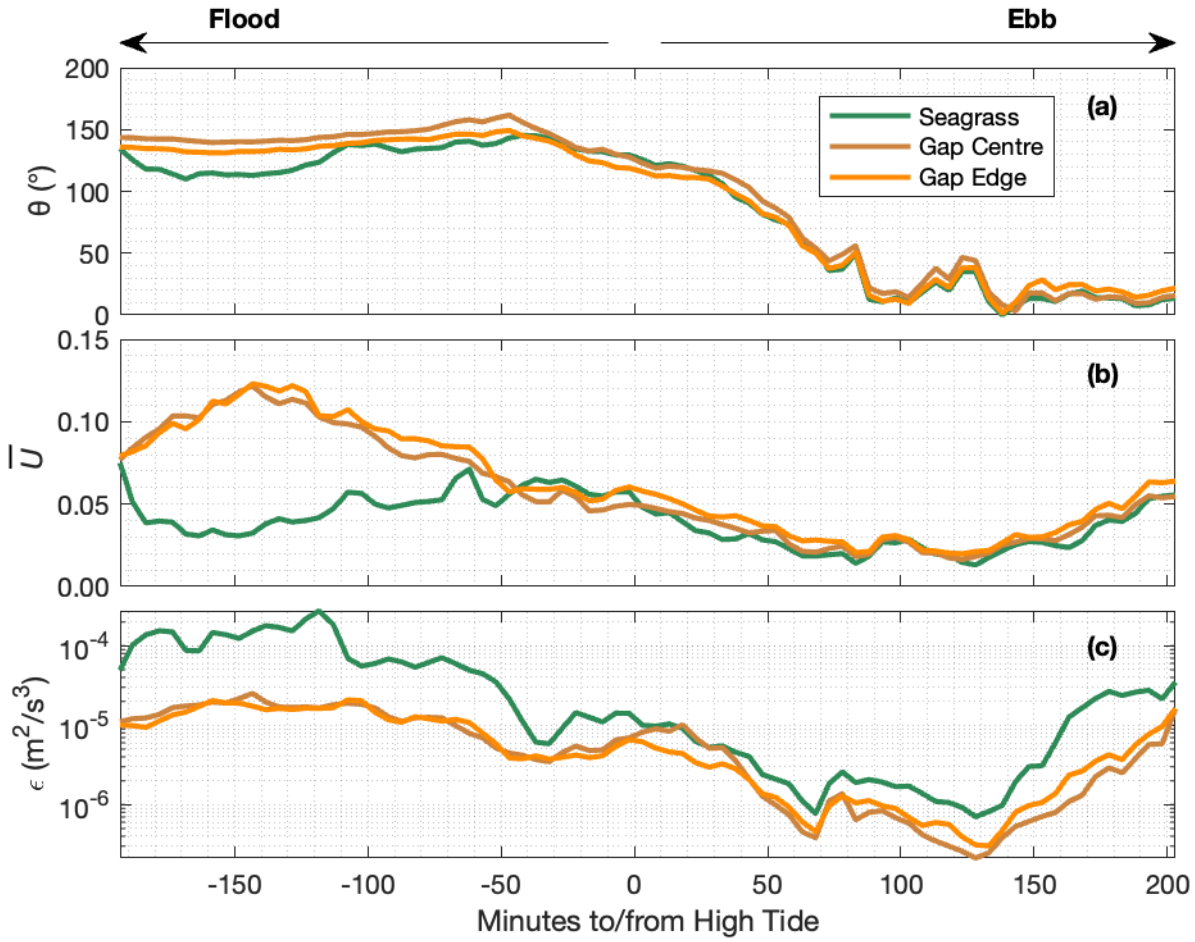

Figure 2.5: Time-series of (a) direction (θ) and (b) speed of horizontal flows ($\overline{U}$), and (c) rates of dissipation of turbulent kinetic energy (ε) over the seagrass (green) and within the gap (brown for gap centre and orange for gap edge), averaged in 10-min velocity segments with 50% overlap. The flow direction refers to the azimuth angle relative to true north.

The calculated rates of dissipation of turbulent kinetic energy (ε) shown in Figure 2.5c, varied from O(10^{-6}) to O(10^{-4}) m^2/s^3, consistent with the dissipation rates measured by others in seagrass canopies (Hansen & Reidenbach, 2017), including *Z. muelleri* (Bryan et al., 2007). Despite slower flow speeds above the seagrass, the rates of dissipation of turbulent energy are consistently around an order of magnitude larger than those over the gap, except for a short period during the beginning of the ebb tide (0 to 30 min after the high tide) when the dissipation rates are approximately the same at all locations. During both flood and ebb tides, the mean dissipation rates differed up to one order of magnitude between the seagrass and the gap,

although they were found to be on the same order of magnitude within the two locations within the gap.

Table 2.1: Summary statistics of mean flow direction (θ), speed ($\overline{U}$), and dissipation rates of turbulent kinetic energy (± 95% confidence interval) for the flood and ebb tidal stages, calculated from the time series shown in Figure 2.5.

Parameter	Tidal stage	Seagrass	Gap Centre	Gap Edge
θ (°)	FLOOD	129 ±4	145 ±3	136 ±2
	EBB	37 ±15	41 ±16	34 ±16
$\overline{U}$ (m s^{-1})	FLOOD	0.05 ±0.004	0.08 ± 0.008	0.09 ± 0.007
	EBB	0.03 ±0.004	0.03 ± 0.004	0.04 ± 0.004
ε (m^2/s^3)	FLOOD	8.5×10^{-5} $\pm2.2\times10^{-5}$	1.2×10^{-5} $\pm1.9\times10^{-6}$	1.2×10^{-5} $\pm1.8\times10^{-6}$
	EBB	7.8×10^{-6} $\pm2.9\times10^{-6}$	2.8×10^{-6} $\pm1.1\times10^{-6}$	2.7×10^{-6} $\pm9.7\times10^{-7}$

We quantify the extent to which the gap influences local flows as a function of tidal stage by comparing synoptic speeds above the gap and the speeds. The horizontal flow speeds measured within the gap relative to those above the seagrass are shown in Figure 2.6. During the incoming flood tide, flow is intensified within the gap (blue symbols), and there is a negative relationship with slower speeds over the seagrass corresponding to faster flow speeds within the gap. Conversely, during the ebb tide, the intensification of speeds within the gap is minimal and flow speeds within the gap are positively correlated with those above the seagrass (brown symbols).

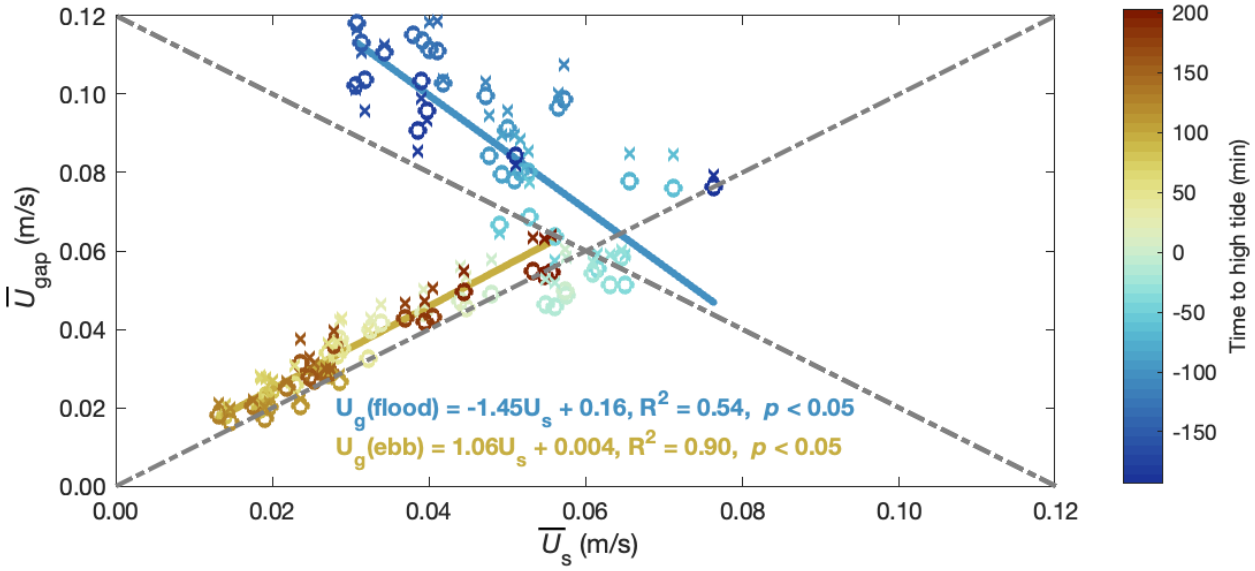

Figure 2.6: Horizontal flow speeds measured above the seagrass ($\overline{U}_s$) plotted against the flow speeds measured at the gap centre (o) and edge (x) coloured by tidal stage ($\overline{U}_{gap}$). The blue and brown solid lines are robust linear fits across all three locations during the flood and the ebb tides, respectively.

Often, the dissipation rate of TKE (ε) scales as $\frac{\overline{U}^3}{L}$, where $\overline{U}$ and L are the mean flow speed and length scales, respectively. We used the ratio $\left(\frac{\overline{U}^3}{H}\right)/\varepsilon$ (where H is the water depth), as an indicator of the turbulence levels in relation to flow conditions (Pope, 2000). The ratios relative to the different measurement locations are plotted in the Figure 2.7. Within the gap, turbulent dissipation rates consistently exhibit a cubic relationship with flow speeds throughout the entire tidal cycle. However, during the incoming flood tide, this relationship does not hold true over seagrass, where turbulence levels remain elevated despite slower flow speeds.

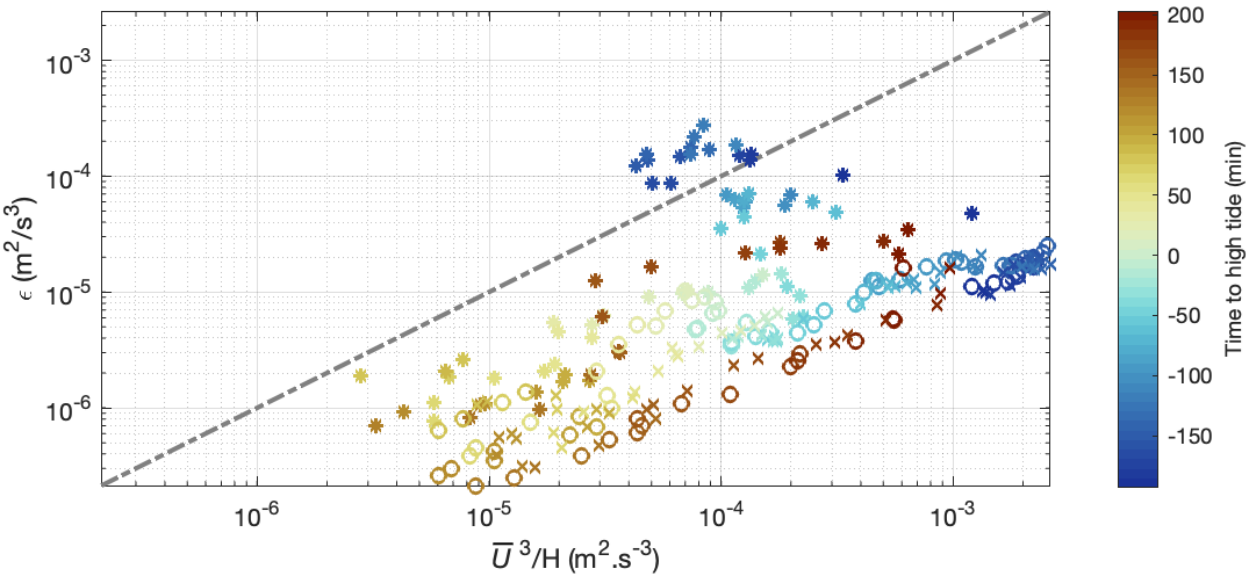

Figure 2.7: Dissipation rates of turbulent kinetic energy (ε) against the cube of flow speeds normalised by water depth ($\left(\frac{\bar{U}^3}{H}\right)/_{\varepsilon}$) with tidal stage measured above the seagrass (*), in the centre of the gap (x) and on the vegetated gap edge (o). The grey dot-dashed lines show a 1:1 slope.

A quadrant analysis of the Reynolds stresses was used to examine how the key processes controlling the transfer of momentum changed over the tidal cycle (Figure 2.8). For each location, the probability density function (pdf) of the fluctuations of the streamwise (u') and vertical velocities (w'), was calculated, normalised by the standard deviation over 10-min windows. Dominance in the first and fourth quadrants (Q1: u' > 0 and w' > 0; Q4: u' > 0 and w' < 0) indicates ejections and sweeps, respectively. Dominance of the second and third quadrants (Q2: u' < 0 and w' > 0; Q3: u' < 0 and w' < 0) indicates up-acceleration and down-deceleration, respectively (Kline et al., 1967; Pope, 2000).

A preliminary analysis revealed that the predominant turbulent events remain relatively consistent within the gap throughout the tidal cycle but vary over the seagrass during different stages of the flood tide (but not the ebb tide). Hence, we show examples of quadrant analysis from during the incoming flood tide (133 min before high tide), later flood tide (97 min before high tide), and ebb tide (173 min after high tide). Within the gap, both at its centre and edge, turbulent processes are primarily characterised by sweeps and ejections, with no clear

dominance of one or the other in the entire tidal cycle (Figure 2.8b, c, e, f, h and i). However, over the seagrass, during the initial influx of faster flood currents (up to 100 min before high tide), turbulence predominantly manifests as downward deceleration (Figure 2.8a). As the flood tide progresses and the tidal currents become slower and more uniform both within and around the gap, turbulence over the seagrass undergoes a transition from down-deceleration to sweeping patterns (Figure 2.8d). During the ebb turbulent processes are dominated by sweeps and ejections with a slight dominance of ejections (Figure 2.8g).

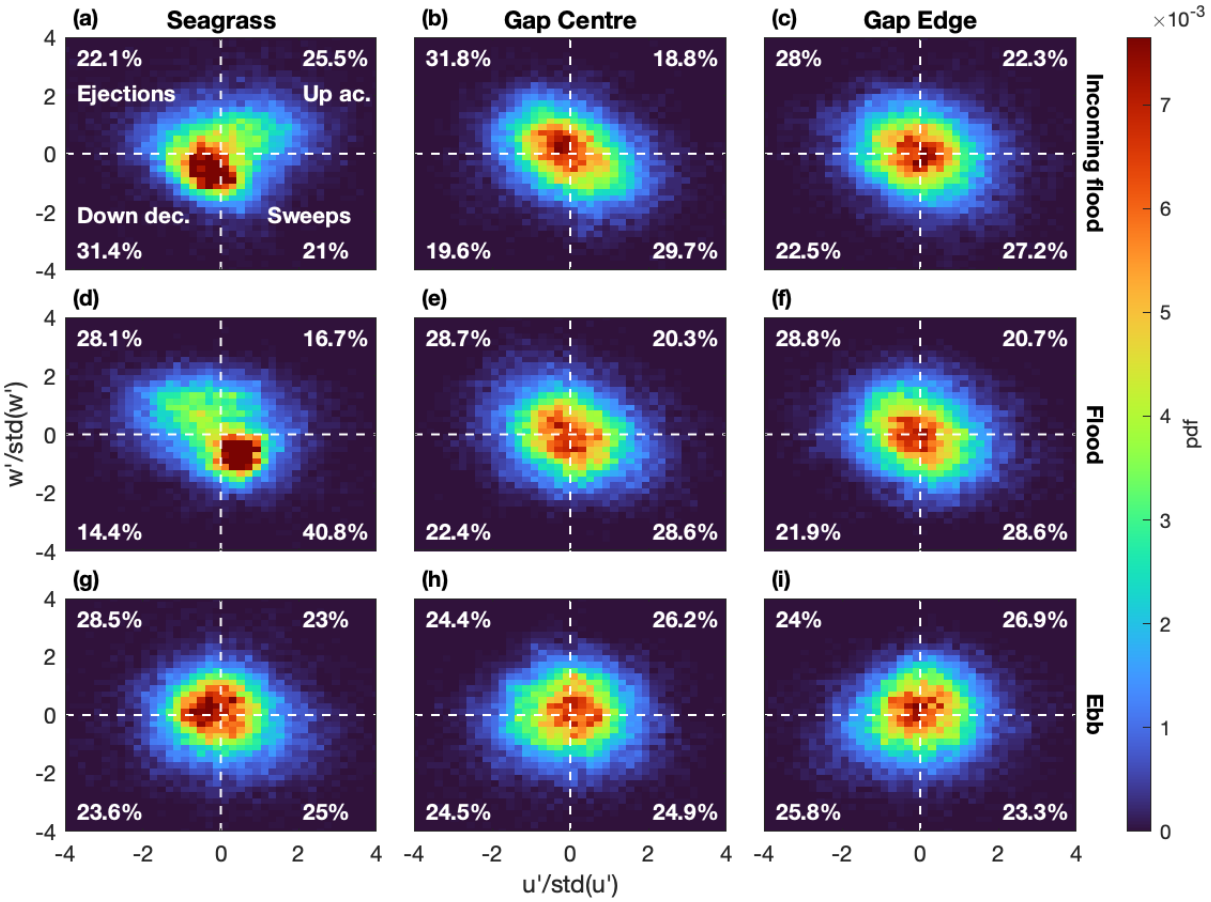

Figure 2.8: Quadrant analysis of the Reynolds Stresses expressed by the probability density function (pdf) of the velocity fluctuations of the streamwise (u') and vertical (w') velocities normalised by their standard deviation (std). The top row (a-c) corresponds a 10-min data segment during incoming the flood tide (133 min before high tide), the middle row (d-f) corresponds to the final stage of flood tide (97 min before high tide) and the bottom row (g-i) during the ebb tide (173 min after the high tide). The percentages indicate the contributions of the stresses in each quadrant.

2.3.4 Tide and vegetation interactions at different spatial scales

The variogram maps presented in Figure 2.9a and b show the alignment between the major and minor axis of spatial continuity and the tidal ellipse derived from flow velocities at both spatial scales analysed. For both scales, the major continuity axis of vegetation (10° at the gap scale and 20° at the meadow scale) nearly coincides with the minor axis of flow (23°), i.e., the vegetation is more variable along the dominant direction of flow. The anisotropy ratio (between the lengths of the major and minor axes) indicates the degree of non-uniformity or directional variability in the seagrass distribution. At the gap scale the anisotropy ratio is 1.4 (=1.59 m/1.13 m). While at the meadow scale the major axis is 96 m long, and the minor axis is 30 m long, yielding an anisotropy ratio of 3.

The seagrass continuity is visually discernible through the high-resolution aerial imagery, shown in Figure 2.9c. Within our study site, the seagrass vegetation displays a mosaic-like colonization of the bed, interspersed with anisotropic gaps separating the rows. These patterns indicate that the rows of vegetation are arranged perpendicularly to the dominant flow direction, as supported by the variogram maps.

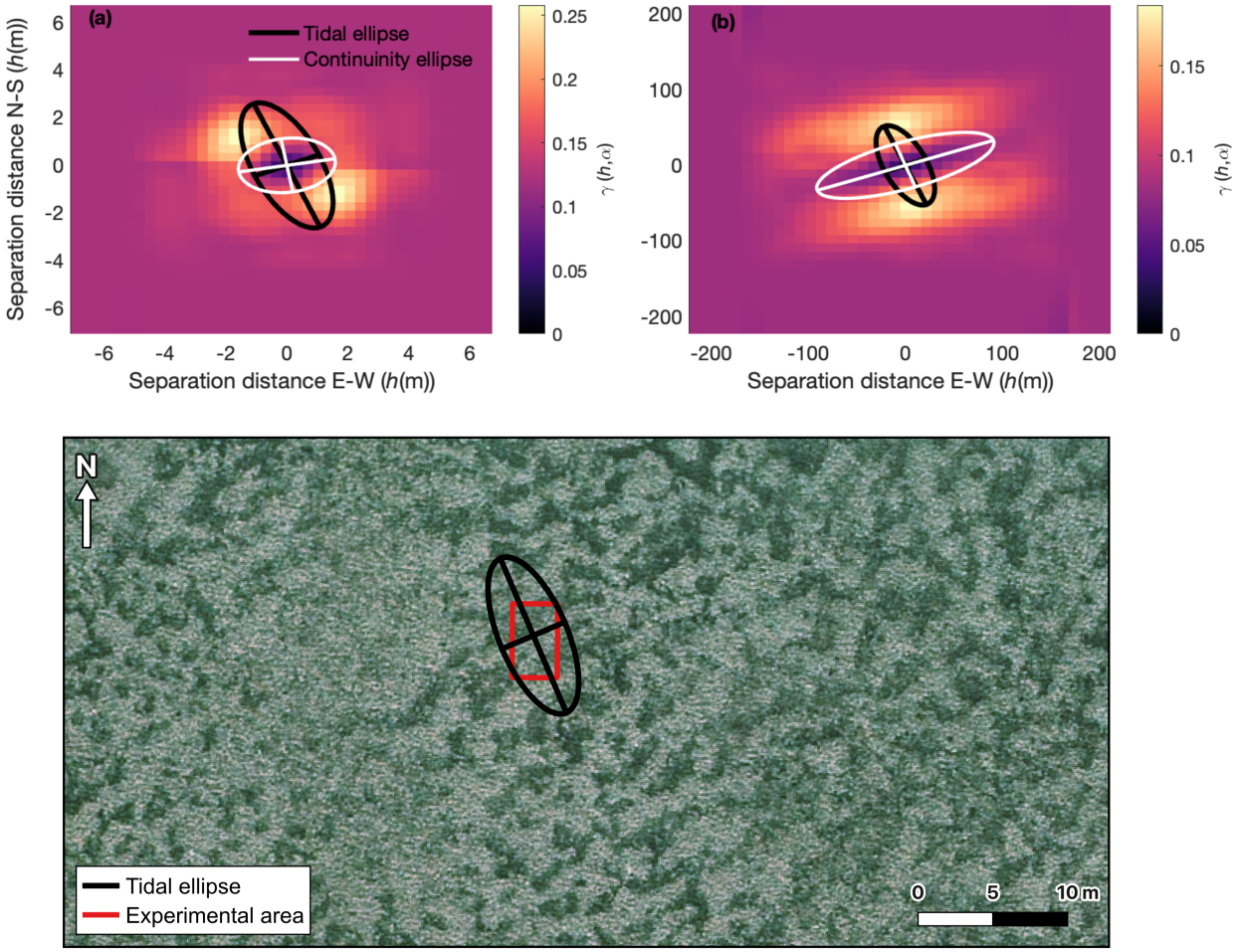

Figure 2.9: (a) Gap scale and (b) meadow scale variogram maps. The black and white ellipses show the tidal (not to scale) and continuity ellipses, respectively. (c) 0.1 m resolution aerial imagery of the study site (provided by Tauranga City Council, 2022), illustrating the approximate distribution of seagrass across the dominant flow direction. The red box indicates the experiment area shown in Figure 2.1e.

2.4 Discussion

Our measurements demonstrate the complexity of tidal flow interactions in fragmented intertidal seagrass meadows and the resulting variability of flow conditions within these habitats at a small scale (O(10^0 m)). Results suggest that, at this site, the small-scale interactions between vegetation and bare patches are driven by larger-scale interactions in tidal asymmetry. In shallow coastal estuaries, tidal asymmetry is influenced by a combination of factors. Interactions between estuarine morphology and tidal constituents result in asymmetrical tides (Dronkers, 1986). The phase difference between these constituents determines the flood or ebb dominance, while the ratio of constituent amplitudes indicates the degree of distortion (Boon

& Byrne, 1981; Friedrichs & Aubrey, 1988). In addition, constricted basins with deep entrance channels, such as the south basin of Tauranga Harbour (Figure 2.1b), often exhibit flood-dominant peak tidal velocity asymmetries, with the most significant tidal distortions occurring in the intertidal flats (de Ruiter et al., 2019). Our results are consistent with these observations as illustrated in Figure 2.5b and further detailed in Figure C.2 in Appendix C.

In vegetated beds, the drag experienced by the water column is controlled by canopy structure and flow speeds, with faster flows resulting in increased drag (Mullarney & Henderson, 2018). Consequently, at our study site only the faster currents of the incoming flood tide generated sufficient vegetation drag to cause flow diversion towards the bare patches. During slower flow conditions, such as during the ebb tide, the vegetation exerts minimal drag, leading to negligible differences in flow speeds between vegetated and bare patches (Figure 2.5b). During the flood tide, downward-directed turbulent motions such as down-deceleration and sweep events enhance the delivery of solutes like nutrients and carbon dioxide to the seagrass canopy, promoting plant health and growth. Although solute concentrations were not directly measured in this study, the beneficial role of turbulence-driven exchange processes for aquatic vegetation is well established in the literature (Hansen & Reidenbach, 2013). Therefore, these observations suggest that perpendicular to the axis of dominant flow the attenuation of near-canopy currents might be beneficial for plant development, as also supported by the observation of denser vegetation on the sides of the bare gap.

At a broader spatial scale ($O(10^2$ m)), the similarity between tidal and continuity ellipses supported by the aerial image (Figure 2.9) indicates a connection between tidal transience and flow variability within and around the gap. This correlation suggests that in fragmented seagrass meadows, plant-flow interactions are shaped by prevailing flow conditions, leading to distinct strategies of seabed colonization. Tidal variability and canopy continuity were correlated not only at the gap scale but also at the meadow scale, underlining the potential

feedback between tidal flows and seagrass habitats. The spatial configurations of vegetated canopies and their edges are influenced not only by alterations in hydrodynamics but also by small-scale interactions resulting from internal structural factors and alterations(Colomer & Serra, 2021; Roca et al., 2016). Under unidirectional flow, the patterns of seagrass beds at various scales may be significantly influenced by the collective growth of individual shoots, which respond to the average direction dictated by hydrodynamic forces over time (Adhitya et al., 2014; Fonseca et al., 2007). The colonization of seagrass beds in a direction perpendicular to the main flow axis may be further enhanced due to the increased likelihood of reduced disturbance on the patch edges that are perpendicular to the flow, as opposed to the edges that face the flow.

In environments with complex flow patterns such as coastal areas, self-organization mediated by flow and vegetation interactions often results in rows of vegetation aligned perpendicular to the dominant flow axis, leading to the formation of anisotropic gaps (Fonseca et al., 2007). This process contrasts with riverine systems, where vegetation tends to organize into patches aligned with the stream flow (Cornacchia et al., 2018). The correlation between tidal forcing and the spatial distribution of seagrass suggests that tidal flow influences plant development, particularly along the borders of gaps, as reported in previous studies (Barcelona et al., 2021; Fonseca et al., 2019). This influence becomes more pronounced under stronger hydrodynamic conditions, as the transport of particles and solutes is affected by vegetation positioning relative to the upstream and downstream edges of the gap (Koehl, 2022b). Our findings support the idea that vegetation structure, especially the geometry of bare gaps within seagrass meadows, may reflect prevailing hydrodynamic regimes, as proposed by Fonseca et al. (2007). For example, elongated gaps aligned with dominant flow directions or asymmetrical contours may indicate cumulative flow exposure or tidal asymmetry. When such configurations are consistently observed in satellite-derived vegetation maps, these patterns may provide a basis

for inferring long-term hydrodynamic forcing, complementing in situ measurements and enabling broader spatial or retrospective assessments of flow conditions.

The results presented illustrate how patchiness locally modifies hydrodynamics at the gap scale. Flow modification is a crucial mechanism that influences ecomorphological processes, thereby shaping the development of patches. These processes, in turn, affect landscape dynamics, habitat diversity, and species richness, with implications for ecosystem resilience and biodiversity conservation (Folkard, 2019). Such observations draw attention to a noteworthy obstacle in modelling the ecomorphodynamics of seagrass meadows as they must account for this fine-scale spatial heterogeneity and the dynamic feedback mechanisms between seagrass and tidal flows. Sufficient spatial resolution of models is required to correctly represent the macroroughness of meadows, which is substantially influenced by patchiness. Incorporating these complexities will enhance predictive accuracy of models.

Furthermore, the observed relationships may not be universally applicable to patches of varying sizes. Existing literature suggests that the density of surrounding vegetation around bare gaps can be influenced by gap size (Barcelona et al., 2021; Colomer et al., 2017), probably due to the capacity of bigger gaps to concentrate more flow. The influence of gap size on flow modification and subsequent implication for vegetation growth remains a prospect for future research. It is also important to note that other physical drivers, such as wind-driven waves on shallow intertidal flats, may influence the spatial organization of vegetation. However, their relative importance varies with local conditions such as wind fetch and water depth.

Our findings indicate that closing of gaps through vegetative growth inward may be hindered by drag forces arising under fast flows. The outcome may vary depending on the specific local flow conditions. Hence, the thorough understanding of the physical settings is crucial when establishing strategies for the restoration of bare patches within seagrass meadows. Such

knowledge can inform more effective and site-specific approaches to ensure the successful recovery and conservation of seagrass ecosystems.

2.5 Conclusions

Our observations have relevance to restoration strategies for seagrass meadows that are susceptible to loss of vegetation cover and consequently meadow fragmentation. As the flow can shape the gap and create flow-induced stress that can affect the survival and growth of seagrass plants, understanding the flow conditions experienced by seagrass seedlings is fundamental for management and restoration of these habitats. The implications for sediment transport, nutrient cycling, and seagrass organization emphasize the importance of considering fine-scale flow variability in conservation and restoration efforts. As coastal ecosystems face increasing anthropogenic pressures, these understandings can guide strategies aimed at preserving and rehabilitating seagrass habitats, contributing to the overall health and stability of coastal environments.

Chapter 3: The impact of bare gaps on meadow-scale flows within fragmented emergent aquatic vegetation

Contribution of authors

Chapter 3 reproduces the paper titled “The impact of bare gaps on meadow-scale flows within fragmented emergent aquatic vegetation”, authored by Tiago D. da Silva, Julia C. Mullarney, Conrad A. Pilditch, and Giovanni Coco, which has been submitted to *Advances in Water Resources*. The text and figures are largely unchanged from the submitted version, aside from relabelling of figures, tables, and equation numbers, along with minor revisions. I conducted the simulations, wrote Matlab scripts for processing and analysing the model results, and prepared all the figures for the manuscript. I also contributed to both the initial and subsequent drafts. My co-authors, Julia C. Mullarney, Conrad A. Pilditch, and Giovanni Coco, assisted in designing the experimental modelling setup and provided editorial support, guidance, and constructive feedback throughout the drafting process.

Abstract

Aquatic vegetation has been shown to shape landscape morphology by interacting with flows and influencing sedimentological processes. These interactions are modulated by the spatial distribution and density of the vegetation. We conducted idealised numerical simulations using a depth-averaged hydrodynamic model to explore how gaps within otherwise continuous beds of emergent aquatic vegetation alter in-canopy horizontal flow patterns. Our findings indicate that gaps reroute and concentrate horizontal flow, creating areas of accelerated flows within the canopy. As gap size increases, horizontal flow speeds also increase, though the rate of increase diminishes as the gap size becomes larger. In cases with pairs of gaps, the maximum flow change within the canopy occurred at streamwise gap separations of 2 gap diameters. The increase in horizontal flow speeds was directly proportional to the percentage of bare bed cover. Moreover, for a specified percentage of bare bed cover, flow changes were also modulated by the fragmentation level, which is determined by the number and size of gaps. Fewer, larger gaps exerted a more pronounced impact on in-canopy horizontal flow speeds compared to numerous smaller gaps. The interconnected nature of vegetation coverage and gap distribution underlines the role of fragmentation levels in controlling in-canopy flow speeds and related ecohydrological dynamics.

3.1 Introduction

Aquatic vegetation such as marsh plants, seagrass and mangroves provides a variety of ecosystem services in coastal, fluvial, and lacustrine systems, including habitat provision, sediment stability, carbon storage, and shoreline protection (Bouma et al., 2009; Irving et al., 2011; Thomaz & Cunha, 2010). Often referred as ecosystem engineers, aquatic plants have the ability to regulate flow, which in turn shape landscapes (Cornacchia et al., 2016; Mullarney & Henderson, 2018; Norris et al., 2021). Drag resistance induced by aquatic canopies can reduce flow speeds, enhance sedimentation, and prevent erosion, thereby facilitating plant growth through stress reduced hydrodynamic stress and improved resource retention (Loidi, 2017).

In fragmented canopies, spatial variations in drag resistance at the interface between vegetated and unvegetated areas lead to flow deceleration within vegetation patches and flow acceleration in adjacent bare zones (Gambi et al., 1990; Schoelynck et al., 2012). Therefore, the fragmentation of aquatic canopies affects flow patterns and sediment dynamics, driving morphological transformation over time. Flow acceleration between bare gaps and patches of vegetation may enhance the transport and exchange of solutes at the edges of the vegetated patches, creating a positive feedback (Adhitya et al., 2016; Granata et al., 2001). However, depending on the intensity of flow acceleration, these faster flows can sometimes create a negative feedback by establishing an environment where plant recruitment and growth might be inhibited due to hydrodynamic stress and/or a reduction of resources (Bouma et al., 2013; Schoelynck et al., 2012). The interplay of these ecological processes can lead to changes in sediment deposition, and the formation of distinct topographic gradients within aquatic environments.

Different landscape patterns can be observed with varying levels of aquatic canopy fragmentation. The colonization of pioneer vegetation on riverine and coastal marine sediments often results in landscapes composed of isolated patches at a variety of spatial scales

(Schoelynck et al., 2012). However, relatively uniform meadows with isolated bare areas (hereafter called gaps) are also observed in aquatic landscapes (Folkard, 2019; Ruiz-Reynés et al., 2017; Swadling et al., 2023). Such mosaic-like patterns of alternating vegetated and unvegetated patches are commonly observed in seagrass meadows and salt marshes (Figure 3.1). This landscape pattern can be formed via multiple different mechanisms and at different spatial scales (Abadie et al., 2015; Larsen & Harvey, 2011; Montefalcone et al., 2010). In salt marsh systems for example, vegetation die-off may result in bare patches characterised by a shallow depression, commonly known as salt marsh pans, ponds or pools (Escapa et al., 2015; Reidenbaugh & Banta, 1980). Discontinuities in aquatic vegetation can also be a result of waterfowl herbivory (Dos Santos et al., 2013; Silliman et al., 2005; Van Der Heide et al., 2012), bioturbation from stingray feeding (Grew et al., 2024), differential growth or recruitment of vegetation (Bell, 1999; Boudouresque et al., 2009), or anthropogenic activities such as boating and mooring (Colomer et al., 2017; Sagerman et al., 2020).

Most past research dedicated to assessing the impacts of fragmentation of aquatic vegetation on hydrodynamics have focused on landscapes consisting of a bare matrix interspersed with vegetated patches (e.g., de Lima et al. 2015; Yamasaki et al. 2019; Licci et al. 2022). Although ecologically relevant, the hydrodynamic impacts of fragmentation caused by bare patches within aquatic canopies remain underexplored (Colomer & Serra, 2021; Folkard, 2019). The few existing studies have predominantly focused on the propagation of turbulent wakes developed at the gap edges, resulting from the interaction between the top of submerged canopies and the increased skimming overflow. Depending on the gap length and vegetation height, this turbulent wake eventually reaches the bed and induces sediment resuspension (Chung et al., 2021; Chung & Koseff, 2021; Hamed et al., 2020).

Figure 3.1: Fragmented intertidal seagrass meadow (*Zostera muelleri*) in Tauranga Harbour, New Zealand (reference coordinates: 37°28'56.67"S 175°57'1.40"E). The meadow is composed by a mosaic of bare gaps that remain waterlogged during low tide. (Photo credit: Tiago D. da Silva). Threats to seagrass meadows in Tauranga Harbour include waterfowl overgrazing, boating activities, mooring disturbances, and eutrophication.

Field observations have shown that bare gaps within seagrass meadows influence flow patterns at multiple spatial scales, leading to localized acceleration, enhanced dissipation of turbulent kinetic energy, and potential feedbacks that shape meadow structure (da Silva et al., 2024). These findings emphasize the role of spatial heterogeneity in modifying hydrodynamic conditions, which in turn can impact sediment transport, nutrient cycling, and seagrass resilience. The spatial influence of bare gaps on hydrodynamics extends beyond the immediate area of the gaps (Carr et al., 2016), and is dependent on the size, arrangement and density of vegetation (Maji et al., 2020; Schepers et al., 2017). However, the effects of such spatial heterogeneity are still insufficiently documented (Folkard, 2019; Tinoco et al., 2020), particularly in real aquatic ecosystems, where vegetation coverage exhibits complex patterns. Moreover, previous studies have predominantly undertaken experiments involving the

existence of either one or two transverse gaps (i.e., gaps spanning the entire width of the flume) (Chung et al., 2021; Ranjan et al., 2022).

This study presents a first-order investigation into how variations in landscape structure affect horizontal flow at a meadow scale, with a particular focus on the extent and configuration of bare patches within vegetated areas. To support this perspective, numerical modelling is employed as a tool to systematically isolate and analyse the effects of gap configurations on flow dynamics. This approach enables controlled exploration of fragmentation scenarios that are difficult to replicate in field or laboratory conditions. Accordingly, we use a depth-averaged numerical model to capture dominant patterns in horizontal flow while avoiding the computational demands of three-dimensional simulations. The model deliberately excludes vertical variability and small-scale turbulence, thereby emphasizing bulk changes in flow resulting from bare patches.

Landscape fragmentation was characterised using quantitative descriptors that reflect both the extent and spatial arrangement of bare areas, namely the total area occupied by bare gaps and their size and number (gap density). These metrics, which have been employed in previous studies to characterize vegetation structure and morphodynamics (Aranda et al., 2022; Hargis et al., 1998), provide a basis for assessing how gap-induced fragmentation influences flow dynamics in vegetated aquatic systems. Specifically, we examine configurations involving (1) single gaps of varying sizes, (2) pairs of gaps with varying sizes and separation distances, and (3) multiple gaps spanning different total unvegetated areas and spatial arrangements.

3.2 Methods

3.2.1 Validation of Delft3D rigid vegetation model (RVM)

The numerical simulations were carried out in a depth-averaged hydrodynamic model, implemented in the Delft3D modelling software using the non-linear shallow water equations,

assuming incompressible free surface flow. In this study we used the Rigid Vegetation Model (RVM) to simulate the effect of vegetation on the flow. This approach directly calculates the drag exerted on flow by aquatic vegetation, assuming the canopy is composed of rigid cylinders with a geometry specified by the user (Uittenbogaard, 2003). The drag exerted by the vegetation in the water column is included in the model as an additional resistance term (F, in N/m^3), calculated by the product between the density of the vegetation, represented by number of stems per unit area (n) and the diameter of each cylinder (d),

$$F = \frac{1}{2}\rho_0 C_d dn|\mathbf{U}|/H\,, \quad (1)$$

where ρ_0 is the water density (kg/m^3), C_d is the cylindrical resistance coefficient, $|\mathbf{U}|$ is the depth-averaged horizontal flow speed, and H is the water depth. More information about the hydrodynamic model implemented in Delft3D can be found in (Deltares, 2024). It is important to clarify that this method does not explicitly resolve individual rigid stems. Instead, the hydraulic influence of vegetation is represented through enhanced bottom friction and the inclusion of additional turbulence or momentum loss within the water column. Since a depth-averaged model was used, the additional resistance term accounting for the impact of plants on flow is applied uniformly throughout the water column, thus simulations are representative of emergent vegetation.

The RVM implemented in Delft3D has been previously calibrated and validated by comparison to field measurements in different types of vegetation, e.g., saltmarsh (Temmerman et al., 2005), seagrass (Bouma et al., 2007), and mangrove pneumatophores (Horstman et al., 2013). However, in these previous studies, the aquatic vegetation was not spatially fragmented. In order to verify the ability of the model to reproduce changes in flow across the transition between vegetated and non-vegetated areas, we validated the RVM using experimental data from (Vandenbruwaene et al., 2011), who investigated the interaction of unidirectional flow

with multiple vegetated patches in a flume. The calibration results and performance statistics indicate the model is capable of reproducing changes in the horizontal flow speeds over the transition between the vegetation and the bare patches (see Appendix E for details).

3.2.2 Model settings

Simulations were performed in a 50-m wide, 100-m long channel, with a 1-m mean water depth (Figure 3.2a). The grid resolution was 0.05 m (identical to the resolution used in the model validation – see Appendix E). We also applied the same values from the validation model for the horizontal eddy viscosity ($\nu_H = 0.002$ m^2/s^2) and the cylindrical resistance coefficient ($C_d = 1.0$). Flows were forced by a constant discharge (7.5 m^3/s) at the inflow boundary and a current speed (0.1 m/s) at the outlet open boundary. Flow speeds of order 0.1 m/s are consistent with values observed in natural salt marshes with emergent vegetation (Sullivan et al., 2015).

Vegetation was characterised by a stem density of 100 stems/m^2 and a stem diameter of 0.03 m, resulting in a frontal area per bed area of 3 m^{-1} and a Solid Plant Fraction (SPF) of 0.07, consistent with observed values for sparse vegetation (Mullarney & Henderson, 2018). Circular gaps were included in the domain by prescribing a plant density of 0 stems/m^2 in the gap locations. Each simulation was conducted for a total run time of 30 min, ensuring sufficient duration for flow adjustment within the domain, indicated by stable water levels and velocities. Flow was considered steady when water levels changed by less than 1 mm and depth-averaged velocities varied by less than 1% over the final 5 min of the simulation period.

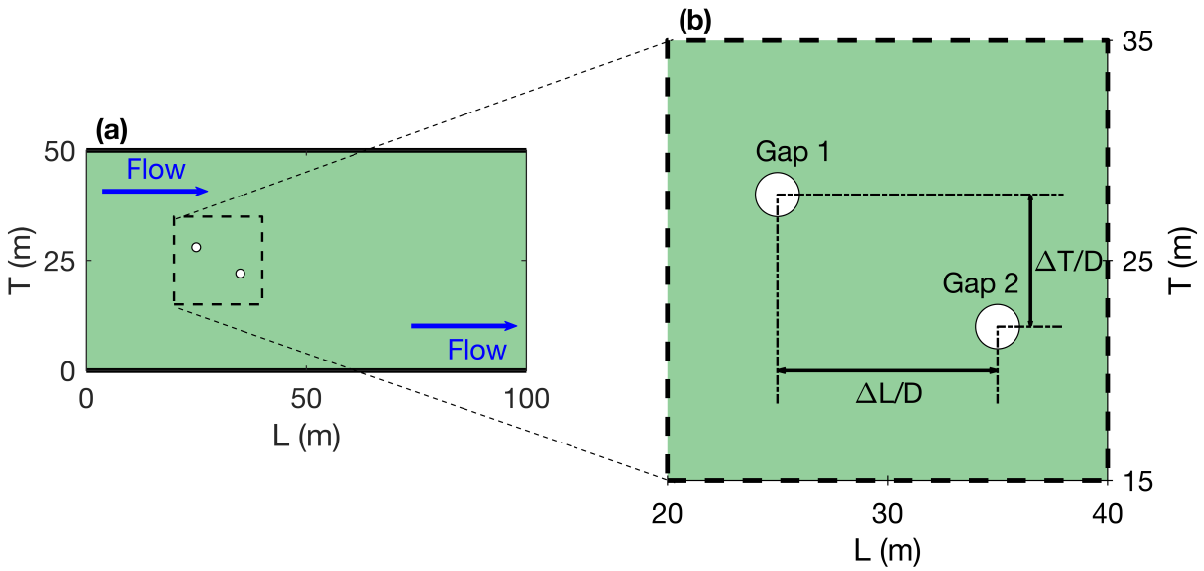

Figure 3.2: (a) Schematic of the model domain showing an example of a simulation with a pair of gaps and (b) a close-up view of the gaps indicating the longitudinal (ΔL/D) and transverse (ΔT/D) distances separating them (here gap diameter D = 2 m, ΔL/D = 10, ΔT/D = 6).

3.2.3 Simulations undertaken

The effect of gap size on horizontal flow was analysed by simulating flows around single gaps of 10 different diameters (D= 0.4, 1, 2, 3, 4, 5, 6, 7, 8 and 9 m). The gap was located at the centre of the channel in each simulation (L = 50 m and T = 25 m).

A second set of simulations with two gaps, each having the same diameter, was performed with gap diameters of D = 0.4, 1, 2, 3 and 4 m. Distances between gaps in the longitudinal (L) and transverse (T) directions measured from the gap centres were scaled by the gap diameters and denoted as ΔL/D and ΔT/D, respectively (Figure 3.2b). Simulations encompassed values of both ΔL/D and ΔT/D spanning from 0 to 10 with increments of 1, resulting in a total of 110 pairs of simulated ΔT/D and ΔL/D distances for each simulated gap diameter. Note that ΔL/D = ΔT/D = 0 corresponds to the limiting case of a single gap; and cases in which ΔL/D = 0 and ΔT/D = 1 or ΔL/D = 1 and ΔT/D = 0, correspond to gaps with direct contact at their borders.

A third series of simulations was designed to assess how gap configuration influences flow dynamics within the canopy. Specifically, the analysis focused on two main factors: coverage

levels (CL) and gap density (GD). Coverage levels were defined as the percentage of unvegetated (bare) area relative to the total domain area, calculated as $CL = (A_b / A_t) \times 100$, where A_b is the total bare area and A_t is the total channel area. Gap density (GD) was defined as the number of gaps per square meter (gaps/m^2), representing how densely gaps are distributed within the canopy. Gap configurations were characterized by the specific combination of gap size and number that produced a given coverage level. For a fixed coverage level, configurations with many small gaps correspond to greater gap density fragmentation, while fewer, larger gaps correspond to smaller gap density and reduced fragmentation. Likewise, for a fixed gap size, increasing bare bed coverage (CL) also results in more fragmented conditions. These relationships were used to examine how fragmentation influences flow dynamics within the canopy.

Simulations were conducted at five distinct coverage levels: 8%, 16%, 24%, 32%, and 40%. For each CL, five gap diameters (1, 3, 5, 7, and 9 m) were tested by adjusting the number of gaps accordingly to maintain a constant total bare area (Table 1). Gaps were randomly distributed within the central portion of the domain (from L = 11 to 89 m and T = 2 to 48 m), with a minimum distance of 2 m from the lateral walls and 11 m from the open boundaries. Overlapping gaps were not permitted, though edges could touch. For each combination of CL and GD, 10 simulations were conducted using different random gap placements, resulting in a total of 250 model simulations.

Table 3.1: Fragmentation metrics for the numerical simulations with multiple gaps. For each level of bare bed coverage (CL), gap configuration was varied by changing the gap diameter and number of gaps, resulting in different gap densities (GD). Five gap diameters (ranging from 1 to 9 m) were used to generate configurations ranging from many small gaps (high GD) to few large gaps (low GD), while maintaining the same CL. For each configuration, 10 simulations were performed with different randomly distributed gap arrangements (totalling 250 simulations). (a) Number of gaps required to achieve each CL for a given gap diameter (and corresponding gap area). (b) Gap density (GD, in gaps/m² × 10²) corresponding to each configuration.

(a)		**Number of gaps**				
Gap diameter (m)		**1**	**3**	**5**	**7**	**9**
Gap area (m^2)		**0.79**	**7.1**	**19.6**	**38.5**	**63.6**
Gap Coverage Level (CL):	**8%**	509	57	20	10	6
	16%	1019	113	41	21	13
	24%	1528	170	61	31	19
	32%	2037	226	81	42	25
	40%	2546	283	102	52	31
(b)		**Gap density (GD, gaps/$m^2 \times 10^2$)**				
Gap Coverage Level (CL):	**8%**	10.2	1.1	0.4	0.2	0.1
	16%	20.4	2.3	0.8	0.4	0.3
	24%	30.6	3.4	1.2	0.6	0.4
	32%	40.7	4.5	1.6	0.8	0.5
	40%	50.9	5.7	2.0	1.0	0.6

3.2.4 Parametrization of changes in mean flow

To derive a simple proxy for summarizing changes in horizontal flow caused by the presence of gaps in the model domain of uniform aquatic vegetation, we normalised the depth-averaged horizontal flow speeds (|**U**|) in simulations with gaps by the speeds from a simulation without any gap in the domain (fully vegetated case). This spatially resolved dimensionless parameter was denoted Normalised Flow Change Index (NFCI) and is calculated from:

$$\mathrm{NFCI_i} = \frac{|\mathbf{U}|_{\mathrm{Gap_i}}}{|\mathbf{U}|_{\mathrm{NoGap_i}}} - 1, \qquad (2)$$

where $|\mathbf{U}| = \sqrt{u^2 + v^2}$ (where u and v are longitudinal and transverse channel velocities, respectively) and i denotes the i_{th} cell in the model domain. Thus, a value of NFCI=0 indicates no change from the fully vegetated case.

Aiming to enhance the understanding of the potential effect of gaps on aquatic canopies, we focus on the potential negative feedback resulting from the interaction between gaps and flow, namely, the impact of flow acceleration (i.e. positive changes in the NFCI). Here, we define a threshold value of NFCI ≥ 0.05, which represents increases greater than 5% than the flow speed relative to the fully vegetated scenario in a given grid cell. The 5% threshold for NFCI is chosen to exclude areas where flow velocity changes are essentially noise.

We also define a bulk dimensionless index to quantify flow acceleration (BFI – Bulk Flow Intensification) over the whole modelling domain, which accounts for both the magnitude of changes on mean flow (NFCI) and spatial distribution of these changes:

$$BFI_n = \sum_{\forall i \text{ s.t. } NFCI_i \geq 0.05}^{\max(NFCI_i)} NFCI_i * A_{c_i}, \quad (3)$$

where A_{c_i} is the area of the i_{th} cell in the domain, and n is the n_{th} simulation. BFI thus represents a flow-weighted effective area (in m^2), integrating regions where flow speeds surpass a reference condition (NFCI ≥ 0.05). When normalized by the total bare area (A_b), BFI provides a relative measure of flow intensification per unit of bare area, enabling comparison across different fragmentation levels.

For simulations with varying gap densities across different total bare bed coverage levels, we also compared the modelled flow fields to literature derived sediment transport thresholds. Specifically, we evaluated the occurrence of flow speeds exceeding the 0.24 m/s threshold for fine sand mobilization on bare beds (Van Veelen et al., 2025) and those falling below the 0.05 m/s threshold for fine sand deposition (de Lima et al., 2015). Given the 0.1 m/s currents

prescribed in the model, these thresholds correspond to NFCI values of 1.4 and -0.5, respectively.

3.3 Results

3.3.1 Effect of a single gap of varying size

For all gap sizes ($D \geq 0.4$ m), the flow patterns arising from the presence of a single gap are similar (Figure 3.3). The horizontal flow is deflected and accelerated longitudinally towards the gap opening, while lobes of reduced speeds form at the lateral edges of the gap. As gap sizes increase from 0.4 to 2 m, the flow changes are indicated by a distinct increase in NFCI within the gap. However, for larger gaps sizes (> 3m), no further increases in NFCI are observed.

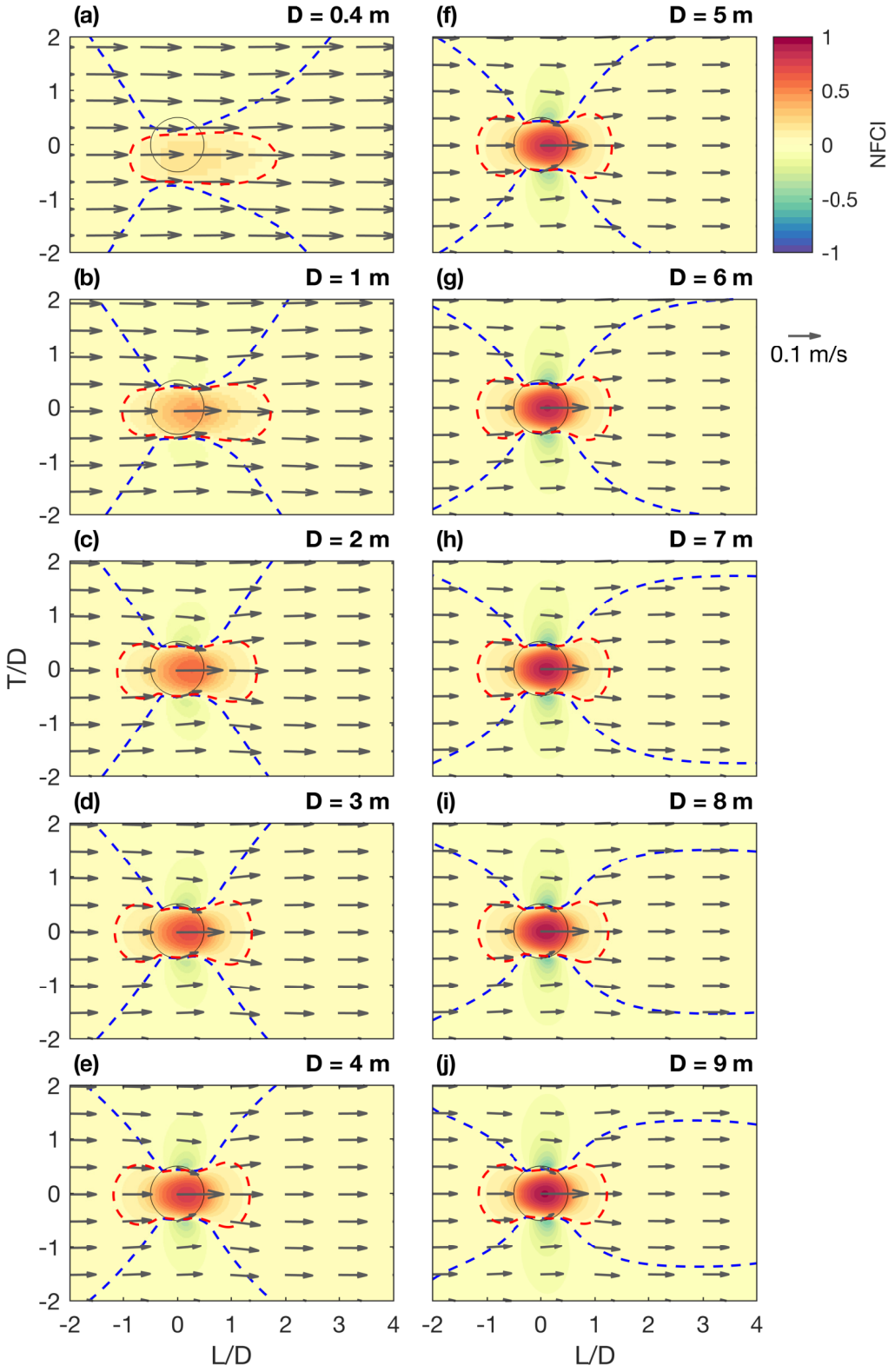

Figure 3.3: Changes in horizontal flow patterns around single gaps of different diameters (D, from e to j), represented by the Normalised Index of Flow Change (NFCI). Arrows show the depth-averaged horizontal velocities **U**. As gap size varied by one order of magnitude, for the sake of visualization, the figures were scaled to a standard size. Black lines show the gap outline, blue and red dashed contours are isolines of NFCI = 0 and 0.05, respectively. L = Longitudinal distance, T = Transverse distance.

Figure 3.4a illustrates how gap size directly impacts the acceleration of horizontal flow, as indicated by the intensification of flow speeds (NFCI ≥ 0.05) along the channel centreline. These longitudinal profiles show that the maximum flow speed occurs near the centre of the gap for larger gaps, while for smaller gaps, the maximum speed is found further downstream (but still within the gap). The relationship between gap size and flow acceleration follows a logarithmic trend, where maximum NFCI increases with gap diameter but at a decreasing rate. The model indicates that gap size alone explains over 99% of the variation in maximum flow speed within the gap ($r^2 > 0.99$), as shown in Figure 3.4b. For gap diameters larger than approximately 4–5 m, the rate of increase in maximum NFCI slows considerably, indicating that further widening of gaps has a diminishing effect on flow enhancement. This result suggests that gap enlargement primarily alters flow distribution rather than continuing to accelerate along-gap flow indefinitely.

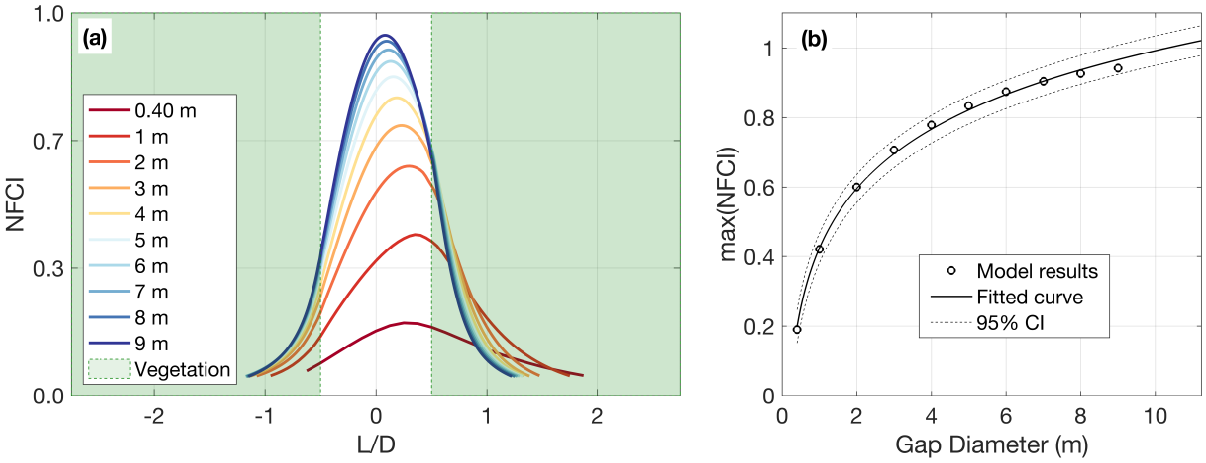

Figure 3.4: (a) Normalised index of flow change (NFCI) for different single gap diameters along the centre longitudinal channel section (T = 25 m) as a function of scaled distances. L/D = 0 at the centre of the gaps (L = 25 m). In this plot, only NFCI ≥ 0.05 is shown. (b) Maximum NFCI found within each gap diameter and the fitted logarithmic curve ($y = 0.43 + 0.25 \log_{10}(x)$, $r^2 = 0.99$ and RMSE = 0.01). L = Longitudinal distance, T = Transverse distance.

3.3.2 Flow interactions of a pair of gaps of varying sizes at different scaled distances

Figure 3.5a and b show an example (for D = 4 m) of the connections of the wake regions when gaps are aligned respectively in the longitudinal and transverse directions. The interconnection

of the zones with flow change is not observed when the gaps are not aligned (Figure 3.5c). When gaps are longitudinally aligned, hydraulic interaction is a result of the interconnection of streamwise zones of accelerated flow. Conversely, the hydraulic interaction of gaps placed transversally arises from the interconnection of the lateral lobes of reduced flow speeds formed across the sides of each gap.

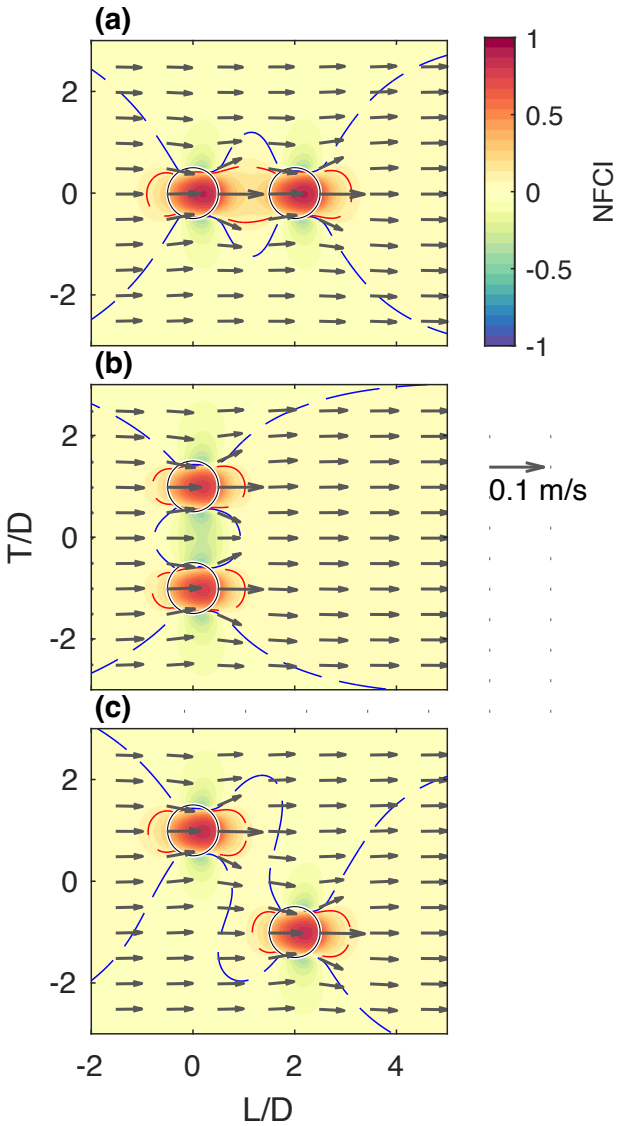

Figure 3.5: Flow changes within and around a pair of gaps for; (a) staggered gaps (ΔL/D = 2, ΔT/D = 0), (b) side-by-side gaps (ΔL/D = 0, ΔT/D = 2) and (c) when gaps are not staggered or side-by-side (ΔL/D = 2, ΔT/D = 2). The gaps shown have a diameter of 4 m. Grey lines show the gap boundaries, red and blue dashed contours represent NFCI = 0 and 0.05 isolines, respectively. L = Longitudinal distance, T = Transverse distance.

To better evaluate changes in flows resulting from the hydraulic interaction between two gaps at varying spacing within the domain, Figure 3.6 shows the maximum NFCI (panels a-e), the total area where NFCI ≥ 0.05 normalised by $2\times A_{gap}$ (panels f-j), and the bulk flow changes (shown by BFI) for each simulation (panels j-o), as a function of scaled separation distances (L/D and T/D). These parameters serve as indicators of the intensity and spatial extent of accelerated flow and their combined effect, as represented by the BFI.

The greatest levels of flow intensification resulting from the interaction between the pair of gaps occur when the gaps are aligned in the longitudinal direction ($\Delta T/D = 0$), particularly at shorter separation distances ($\Delta L/D < 3$). Conversely, less pronounced flow acceleration is observed when the gaps are positioned side by side ($\Delta L/D = 0$). These patterns are observed for both the magnitude of flow concentration (maximum NFCI), and the area of flow change (and summarized by the BFI), irrespective of the gap size.

When comparing parameter values across various gap sizes, it becomes apparent that smaller gaps yield small relative changes in flow, while larger gaps cause larger relative changes in flow speeds, as in the case with a single gap. However, the area over which flows are changed (second row) is relatively insensitive to the gap size, with maximum values of around 3.75 times larger than the area of the gaps in all cases (at $\Delta L/D = 3$ and $\Delta T/D = 0$). Greater BFI values are observed when the gaps are staggered at distances where $\Delta T/D = 0$ and $\Delta L/D = 2$, indicating that this configuration of gaps resulted in greatest changes in flow within the full domain.

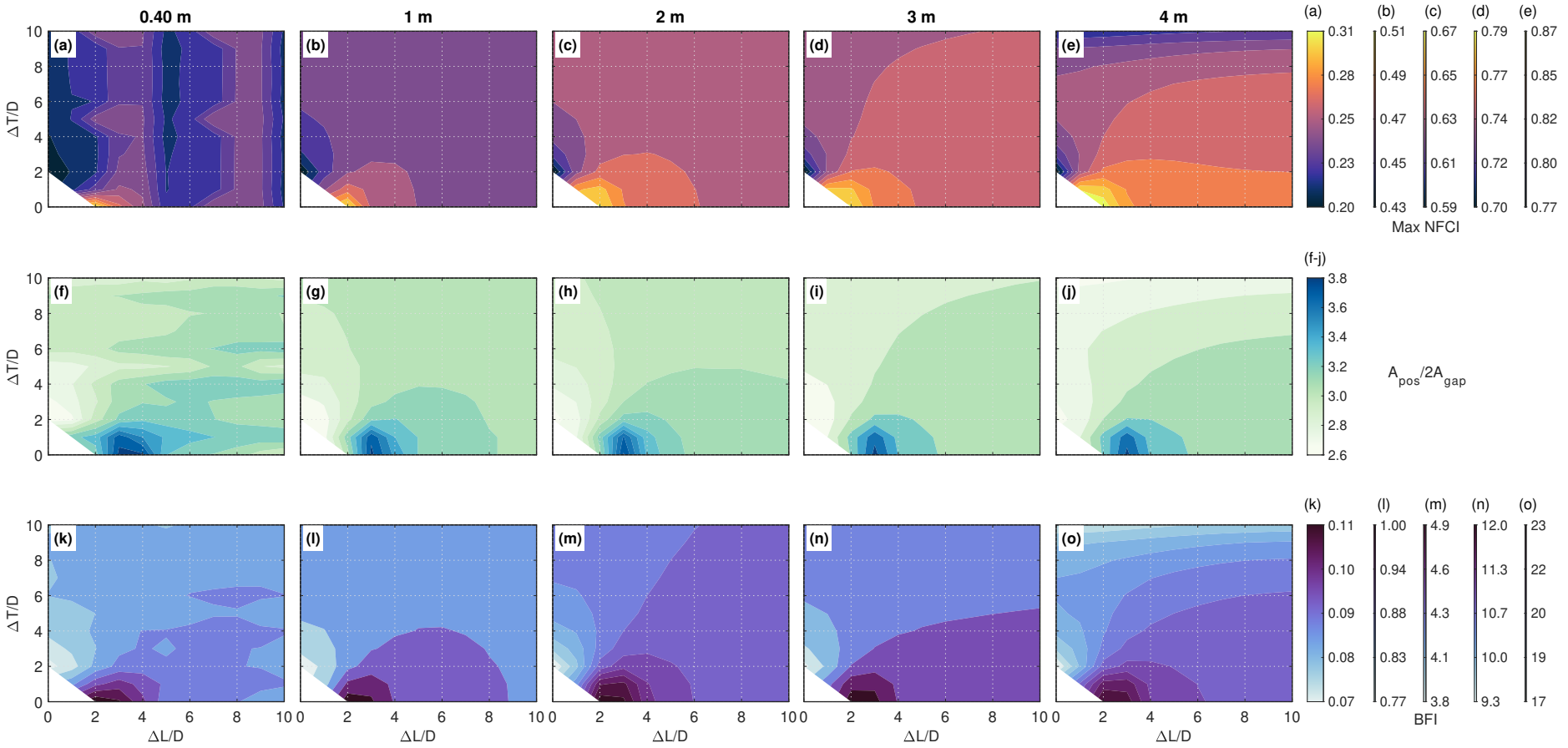

Figure 3.6: Flow change parameters as a function of the inter-gap scaled distances for different gap sizes (columns). (a-e) maximum Normalised Flow Change Index (NFCI) observed across the domain; (f-j) ratio of the area within the domain where NFCI ≥ 0.05 and the area of the gaps; (k-o) Bulk Flow Intensification Index (BFI). Note in each case the two gaps are of the same size. L = Longitudinal distance, T = Transverse distance. The white triangle in the bottom left of each panel corresponds to situations in which gaps are overlapping which were not permitted.

3.3.3 Flow interactions with multiple gaps of varying sizes at different levels of fragmentation

The probability density functions (PDFs) of the Normalised Flow Change Index (NFCI, Figure 3.7) illustrate the variation in flow conditions across different fragmentation levels, defined by the combined effects of gap density (GD) and bare bed coverage (CL). Overall, across all simulated coverage levels, configurations with fewer, larger gaps, corresponding to lower gap densities, produce a wider range of flow modifications, resulting in more pronounced flow heterogeneity within the domain.

At the lowest bare bed coverage level (CL = 8%, panel a), the distributions exhibit a pronounced peak near NFCI = 0, indicating minimal flow alteration across most of the domain. However, the spread of the distributions varies with gap density. Higher GD (smaller, more numerous gaps) yields a narrower distribution centred around zero, while lower GD (fewer, larger gaps) results in a broader range of NFCI values.

As CL increases (from 16% to 32%, panels b–d), the distributions shift progressively toward higher NFCI values, indicating a greater likelihood of intense flow acceleration and erosion-prone conditions. This trend is most pronounced in configurations with fewer, larger gaps, where the right tail of the distribution extends further, reflecting localised intensification of flow. In contrast, configurations with smaller, more numerous gaps show higher probability densities at lower NFCI values (NFCI < –0.5), especially at lower CL, indicating more frequent flow deceleration and increased potential for sediment deposition.

At the highest bare bed coverage (CL = 40%, panel e), the distributions become more dispersed, demonstrating increased spatial variability in flow conditions. Configurations with fewer, larger gaps resulted in a marked shift toward higher NFCI values, with the occurrence of intensified flow acceleration and a greater potential for bed erosion under low-gap-density

conditions. Conversely, configurations with smaller, more numerous gaps yield more symmetrical distributions, consistent with a dampening effect on flow variability.

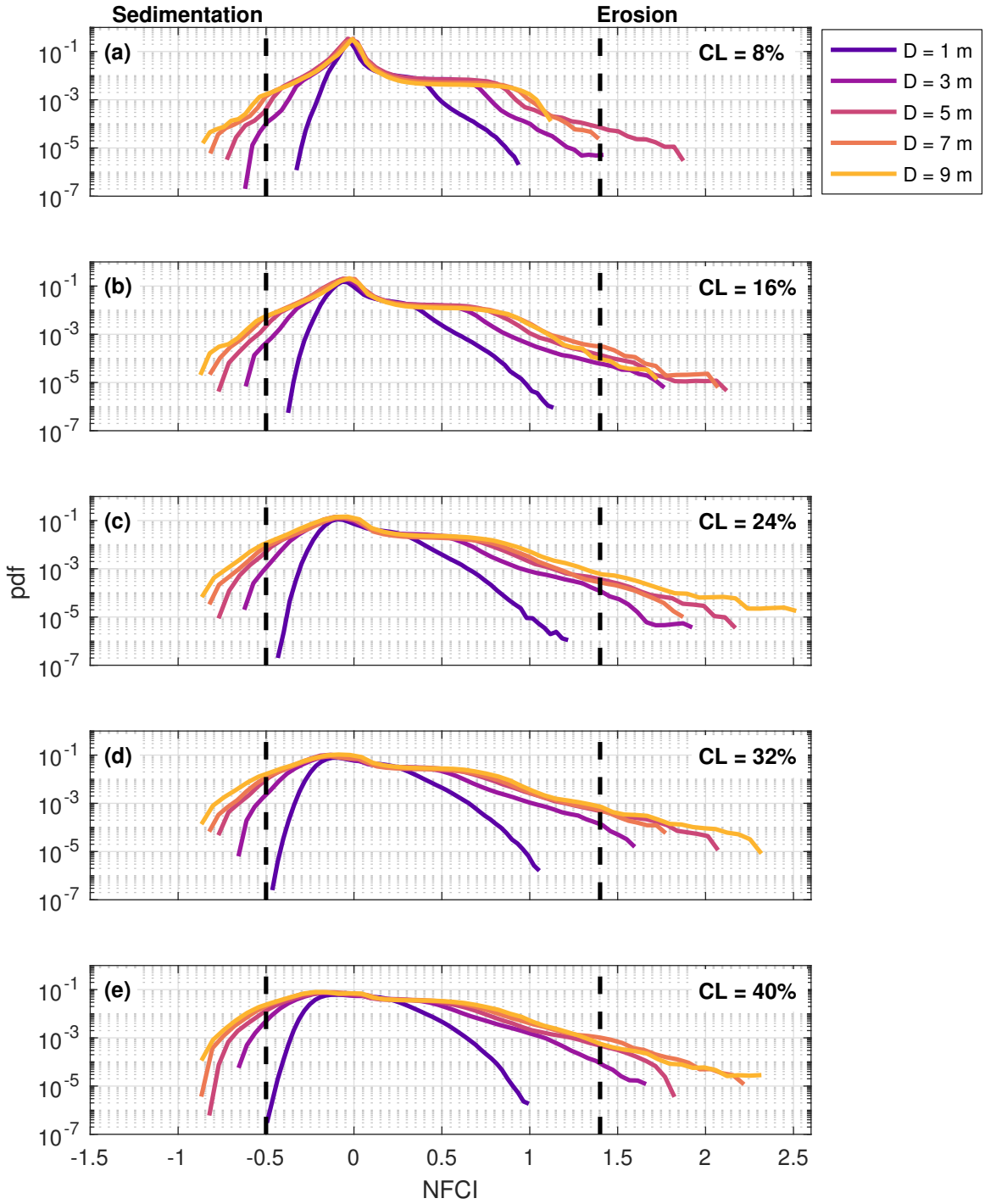

Figure 3.7: Histograms showing the probability distribution function (pdf) of the Normalised Flow Change Index (NFCI) across different gap configurations, defined by gap diameter (m), for each bare bed coverage level (CL, panels a–b). The probability density function (pdf) represents the aggregated NFCI values from 10 simulations with randomly placed gaps for each configuration. Vertical dashed lines indicate thresholds associated with sedimentation (left) and erosion (right) regimes. For the corresponding gap density associated with each CL and gap diameter, refer to Table 3.1.

The colormaps in Figure 3.8 illustrate the spatial distribution of the Normalized Flow Change Index (NFCI) across the different CL and GD simulated. At smaller bare bed coverage levels (CL = 8%, panel a), the NFCI field remains relatively uniform, with only minor variations in flow change surrounding the smaller gaps (D = 1 m). The weak NFCI gradients indicate that flow modifications are minimal, with no widespread acceleration or deceleration zones. As the area occupied by the gaps increase (CL = 16% to 40%, panels b–c), the NFCI field becomes increasingly heterogeneous, with regions of flow acceleration (red) and deceleration (blue) developing within around individual gaps, respectively. Lower gap density scenarios, with larger, fewer gaps (D ≥ 5m) exhibit more pronounced NFCI gradients, particularly at CL = 32% (panel d), where flow acceleration extends downstream of the gaps while recirculating zones of reduced NFCI form along their peripheries.

At greater bare bed coverage levels (CL = 40%, panel e), the colormaps reveal a transition from isolated flow disturbances to a more interconnected pattern of flow modification. The red zones surrounding gaps become more widespread and begin to merge, forming elongated regions of increased flow, while the blue zones become more concentrated in narrow regions along gap edges. These flow patterns emphasize that when gaps are larger and more numerous, the canopy no longer provides continuous resistance to flow, leading to more extensive flow acceleration across the domain. The strengthening of high NFCI regions with increasing CL illustrates the trends observed in the probability density functions (**Error! Reference source not found.**), where the likelihood of erosion-prone conditions rises with both CL and GD.

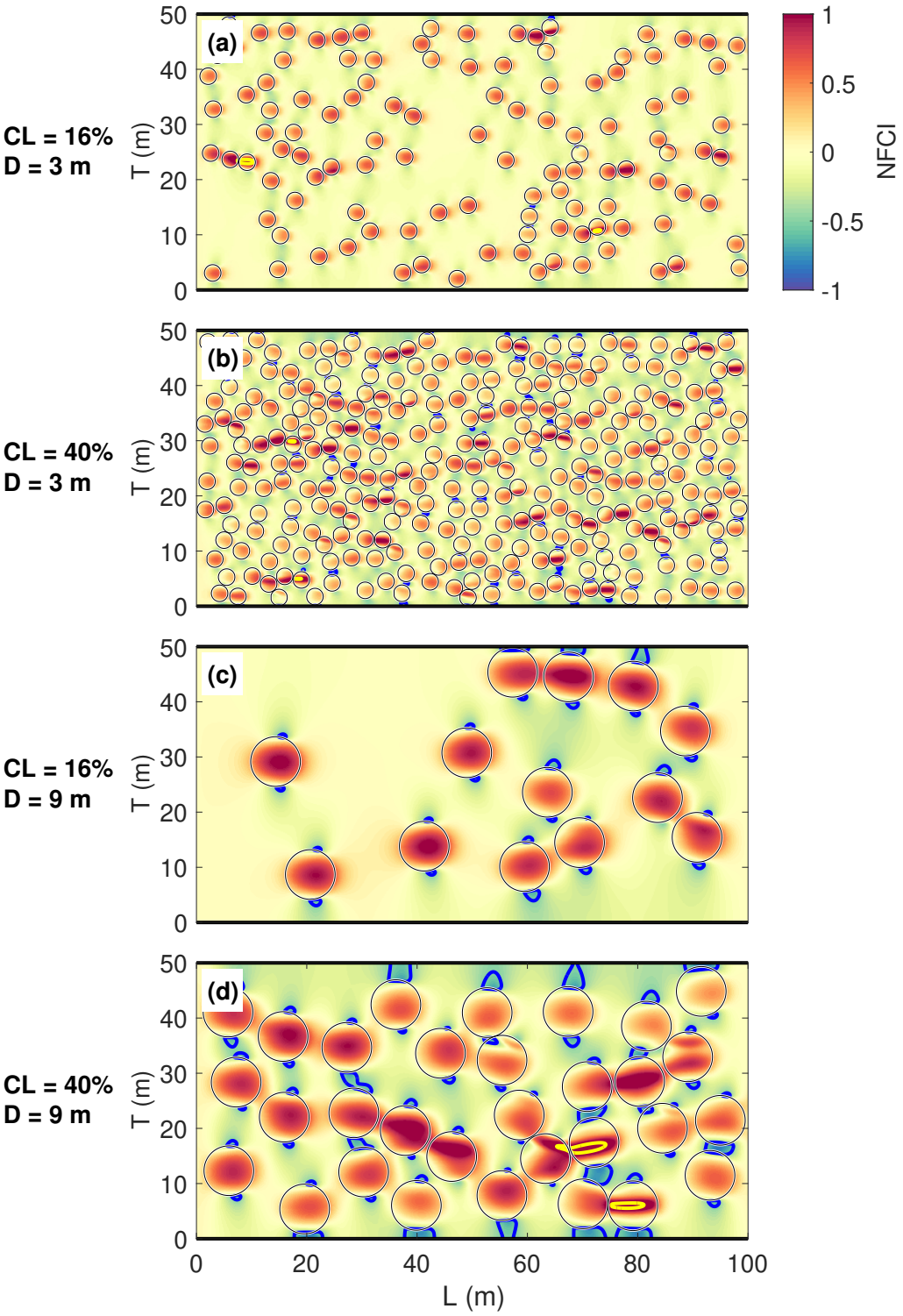

Figure 3.8: Normalized flow change index (NFCI) across two different total bare bed coverage and gap configurations. Panels (a) and (b) correspond to gap configurations with 3 m diameter gaps with 16% and 40% bare bed coverage, respectively. Panels (c) and (d) correspond to gap configurations with 9 m diameter gaps with 16% and 40% coverage. Positive NFCI values (red) indicate flow acceleration relative to the reference (no-gap) condition, while negative values (blue) indicate flow deceleration. Black circles denote gap locations. Blue and yellow contours highlight regions exceeding sedimentation and erosion thresholds (NFCI < –0.5 and NFCI > 1.38), respectively.

The relationship between gap density and the relative flow intensification per unit of bare bed area (expressed as BFI/A_b, Figure 3.9) shows that configurations composed of many small gaps (i.e., high gap density) are associated with reduced BFI/A_b, indicating a smaller effective area where flow is intensified. In contrast, configurations with fewer, larger gaps (i.e., low gap density) yield higher BFI/A_b values. This pattern is consistent across all tested bare bed coverage levels (CL). Notably, the rate of decline in BFI/Ab with increasing gap density remains approximately consistent across all simulated bare bed coverage levels, as indicated by the similar slopes of the curves.

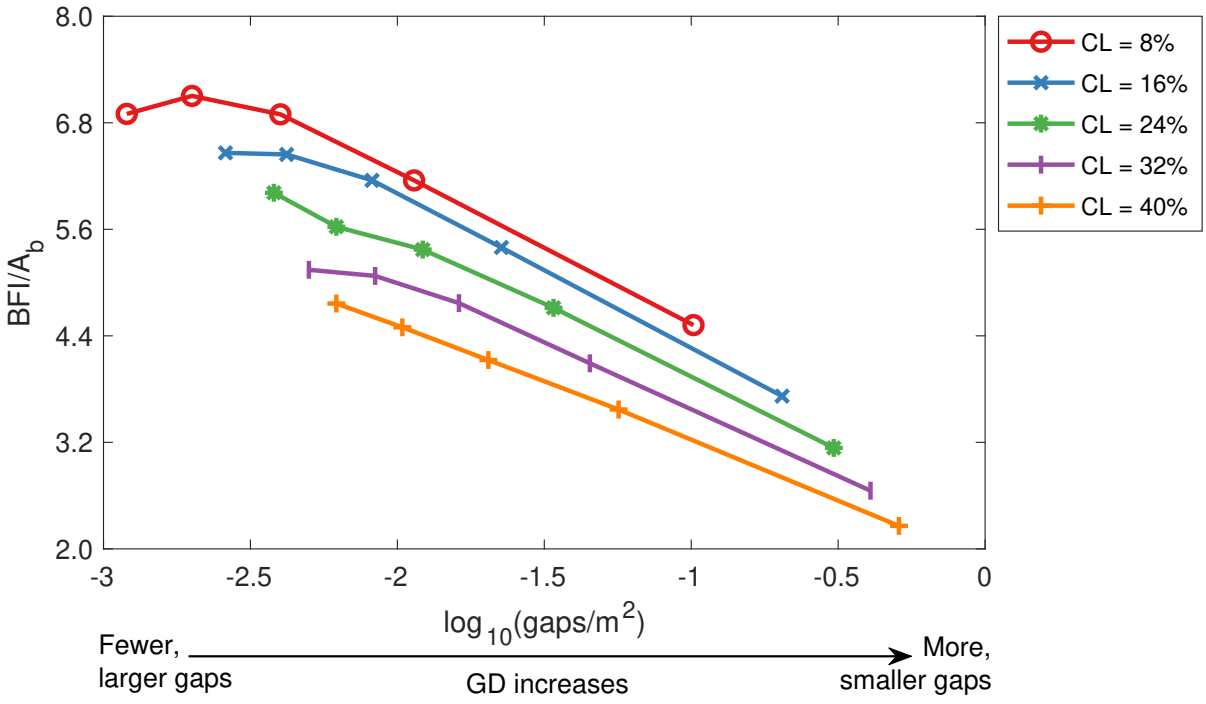

Figure 3.9: Bulk Flow Intensification Index (BFI) normalized by the total bare bed area (A_b) as a function of gap density (GD) across fixed bare bed coverage levels (CL).

3.4 Discussion

Although this study employs a simplified, depth-averaged modelling framework, the results provide a novel mechanistic baseline for understanding how fragmentation induced by bare gaps alters horizontal flow within emergent vegetated canopies. Despite their limitations, the simulations demonstrated how flow redistribution within fragmented canopies is modulated by gap size, inter-gap spacing, and overall fragmentation levels. Flow patterns around a single gap

remain consistent across varying gap sizes, with accelerated flow concentrated within the gap. Although flow acceleration in bare gaps is well established (Schepers et al., 2020), our simulations show that this acceleration also reduces lateral flow at the edges of the gap, a feature not captured in previous flume studies but consistent with field observations (da Silva et al., 2024). The logarithmic increase in maximum flow speed with gap size shows that while widening of a single gap can enhance flow, this effect plateaus beyond gaps with diameters of 4–5 m (Figure 3.4b). As the bare gap occupies a larger proportion of the domain, the influence on horizontal flow diminishes due to the fixed input flow rate and the consequent reduction in the pressure gradient, which is the primary driver of momentum under the assumed flat-bed conditions (Peterson et al., 2004).

Two distinct interaction modes between gaps were identified, each influencing flow redistribution. Side-by-side gaps divide the incoming flow between them, reducing acceleration within individual gaps and promoting a more uniform flow distribution across the meadow. In contrast, gaps aligned with the flow direction reinforce the influence of one gap on the other, concentrating momentum and directing flow along narrow corridors. Both interaction modes operate over short spatial scales, on the order of two gap diameters (Figure 3.6), as longer stretches of vegetation between gaps dissipates flow wakes and prevents merging. The canopy surrounding bare gaps acts as a momentum sink, limiting the propagation of accelerated flow and preventing hydraulic connectivity from extending over large distances. These short-scale interactions differ from those observed in bare landscapes with vegetated patches (de Lima et al., 2015; Yamasaki et al., 2019), where wake interactions can persist over broader spatial scales.

The results consistently show that fragmentation into fewer, larger gaps, rather than numerous, smaller gaps result in stronger flow alterations in intra-meadow flow. Larger gaps create direct pathways for momentum transfer, reducing flow resistance, while numerous smaller gaps

distribute flow acceleration across a broader area, leading to weaker overall flow changes. At larger bare bed coverage levels (CL ≥ 32%, Figure 3.7**Error! Reference source not found.**, p anel d-e), increasing gap proximity funnels flow into distinct channels, forming preferential pathways (Figure 3.8). This transition results in a patchwork of accelerated and reduced flow zones.

Preferential flow pathways within vegetated aquatic environments influence key ecosystem processes by enhancing water exchange, promoting nutrient transport, and facilitating oxygen renewal and propagule dispersal (Gaylord et al., 2006; Granata et al., 2001; Kaller et al., 2015). These pathways can increase flushing and connectivity in fragmented meadows, improving water quality. However, the simulations showed that areas adjacent to accelerated flow corridors can exhibit reduced velocities, which in turn may lead to reduced mixing and water renewal (Hurd, 2000; Lightbody et al., 2008). The spatial configuration of gaps modulates these outcomes, with closely spaced gaps strengthening hydraulic connectivity and enhancing flushing efficiency. In contrast, widely spaced gaps reduce flow continuity across the canopy, leading to zones of low flow exchange within vegetated areas and limiting their connection to the main transport pathways. Percolation theory suggests that continuous hydraulic networks develop when the fraction of open area surpasses a critical threshold, typically around 60% coverage (Luhar et al., 2008). Nonetheless, the present results demonstrate that coherent preferential pathways can form even below this threshold, particularly when gap alignment and clustering enhance directional flow organization.

Overall, the results indicate that the spatial orientation of fragmentation features influences hydrodynamic connectivity, which may contribute to longer-term morphological change. However, the simulations also indicate that the capacity of bare gaps to mobilize sediment is limited under most conditions, suggesting that any resulting morphological adjustments are likely to be gradual. It is noteworthy that neither single gaps nor pairs of gaps produced flow

speeds exceeding the erosion threshold defined in this study (see maximum NFCI for single gaps in Figure 3.4 and for pairs of gaps in Figure 3.6, panels a-e). For smaller gaps (1 m in diameter), flow conditions remained within an intermediate range that allowed sediment to be transported without being resuspended or deposited. At low bare bed coverage (CL = 8%), only 5 m diameter gaps had flow speeds reaching the sediment mobilization threshold (Figure 3.7a). When CL reached 16%, most gap configurations exceeded this threshold, implying potential for scour within gap (Figure 3.7b to e).

While flow speeds exceeding erosion thresholds or falling below sedimentation thresholds were confined to a small portion of the modelling domain (see the yellow lines in Figure 3.8, panels c–e), the simulations suggest that localized erosion may still occur within flow-aligned gaps. However, the limited spatial extent of these conditions indicates that sediment transport and morphological changes under typical flow scenarios are likely to occur at slow rates. The potentially gradual nature of these changes as indicated by the simulations is consistent with observations in ecosystems such as saltmarshes, where the morphological development of bare gaps has been shown to unfold over extended timescales (Mariotti et al., 2020). In Figure 3.10, an aerial image of a saltmarsh meadow reveals elongated, parallel channelized gaps, resembling the flow-driven patterns depicted in Figure 3.8. This similarity suggests that the preferential flow acceleration pathways along gaps, as observed in the simulations, could contribute to the elongation and alignment of bare patches in saltmarsh environments.

In wave-driven canopies, fragmentation also modifies canopy structure and hydrodynamic sheltering. Laboratory studies on submerged flexible canopies (El Allaoui et al., 2016) have shown that larger gaps can lead to increased orbital flow velocities and greater turbulent energy levels. Although the magnitude, vertical structure, and spatial extent of flow–canopy interactions may vary under wave forcing, along with associated patterns of erosion and sediment transport, some parallels in the spatial feedbacks between canopy discontinuities and

local hydrodynamics have been observed across flow regimes. These similarities indicate that certain elements of the conceptual framework developed here may be applicable to other types of aquatic vegetation and hydrodynamic conditions, particularly regarding how fragmentation modifies flow exposure.

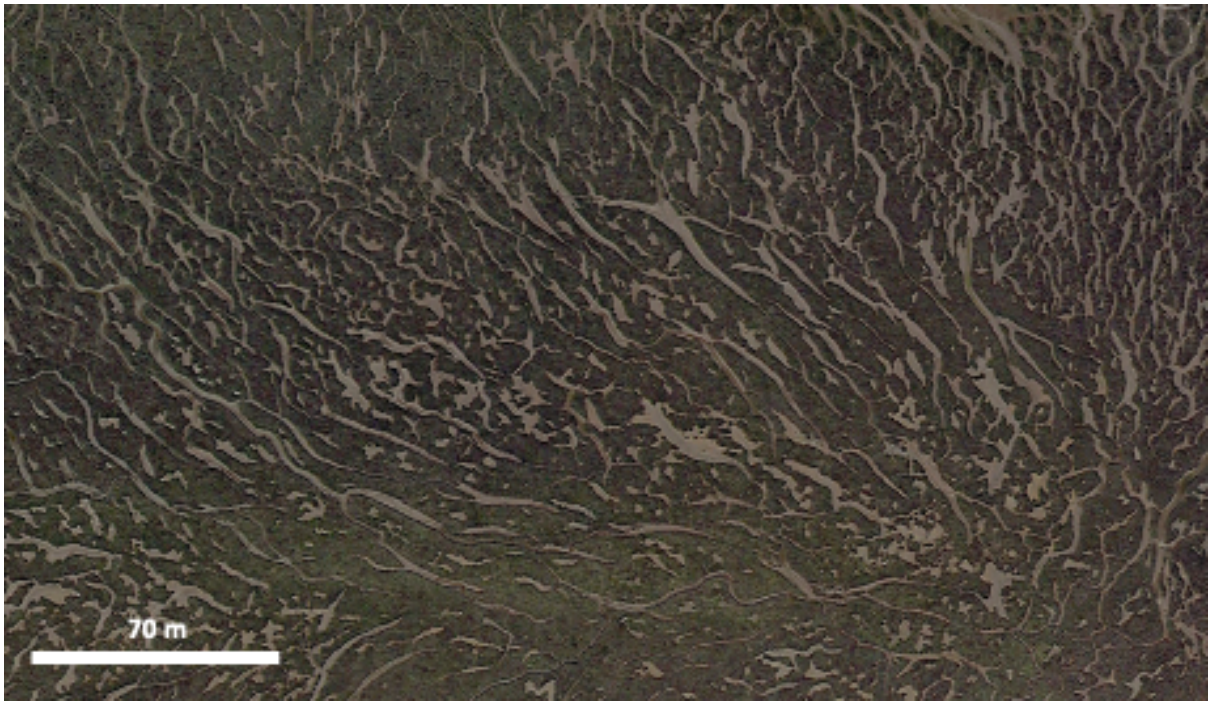

Figure 3.10: Elongated gaps of vegetation in the *Salicornia* salt marsh flats at Hooge Platen, Western Scheldt Estuary, Netherlands (reference coordinates: 51º23'11.04"N 3º40'51.46"E). The spatial patterns noticed in the salt marsh resemble those identified in the simulations, with bare areas positioned longitudinally in the direction of flow. Source: Google Earth.

The more pronounced flow modifications observed in scenarios with fewer, larger gaps in the modelling domain have important implications for management of vegetated aquatic ecosystems. Stressors that create bare gaps, such as anchor damage, mooring scars, or herbivory, are often concentrated in specific areas, resulting in closely spaced gaps (Dos Santos et al., 2013; Swadling et al., 2023). As demonstrated in our simulations, this spatial clustering can amplify the effects of bare gaps on intra-meadow flow dynamics, potentially accelerating habitat fragmentation. Thus, targeted management strategies should aim to minimize gap clustering, to reduce localized flow acceleration and preserve stable hydrodynamic conditions within the meadow. Building on this mechanistic understanding, future studies should

incorporate three-dimensional flow dynamics, vegetation flexibility, and bidirectional tidal forcing to capture the full range of gap–flow–sediment interactions. Advancing this framework will support more accurate predictions of flow–vegetation interactions and contribute to the development of effective strategies for managing and restoring fragmented aquatic ecosystems.

3.5 Conclusions

This study investigates the relationship between bare gaps and flow dynamics within relatively uniform emergent aquatic vegetation. Numerical simulations demonstrate that gaps in continuous vegetation modify horizontal flow by redirecting and concentrating momentum, thereby intensifying flow-related impacts. Notably, hydraulic interactions between adjacent gaps were only observed at small inter-gap distances. Moreover, flow redistribution is influenced not only by the extent of bare bed area but also by the spatial configuration of gaps. While localized erosion may occur in constrained areas within flow-aligned gaps at higher bare bed coverage levels with configurations involving larger and fewer gaps. However, most conditions remained below sediment mobilization thresholds, indicating a tendency toward gradual morphological change. These findings point to the need to minimize gap clustering and to account for gap size, spacing, and alignment when designing conservation and management strategies for vegetated aquatic ecosystems.

Chapter 4: The influence of topography and sediment composition on habitat suitability and patchiness of temperate shortleaf seagrass

Contribution of authors

Chapter 4 reproduces the paper titled “The influence of topography and sediment composition on habitat suitability and patchiness of temperate shortleaf seagrass,” authored by Tiago D. da Silva, Julia C. Mullarney, Conrad A. Pilditch, and Giovanni Coco, intended for submission to *Science of the Total Environment*. I processed all the geospatial data, developed the Python scripts for the machine-learning models, and contributed to both the initial and subsequent drafts. My co-authors, Julia C. Mullarney, Conrad A. Pilditch, and Giovanni Coco, provided editorial support, guidance, and valuable feedback throughout the drafting process.

Abstract

Seagrass habitats are increasingly threatened by anthropogenic and climate-related stressors, making it essential to understand the factors influencing their extent, patchiness, and biomass to inform effective management and conservation strategies. This study explores the relationship between environmental variables and the intertidal distribution of *Zostera muelleri*, a temperate shortleaf seagrass species, in Tauranga Harbour, New Zealand. Using Random Forest species distribution models, the influence of twenty topographic and substrate variables on seagrass habitat suitability was assessed across a large (~240 km²), predominantly intertidal (~60%) barrier island lagoon. The models showed strong predictive performance, with a mean area under the curve (AUC), a measure of model accuracy, of 0.84. Elevation emerged as the most significant factor (mean importance score = 0.29), followed by sediment composition (mean importance score = 0.17 to 0.22), while other topographic variables had a lesser impact (mean importance score < 0.17). Suitable habitats were mostly located in sandy areas near mean sea level, within a narrow optimal elevation range. The study also revealed that broad-scale patchiness (minimum patch size = 0.1 ha) was significantly influenced by these environmental factors, with seagrass forming smaller, clustered patches in areas of lower habitat suitability, where patches also exhibited a higher presence of bare gaps. The findings suggest plant-substrate feedback mechanisms, emphasizing the importance of considering both large-scale distribution patterns and broader-scale patchiness in developing targeted seagrass conservation and restoration efforts.

4.1 Introduction

Seagrasses form valuable coastal environments that provide essential ecosystem services such as habitat provision, nutrient cycling, and carbon sequestration (Orth et al., 2006; Waycott et al., 2009). However, these plants face significant threats from coastal development, pollution, and climate change, resulting in meadow degradation and loss (Short et al., 2011). Consequently, there has been an increased effort to identify the factors that make coastal areas suitable for seagrass development globally (Bertelli et al., 2022).

Machine-learning algorithms have emerged as powerful tools in species distribution modelling (SDM) to predict the spatial distributions of species based on environmental variables. SDMs assume that the environmental conditions allowing a species to survive and reproduce determine the spatial distribution of that species (Grinnell, 1917; Wiens et al., 2009). These models are fundamental for conservation planning, biodiversity assessments, and understanding species-environment relationships (Guisan & Thuiller, 2005).

Chapters 2 and 3 demonstrated that flow variability across vegetated and unvegetated areas is closely linked to spatial configuration and patch distribution of vegetation, influencing turbulence, flow acceleration, and potentially sediment transport (da Silva et al., 2024). It is worth noting that these hydrodynamic interactions are indirectly imprinted on the seabed, as reflected in topographic gradients and sediment composition, which in turn shape habitat conditions such as light availability, exposure to desiccation, and hydrodynamic stress (Bertelli et al., 2022; Ralph et al., 2007; Rao et al., 2023). Tidal processes influence elevation profiles and patterns of sediment deposition (Van Proosdij et al., 2006), while sediment grain size affects substrate stability, permeability, and nutrient retention, factors essential for seagrass establishment (De Boer, 2007). Wave action and current-driven forces further restructure seabed morphology by redistributing sediments (Perillo, 1995), and bioturbation contributes to microhabitat heterogeneity (Berkenbusch & Rowden, 2007; Townsend & Fonseca, 1998).

These physical imprints can be interpreted as long-term proxies of hydrodynamic forcing, capturing the cumulative effects of environmental gradients and physical processes that ultimately influence seagrass distribution and associated ecological functions **(Maxwell et al., 2017)**.

Patchiness is an intrinsic characteristic of vegetated ecosystems, influencing biodiversity, resilience, and habitat function stability (Rietkerk & Van De Koppel, 2008). In seagrass ecosystems, the mosaic-like distribution of vegetation creates diverse microhabitats that support various species adapted to different conditions within the meadows (Mills & Berkenbusch, 2009). This spatial variability also affects ecological resilience, as smaller, isolated patches may be more vulnerable to environmental stressors (Carr et al., 2016). Furthermore, the arrangement and size of seagrass patches directly affect ecosystem functions such as nutrient cycling and sediment stabilization (Bos et al., 2007). Understanding the factors driving these patterns is essential for predicting changes in seagrass distribution and developing effective conservation strategies (Orth et al., 2006).

Aiming to enhance the understanding of the physical variables influencing the distribution and patchiness of temperate shortleaf seagrass, this study employs a machine-learning approach to evaluate the extent to which intertidal topography and sediment characteristics predict the distribution of *Zostera muelleri* in Tauranga Harbour, New Zealand. The specific objectives are to: (1) identify the key environmental variables governing *Zostera muelleri* distribution within the study area, (2) provide spatial insights into the environmental constraints on seagrass habitat suitability, and (3) examine the relationship between seagrass patchiness and the environmental drivers that shape spatial distribution.

4.2 Methods

4.2.1 Study site

The study was conducted in Tauranga Harbour (Figure 4.1a), a 240 km² micro-tidal estuary (spring and neap tidal ranges of 1.62 m and 1.24 m, respectively) located on the North Island of New Zealand (Heath, 1976; Hume et al., 2007). This semi-enclosed waterbody (Figure 4.1b) is sheltered by a barrier island and consists of two primary basins, the southern and northern basins, between which there is limited hydrodynamic exchange.

Approximately 60% of the harbour area consists of intertidal zones, characterised by extensive sandflats, which are colonised by the perennial shortleaf seagrass species, *Zostera muelleri*. This species is the only seagrass species in the coastal waters of New Zealand, and is also present in Australia and Papua New Guinea (Lee et al., 2016). Some of the seagrass meadows also extend into the shallow subtidal regions. Previous studies have reported a decline in seagrass meadow coverage in Tauranga Harbour , although the rates of seagrass loss have decreased in the last decade (Ha et al., 2021; Park, 2016).

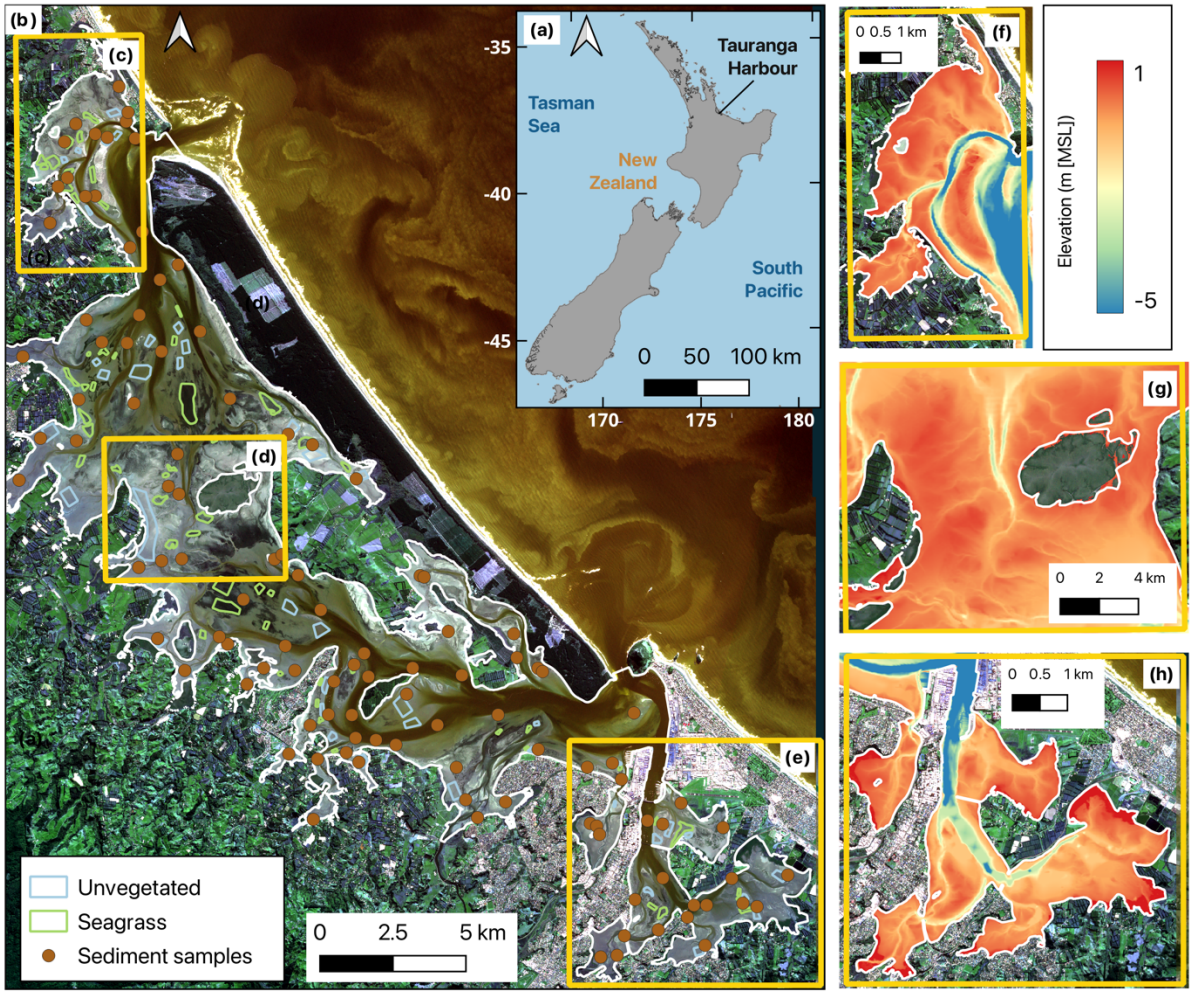

Figure 4.1: (a) Location of the study site in Tauranga Harbour, North Island, New Zealand; (b) Sentinel-2 image captured on July 4, 2021, overlaid with manually geotagged seagrass presence samples and sediment samples collected for sediment properties analysis in past studies; (c), (d), and (e) depict polygons outlining enlarged inset colourmaps of the Digital Elevation Model (DEM) in (f), (g), and (h), respectively.

4.2.2 Random forest methods for seagrass detection and presence/absence sampling

Random forest is an ensemble learning method for classification and regression. This approach uses multiple decision trees to split data based on feature values, with each tree contributing to the final prediction through majority voting (Breiman, 2001). Known for its robustness to overfitting, scalability, and ability to handle high-dimensional data, random forest methods are widely used in various fields, including species distribution modelling (Valavi et al., 2021). In this study, the models were generated using the random forest algorithm from the Sci-kit Learn package in Python (Kramer, 2016).

To ensure reduced inaccuracies in determining habitat suitability for a given species, it is

essential to sample the full range of environmental gradients where the species exist. Incomplete or biased sampling can lead to models that do not accurately reflect the true ecological preferences and potential distribution of the target species (Dubos et al., 2022). Thus, following this consideration, the random forest classifier was initially employed to detect seagrass within the estuary in a 10 m spatial resolution Sentinel-2 image captured on July 4, 2021, during a spring low tide when most of the intertidal flats were exposed (Figure 4.1b), although submerged seagrass in the imagery was also mapped. Considering that seagrass meadows in Tauranga Harbour are monospecific, vegetation coverage can be easily distinguished in the landscape through visual interpretation of moderate to high resolution remote sensing imagery such as Sentinel-2 (as has already been demonstrated by previous studies in Tauranga Harbour; Ha et al. 2021; Shao et al. 2024). Employing this method, polygon samples of vegetated and unvegetated flats were manually geotagged within the estuary, using the multispectral Sentinel-2 imagery, with the 3 visible light and the infrared bands (RGB + IR). The polygon samples are shown in Figure 4.1b. This seagrass detection model was built using 70% of the samples for training/validation and 30% for testing, resulting in a map indicating areas of seagrass presence and absence, which was subsequently sampled for the habitat suitability model.

4.2.3 Seagrass habitat suitability

For seagrass habitat suitability models, a total of 60,000 samples, comprising 30,000 samples of seagrass presence and 30,000 samples of absence were randomly selected from the seagrass classification. The random forest models were constructed using 10-fold cross-validation, where, in each iteration, the samples dataset was split into training/validation (70% of samples) and testing (30% of samples) subsets using stratified sampling to maintain class balance. The outputs of the models included a binary map indicating seagrass presence and absence based on the model decisions. Additionally, the algorithm generated a probability map representing

the likelihood of seagrass presence within the estuary. The probability of a species being present at a given location based on environmental variables is interpreted as a measure of habitat suitability for that species (Phillips et al., 2006), hereafter referred as Habitat Suitability Index (HSI).

4.2.4 Digital Elevation Model (DEM) and topographic variables.

To produce surface gradient variables to be used as potential predictors for seagrass habitat suitability, a Digital Elevation Model (DEM) was created using elevation data from different sources. For the intertidal flats, where most seagrass is found in Tauranga Harbour, a DEM derived from LiDAR data was used. This DEM is available in the Land Information New Zealand (LINZ) data portal (www.data.linz.govt.nz) as raster files with a spatial resolution of 1 m and was derived from an airborne survey, conducted in April-November 2020. The vertical accuracy of the survey is ±0.22 m, while the horizontal accuracy is ±1.0 m. The DEM covers an area of approximately 80 km², representing 40% of the total estuary area or 66% of the intertidal zone. For the remaining of the study area, bathymetric data stored in a grid with 10-m resolution from multibeam bathymetrical surveys were used (de Ruiter et al., 2019). The DEMs were combined to produce a final DEM with 10 m resolution (Figure 4.1d, f and h).

Preprocessing of DEM before computing terrain variables included the conversion of the elevations from the vertical datum NZVD2016 (Lidar) and Moturiki 1956 (bathymetry) to Mean Sea Level (MSL) as per LINZ guidelines for vertical datum transformations. The estuary area was delimited using vector files of mean high-water spring (MHWS) also provided in the LINZ data portal. Similarly, mangroves were removed by clipping the merged mosaic of DEM raster files using shapefiles of mangroves also available in the LINZ data portal.

Different surface variables were calculated for use in seagrass habitat suitability model and. are described below:

- **Bathymetric Position Index (BPI):** is calculated as the difference between the mean elevation within an outer and inner neighbourhood annulus, identifying topographic features like ridges or depressions (Weiss, 2001). The scale of these features depends on the specified inner and outer annuli (Lampietro et al., 2005; Mena & Fernández-Salas, 2024). Various BPIs were evaluated using combinations of inner and outer annuli: 1-3 (10-30 m), 2-5 (20-50 m), 3-7 (30-70 m), 5-12 (50-120 m), 10-20 (100-200 m), 20-40 (200-400 m), 5-50 (50-500 m), and 4-80 (40-800 m) pixels, where the first value indicates the inner annulus and the second the outer annulus.

- **Slope:** the steepness of the terrain is an important parameter for understanding the gradient and potential water flow across the seabed (Walbridge et al., 2018). The gradient of the slope was also computed and considered as a predictor variable in the models.

- **Aspect:** refers to the direction that a slope faces (Burrough & McDonnell, 1998). This parameter influences microclimatic conditions, such as sunlight exposure and wind patterns, affecting seagrass growth.

- **Roughness:** a measure of the variability in elevation within a specified area, providing an indication of surface irregularity and texture. High roughness values indicate more complex and uneven terrain. In seagrass habitats, roughness is related to water flow and sediment stability.

- **Terrain Ruggedness Index (TRI):** quantifies the total elevation change within a local neighbourhood around each cell in a digital elevation model (DEM). TRI reflects the overall terrain complexity by considering the sum of the absolute differences in elevation between each cell and its eight surrounding cells (Riley et al., 1999). Higher TRI values suggest more rugged and steep terrain.

The bathymetric position indexes were computed using Matlab, whereas the remaining DEM

variables were generated using the open-source software QGIS.

4.2.5 Sediment properties

Data on sediment properties, such as percentage of mud, sand, gravel, concentrations of total nitrogen, and total phosphorus were sourced from published environmental reports (Clark et al., 2018; Ellis et al., 2017). Sediment samples from the intertidal flats were collected in 2013 (n = 75), while sampling of the subtidal region occurred in 2016 (n = 34). The sampling locations are indicated in Figure 4.1b. Although the datasets were not collected simultaneously, we assume that over the span of a few years, these sediment properties remain relatively stable within the estuary.

The sediment properties were interpolated across the study area in a 10 m by 10 m grid using a cubic spline algorithm implemented in SAGA/QGIS. This method was selected for its ability to generate smooth, continuous surfaces from scattered point data, preserving local variation while minimizing abrupt transitions. Cubic spline interpolation is particularly suitable for environmental variables such as sediment properties, where gradual spatial gradients are expected (Igaz et al., 2021). The accuracy of the interpolated surfaces was evaluated using the root mean square error (RMSE), which represents the root mean squared difference between observed and interpolated values. The resulting RMSE values were 3.86% for gravel, 17.02% for mud, 6.97% for sand, 171.96 mg/kg for total nitrogen (TN), and 60.54 mg/kg for total phosphorus (TP), indicating reasonable performance across these variables.

Table 4.1 presents a summary of the information on the datasets used in the models.

Table 4.1: Description of the sources of seagrass samples of seagrass training and validation polygons and environmental predictor variables used for habitat suitability modelling, including data sources, acquisition years, and spatial resolutions.

Seagrass Samples / Predictors	Source of the data	Year	Resolution
Seagrass training and validation polygons	Copernicus Sentinel-2	2021	10 m
Digital elevation model (DEM)	Subtidal: de Ruiter et al., 2021	Various (derived from multiple nautical charts)	
	Intertidal: Land Information New Zealand	2020	
BPI 1-3	Derived from the LINZ DEM	Derived from the joined subtidal and intertidal DEM's	
BPI 2-5			
BPI 3-7			
BPI 5-12			
BPI 10-20			
BPI 20-40			
BPI 5-50			
BPI 4-80			
BPI 50-100			
Slope			
Slope of Slope			
Roughness			
TRI			
Aspect			
Mud	Ecological reports - subtidal and intertidal (Clark et al., 2018; Ellis et al., 2017)	2016 - subtidal	Interpolated to 10 m
Sand			
Gravel			
TN		2013 - intertidal	
TP			

4.2.6 Rationale of modelling of seagrass habitat suitability

In species distribution modelling, correlations between variables can bias habitat suitability calculations and should be minimised. To address this issue, collinearity among 20 candidate predictors was analysed using a Pearson (r) correlation matrix. Two variables were considered uncorrelated if $-0.5 \leq r \leq 0.5$, aiming to reduce moderate to strong multicollinearity while preserving a diverse set of predictors. This threshold allowed a maximum of 6 uncorrelated

variables to be grouped together in each set. Based on this threshold, 20 random sets of 6 uncorrelated predictors were selected. This approach ensured each set included a diverse mix of terrain and sediment properties, enhancing model robustness and accuracy by representing a broader range of environmental conditions.

4.2.7 Assessment of model performance and importance of predictors

The effectiveness of the random forest algorithm in identifying seagrass within the study area (supervised classification of the Sentinel-2 image) was evaluated using several key performance metrics: Overall Accuracy, Precision, Recall, F1-Score, and Kappa. While the overall accuracy provides a general idea of how well the model performs across all classes, precision measures the proportion of true positive predictions out of all positive predictions made by the model. Recall, also known as Sensitivity or True Positive Rate, measures the proportion of true positive instances out of all actual positive instances. The F1-score is the harmonic mean of Precision and Recall, providing a single metric that balances both the precision and the recall of the model. These parameters range from 0 to 1, where 0 indicates the worst performance (no correct classifications or random chance agreement) and 1 indicates perfect performance (all correct classifications and perfect agreement).

For the seagrass habitat suitability analysis, the performance of the model was assessed solely using the Area Under the Curve (AUC). AUC represents the probability that a randomly chosen positive instance is ranked higher than a randomly chosen negative one. The AUC ranges from 0.5 to 1, where 0.5 indicates no discriminative power (random guessing) and 1 indicates perfect discrimination between classes. The AUC values can be uses to classify model performance as: < 0.5 – terrible; 0.5-0.6 bad; 0.6-0.7 average; 0.7-0.8 good; 0.8-0.9 very good; and 0.9-1.0 excellent (Swets, 1988).

The importance of each predictor in the 20 models on the output of the models were based on

'feature' importance, a score determined by assessing the contribution of each feature in the prediction of the target variable (HSI). Based on the performance of the 20 models and the most influential variables for seagrass habitat suitability, one set of variables was selected for a 'leave one out' analysis. In this analysis, the model is run discarding one variable and then with only that variable, allowing assessment on the impacts of individual variables on the performance of the model. Partial dependence plots were retrieved and analysed, showing the relationship between a specific predictor variable and the predicted outcome, averaging out the effects of other variables to indicate the specific effects of each individual predictor on the seagrass habitat suitability.

4.2.8 Assessment of the relationship between seagrass patchiness and habitat suitability

To analyse the impact of habitat suitability on seagrass patchiness, vegetated patches were identified from the supervised classified seagrass map by labelling discrete seagrass patches using an 8-connected neighbourhood method, where pixels are considered connected if they share either an edge or a corner. In this analysis, only patches larger than or equal to 10 pixels (0.1 ha) were considered to minimize noise and improve data reliability by excluding smaller patches that could have been misclassified. By setting this minimum patch size, the analysis focuses on medium to larger patches, exploring broader habitat patterns and processes, and improving the interpretability and relevance of the results for management and conservation efforts.

Each patch was characterised based on spatial patch metrics, including area (A) and a shape index ($\mathbf{S} = {}^{\mathbf{P}}\!/_{\mathbf{2\sqrt{\pi A}}}$), where P is the patch perimeter). The area (G_A) and number (N_{gaps}) of bare gaps, defined as distinct empty spaces within each patch and determined through binary inversion and connected component analysis, were also calculated. Finally, the mean habitat suitability for each patch ($\overline{\mathbf{HSI}}_{\mathbf{patch}}$) was computed by averaging the habitat suitability index

values of all pixels within each patch.

The impact of habitat suitability on seagrass patchiness was evaluated using a linear regression model, with $\overline{\mathbf{HSI}}_{\mathbf{patch}}$ as the independent variable. To address issues such as non-normality and the presence of skewed distributions in the patch metrics, the dependent variables were log-transformed. These patch metrics were correlated with $\overline{\mathbf{HSI}}_{\mathbf{patch}}$, and the correlations between these metrics of vegetated and unvegetated patches were assessed trough the Pearson's correlation coefficient (r). Additionally, a robust linear regression model was applied to the log-transformed bare gap metrics.

4.3 Results

4.3.1 Seagrass detection

The random forest model showed an outstanding performance in detecting seagrass within the estuary with very high precision (≥0.97) and confidence (F1-score ≥ 0.98). For unvegetated areas, performance metrics include a precision of 0.97, with a recall of 0.99, and an F1-score of 0.98. In seagrass areas, the model maintained high precision, recall, and F1-score values, all at 0.97. The map of seagrass presence and absence is presented in Figure 4.2b. The total seagrass area for the Sentinel-2 imagery captured in July 2021 used in this study was 3,982 ha, which is consistent with the estimations of previous research for the winter of 2021 (Shao et al., 2024).

Table 4.2: Model performance metrics for seagrass detection model.

Class	Precision	Recall	F1-score	Support (number of samples)
Unvegetated	0.97	0.99	0.98	30409
Seagrass	0.97	0.97	0.97	28593
Overall accuracy (macro avg)	0.98	0.98	0.98	
Overall accuracy (weighted avg)	0.99	0.99	0.99	59002

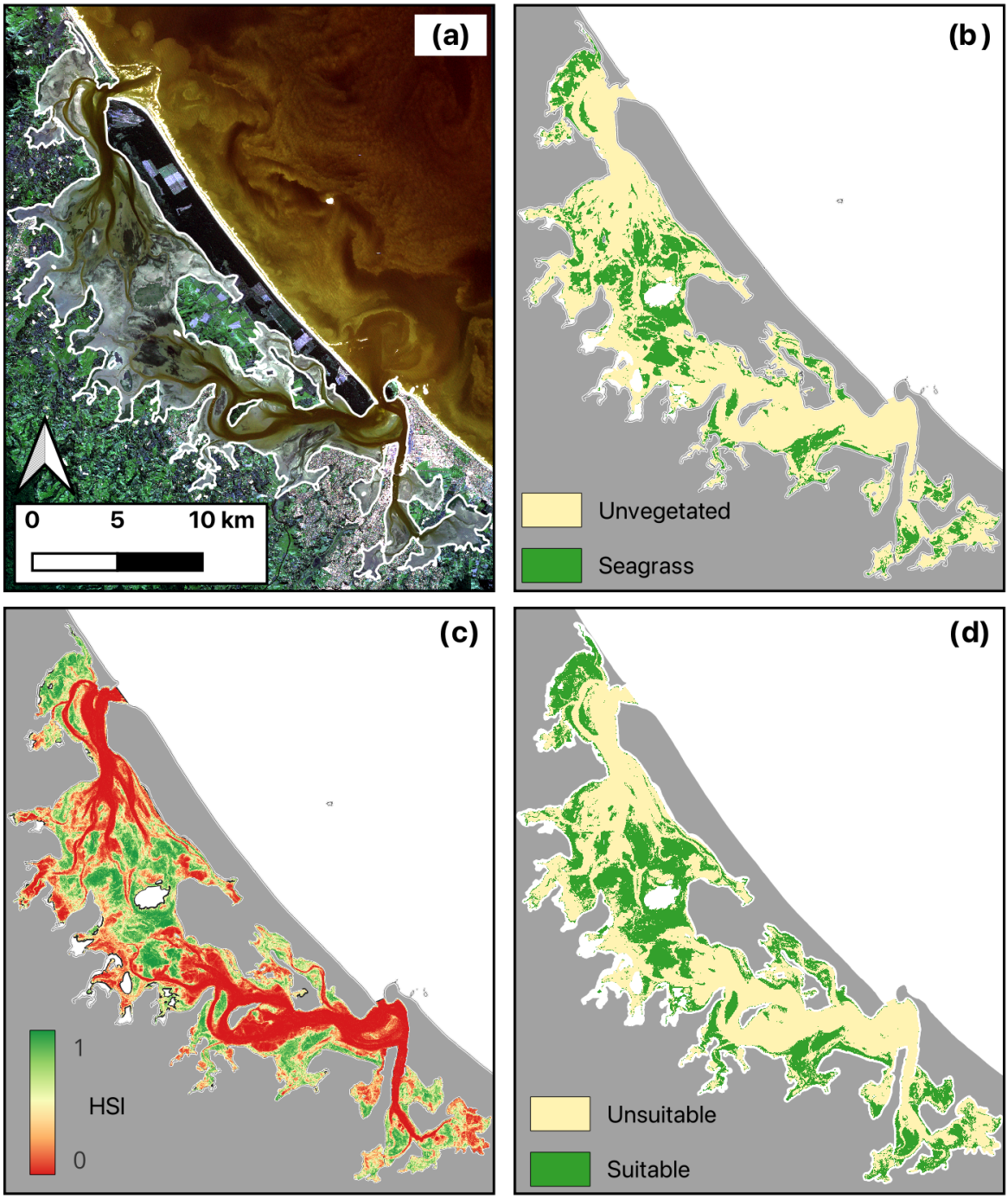

Figure 4.2: (a) Sentinel-2 imagery used for detecting seagrass (for comparison); (b) results of the seagrass detection from the Sentinel-2 imagery; (c) habitat suitability index (HSI) for seagrass, represented as the likelihood of each pixel being classified as seagrass (probability of occurrence) based on the topographic and sediment composition variables (Set 13); (d) binary classification of seagrass based on the topographic and sediment composition variables.

4.3.2 Collinearity among predictor candidates

In the Appendix F, Figure F.1 presents colourmaps of all 20 variables that were used as predictors for seagrass habitat suitability. In addition, the correlation matrix in Figure 4.3 illustrates the multicollinearity among the 20 predictor variables for seagrass habitat suitability. The absolute values of the Pearson correlation coefficients in the Figure 4.3 shows that elevation has a stronger correlation with bathymetric position indexes of larger annulus distances (e.g., BPI 4-80 and BPI 50-100) compared to those with smaller annulus distances (e.g., BPI 1-3 and BPI 3-7). These strong correlations indicate that as the outer annulus distance increases, the relationship between elevation and BPIs becomes more pronounced. Additionally, aspect and gravel stand out as the only variables that are uncorrelated with all other predictors, showing very low or near-zero correlation coefficients. Strong correlations were observed between different bathymetric position indexes with stronger correlations for closer annulus distances, which is expected as these variables are derived measures of bathymetry. Variables such as terrain ruggedness index and slope show moderate correlations with several bathymetric position indexes and each other, indicating a combined influence on terrain characterisation. Conversely, environmental variables such as total nitrogen and total phosphorus display weaker correlations with most predictors, except with each other, where a moderate correlation is observed, reflecting the relatedness in nutrient composition.

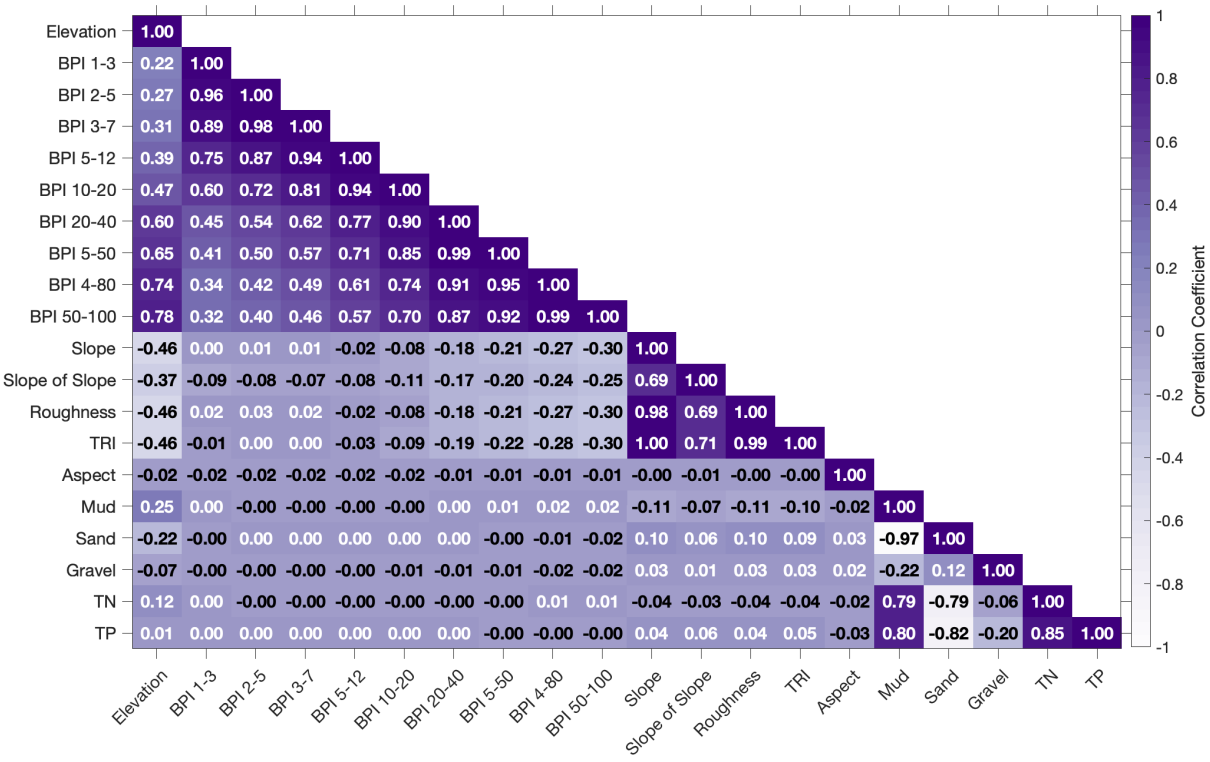

Figure 4.3: Collinearity analysis of the 20 predictor candidates for seagrass habitat suitability, represented by the absolute values of the Pearson correlation. Values indicate the strength of the linear relationship between each pair of predictors. Bathymetric Position Indexes (BPIs) are labelled with the number of cells in the inner and outer annulus, respectively, and are arranged in order of increasing outer annulus distance. TRI stands for Terrain Ruggedness Index, TN for Total Nitrogen, and TP for Total Phosphorus.

Table 1 displays the 20 sets of predictor variables selected for seagrass habitat suitability analysis. Each set was designed to include six uncorrelated variables ($-0.5 \leq r \leq 0.5$) to avoid multicollinearity, as six was the maximum number of uncorrelated variables that could be combined. Aspect and gravel were found to be uncorrelated with all other variables and, therefore, were included in all sets of variables.

Table 4.3: 20 sets of randomly selected uncorrelated variable predictors for seagrass habitat suitability. BPI stands for Bathymetric Position Index, TRI for Terrain Ruggedness Index, TN for Total Nitrogen, and TP for Total Phosphorus.

Set # / Predictors	Elevation	BPI 1-3	BPI 2-5	BPI 3-7	BPI 5-12	BPI 10-20	BPI 20-40	BPI 5-50	BPI 4-80	BPI 50-100	Slope	Gradient of slope	Roughness	TRI	Aspect	Mud	Sand	Gravel	TN	TP
Set 1	X	X									X				X			X	X	
Set 2			X							X				X	X	X		X		
Set 3		X								X			X		X	X		X		
Set 4				X						X	X				X		X	X		
Set 5			X					X			X				X			X		X
Set 6			X							X				X	X	X		X		
Set 7		X					X				X				X		X	X		
Set 8	X				X								X		X			X	X	
Set 9		X					X						X		X			X		X
Set 10	X	X									X				X		X	X		
Set 11	X					X								X	X	X		X		
Set 12		X					X					X			X		X	X		
Set 13	X					X					X				X			X	X	
Set 14		X							X				X		X	X		X		
Set 15			X						X			X			X		X	X		
Set 16	X	X										X			X			X	X	
Set 17		X						X					X		X			X		X
Set 18			X							X				X	X		X	X		
Set 19			X					X					X		X			X		X
Set 20				X						X				X	X			X	X	

4.3.3 Model performance

Figure 4.4 highlights the performance of each of the 20 models (Figure 4.4a) and the mean importance of the predictor variables in modelling seagrass habitat suitability (Figure 4.4b). The AUC scores for the 20 models generally fall between 0.81 and 0.86 with a mean across all models at 0.84, indicating a good performance in distinguishing between suitable and unsuitable habitats (Swets, 1988). The relatively small standard deviations suggest consistent performance across the different subsets (folds) of the data used during the cross-validation

process. Elevation is the most critical variable, with an average importance score of 0.29. The broad-scale group of bathymetric position indexes that are correlated with elevation had mean importances scores varying from 0.12 to 0.23 (Figure 4.4b). Variables within the group of sediment properties such as mud, total phosphorus, sand and total nitrogen had mean importances scores ranging from 0.17 to 0.2. Roughness, terrain ruggedness index, slope, gradient of slope, and the fine-scale bathymetric position indexes had minor importance in the model (average importance < 0.17), with aspect being the least important variable.

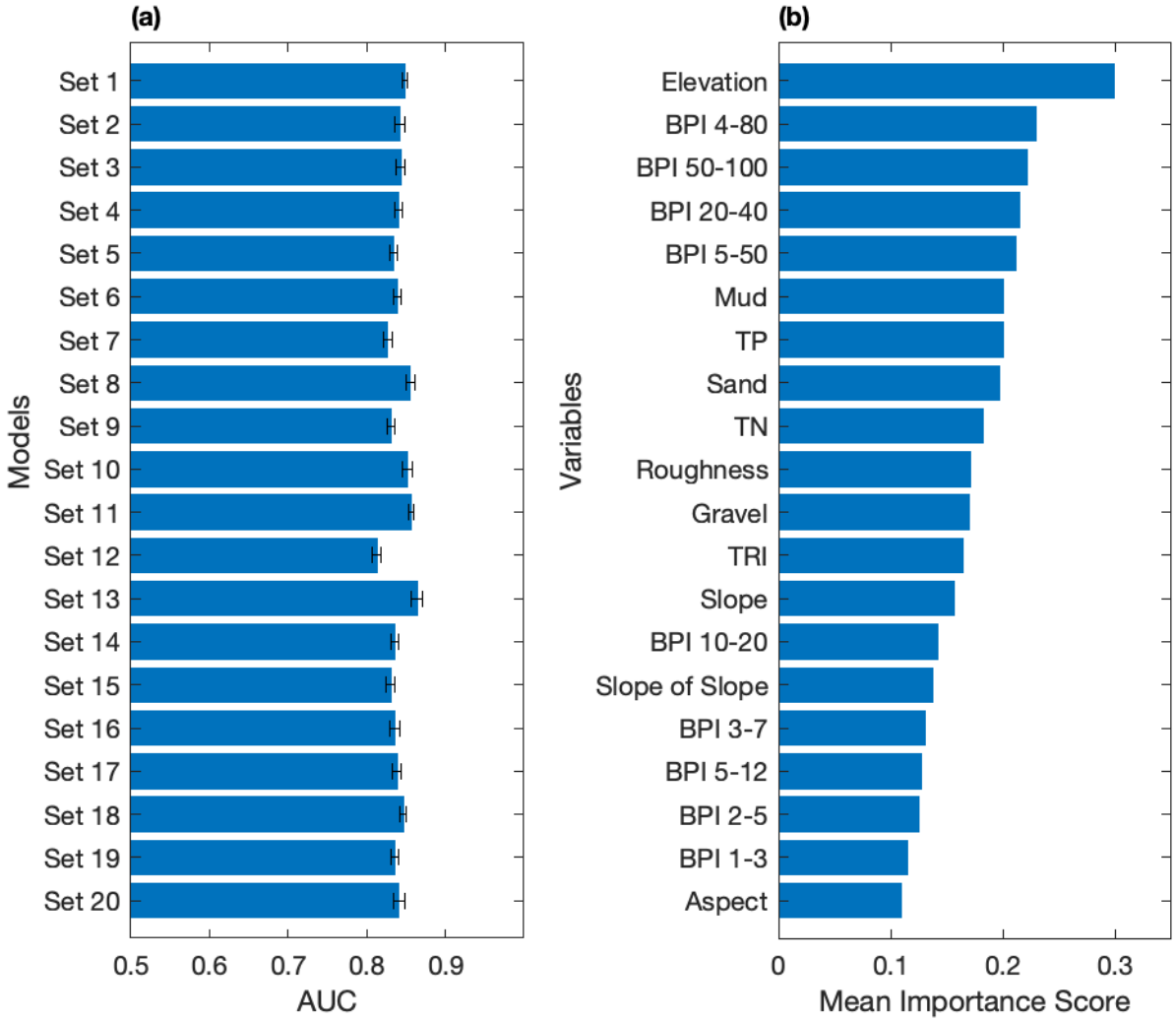

Figure 4.4: (a) AUC scores (mean ± 1 SD, considering the 10-fold cross-validation) for all models with 20 different sets of uncorrelated predictors. (b) Mean importance score of each variable within the sets that include those variables, ordered in ascending mean importance score. BPI = Bathymetric Position Index; TRI = Terrain Ruggedness Index; TN = Total Nitrogen; TP = Total Phosphorus.

Based on the AUC scores of all 20 models and the mean importance of each predictor, the 'leave-one-out' analysis was performed with the variables from Set 13, since this set had the highest AUC. The results of this analysis are presented in Figure 4.5 and evaluate the contribution of each variable to overall model performance. The model shows a large drop in AUC when elevation, gravel, and total nitrogen are removed, indicating their critical importance, whereas the removal of BPI 10-20, slope, and aspect does not affect the AUC score, suggesting these variables are less critical for the accuracy of the model.

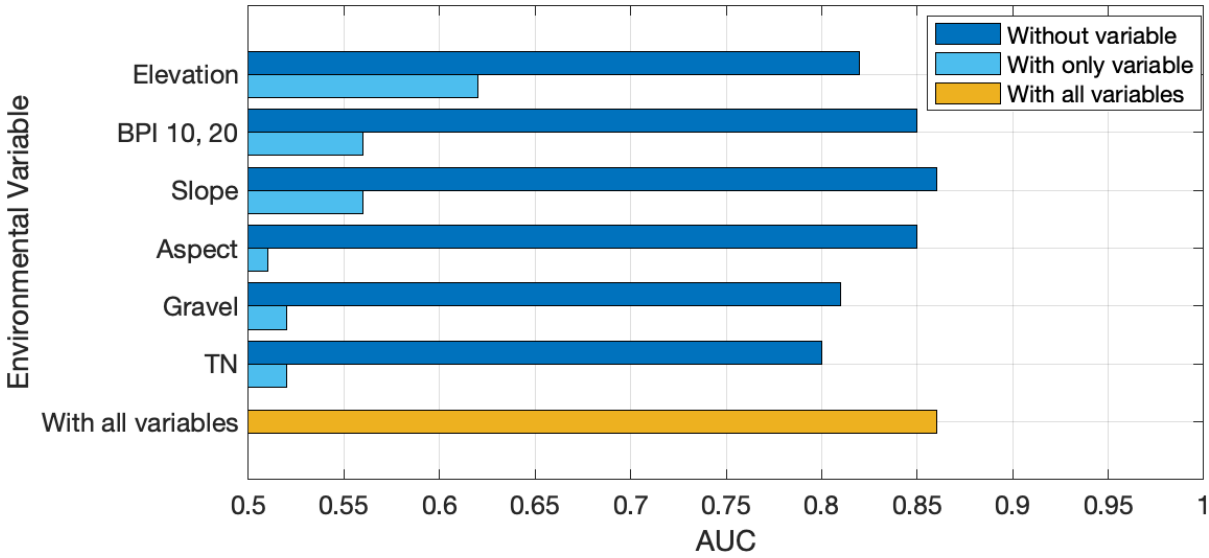

Figure 4.5: Impact of individual predictors on model performance using the 'Leave-One-Out' approach on the variables considered in the Set 13 (Table 4.3). The analysis evaluates the contribution of each variable (elevation, BPI 10-20, slope, aspect, gravel, and total nitrogen) to the overall model performance. Higher AUC scores indicate better model performance, demonstrating the relative importance of each predictor in the context of species distribution modelling.

4.3.4 Dependence of habitat suitability on environmental variables

Given the similar AUC scores across the models, the partial dependence of habitat suitability index on elevation and sediment properties was averaged over all models where each variable was included and then plotted in the Figure 4.6. For elevation, seagrass suitability is very low at elevations < -3 m MSL (mean sea level) but increases sharply as elevation approaches the MSL. Suitability has a maximum within the range starting at approximately -0.5 m MSL, before starting to decrease at elevations higher than 0.6 m MSL. Mud content shows a rapid

increase in suitability at low percentages and then stabilizes, with minor fluctuations around a relatively stable value between 5% and 20%. For sand content, there is noticeable variability across the range of sand percentages. Suitability displays a slight positive trend from 70% to 90%, decreases, and then rises again at very high sand content, indicating an optimal range between 80% and 90%. The impact of gravel content on suitability is relatively stable with slight fluctuations, indicating limited influence. Seagrass habitat suitability remains relatively constant across the gravel content range of 0% to 5%. In terms of total nitrogen, suitability decreases as nitrogen levels increase from 300 mg/kg to 600 mg/kg, showing a negative trend, with optimal suitability below 400 mg/kg. Similarly, total phosphorus shows a decrease in suitability with increasing phosphorus levels from 100 mg/kg to 250 mg/kg, with an optimal range below 150 mg/kg.

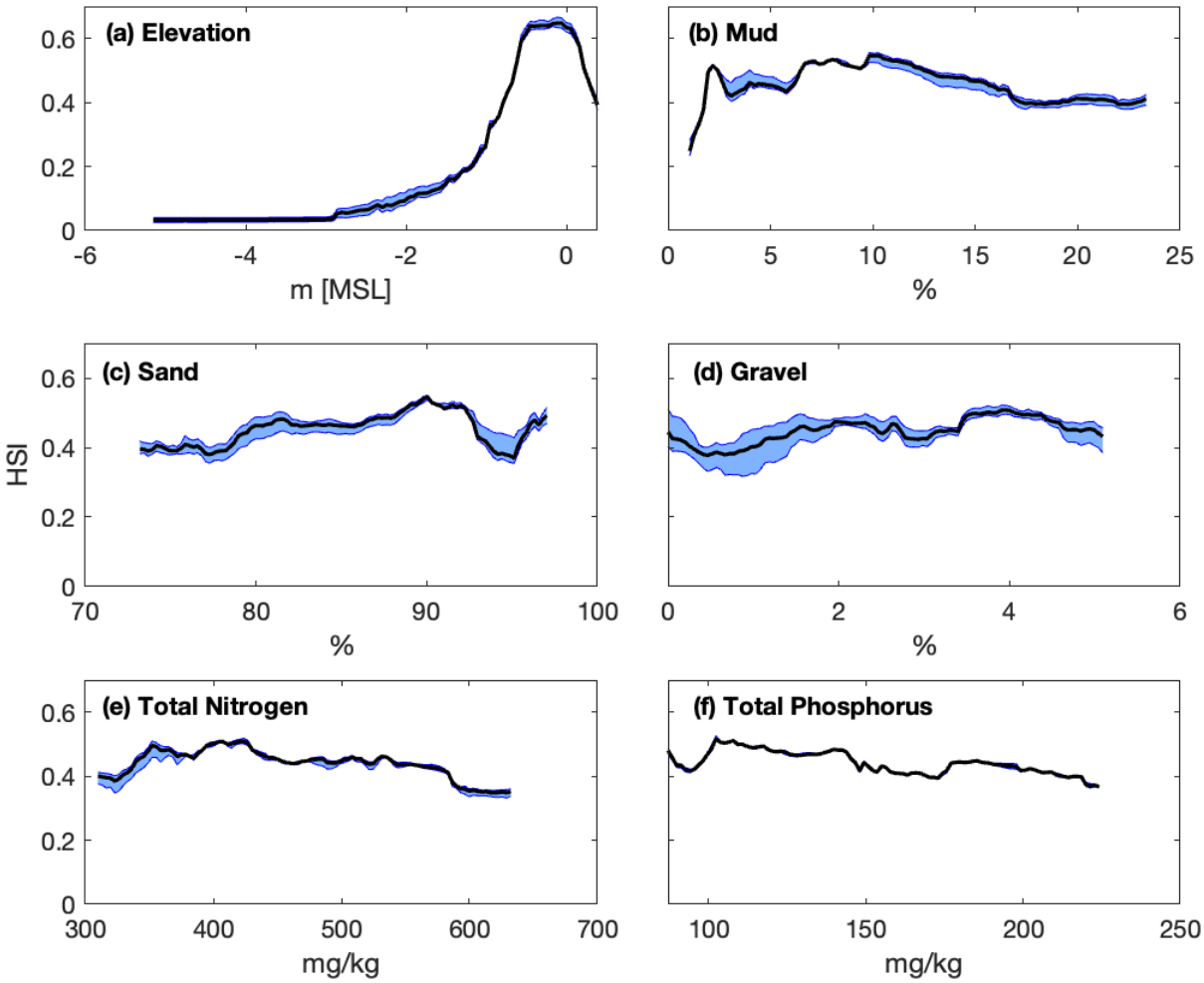

Figure 4.6: Mean (black line) and modelled range (blue area) of the dependence of habitat suitability index (represented as the probability of *Zostera muelleri* presence) on elevation (a) and sediment properties (b-f) across all models in which each variable is included.

The maps with the final binary classification of suitable seagrass habitats as well as the probabilities of having seagrass based on the environmental variables used as predictors in the model with the highest AUC (Set 13) are presented in Figure 4.2, panels (c) and (d). The total suitable habitat area in Tauranga Harbour is estimated to be 6,966 ha, which accounts for approximately 32% of the total area of the estuary.

4.3.5 Dependence of patchiness on habitat suitability

The scatter plots in Figure 4.7 illustrate the relationships between the mean patch habitat suitability index ($\overline{\mathrm{HSI}}_{\mathrm{patch}}$) and patch metrics. While all p-values were below 0.05, indicating statistical significance, the strength and direction of the correlations varied. Panels (a) and (b)

show weak positive trends between $\overline{HSI}_{patch}$ and patch area (A) and patch shape index (S), respectively. In contrast, a strong negative relationship is evident between $\overline{HSI}_{patch}$ and the number of bare gaps per patch area (N_{gaps}/A, panel c), suggesting that patches with higher habitat suitability have fewer gaps. However, there is no meaningful association between $\overline{HSI}_{patch}$ and the ratio of total gap area to patch area (A_{gap}/A, panel d).

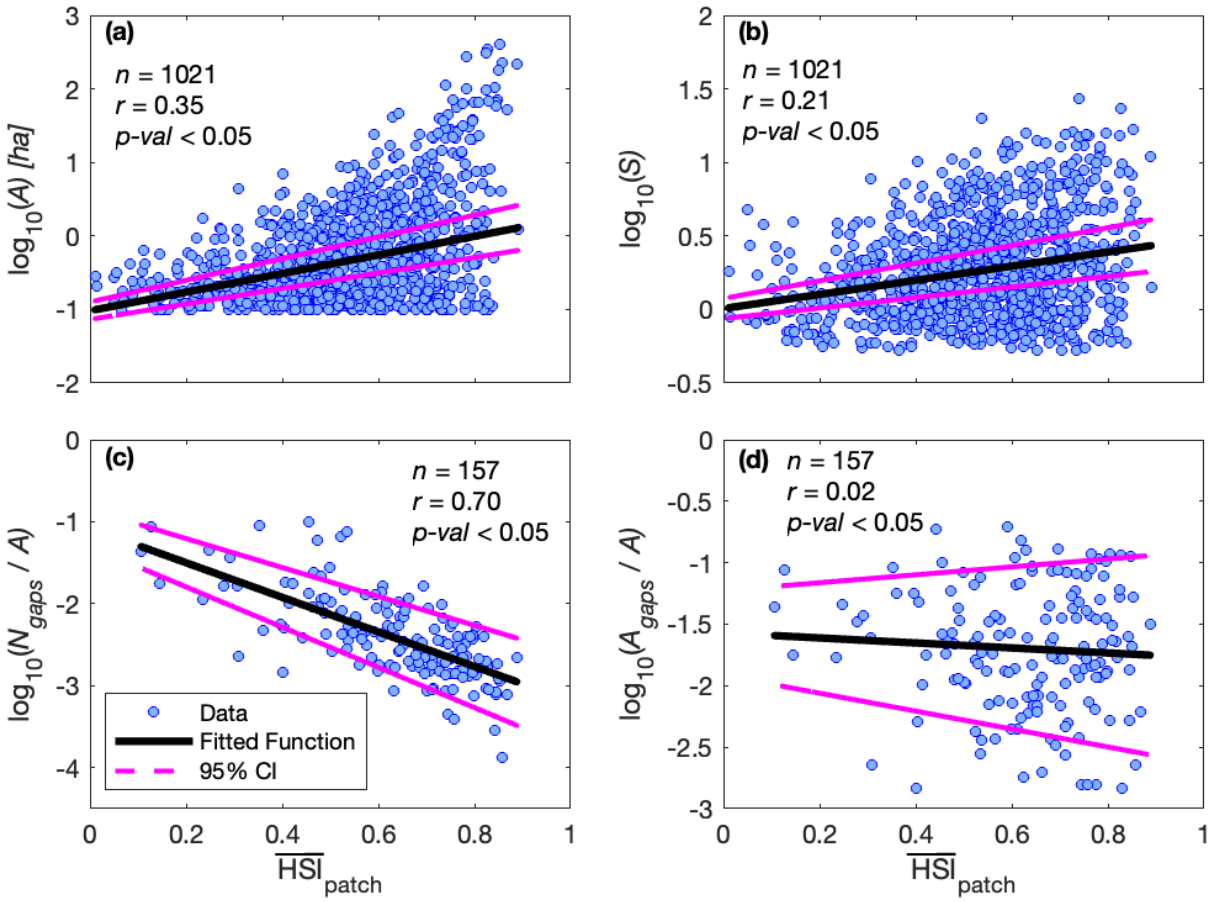

Figure 4.7: Scatterplots showing the relationships between mean patch habitat suitability index ($\overline{HSI}_{patch}$) within each patch and patch metrics: (a) patch area (A), (b) patch shape index (S), (c) ratio between the number of gaps and patch area (N_{gaps}/A), and (d) ratio of total bare gap area to patch area (A_{gaps}/A). The fitted regression lines and 95% confidence intervals (CI) are shown for each relationship.

Figure 8 illustrates the density of mapped seagrass patches across gradients of elevation and sediment properties, expressed as the number of patches per unit of seagrass area ($N_{patches}/A_{seagrass}$) within specific ranges of each environmental variable. Seagrass patch density is highest between -10 and -3 meters relative to mean sea level (panel a). This trend indicates

that patchiness is primarily associated with the lower end of the elevation gradient, while the upper end (higher elevations) tends to have larger, more uniform patches. Seagrass is most fragmented into patches when mud content greater than 30% (panel b). Clustered seagrass patches are most common in areas with sand content between 20% and 70%, decreasing at both lower and higher sand concentrations (panel c). Seagrass patch density is low across all gravel concentrations but is slightly higher at the greater gravel content (> 6%, panel d). The influence of total phosphorus on patch density (panel e) appears more variable, with a noticeable peak in patch density at lower concentrations, around 0 to 100 mg/kg, suggesting that total phosphorus has a limited but distinct impact at these lower levels. Patch density increases significantly in areas where total nitrogen concentrations range from approximately 800 to 1500 mg/kg (panel f), indicating that higher levels of total nitrogen are linked to more fragmented seagrass patches.

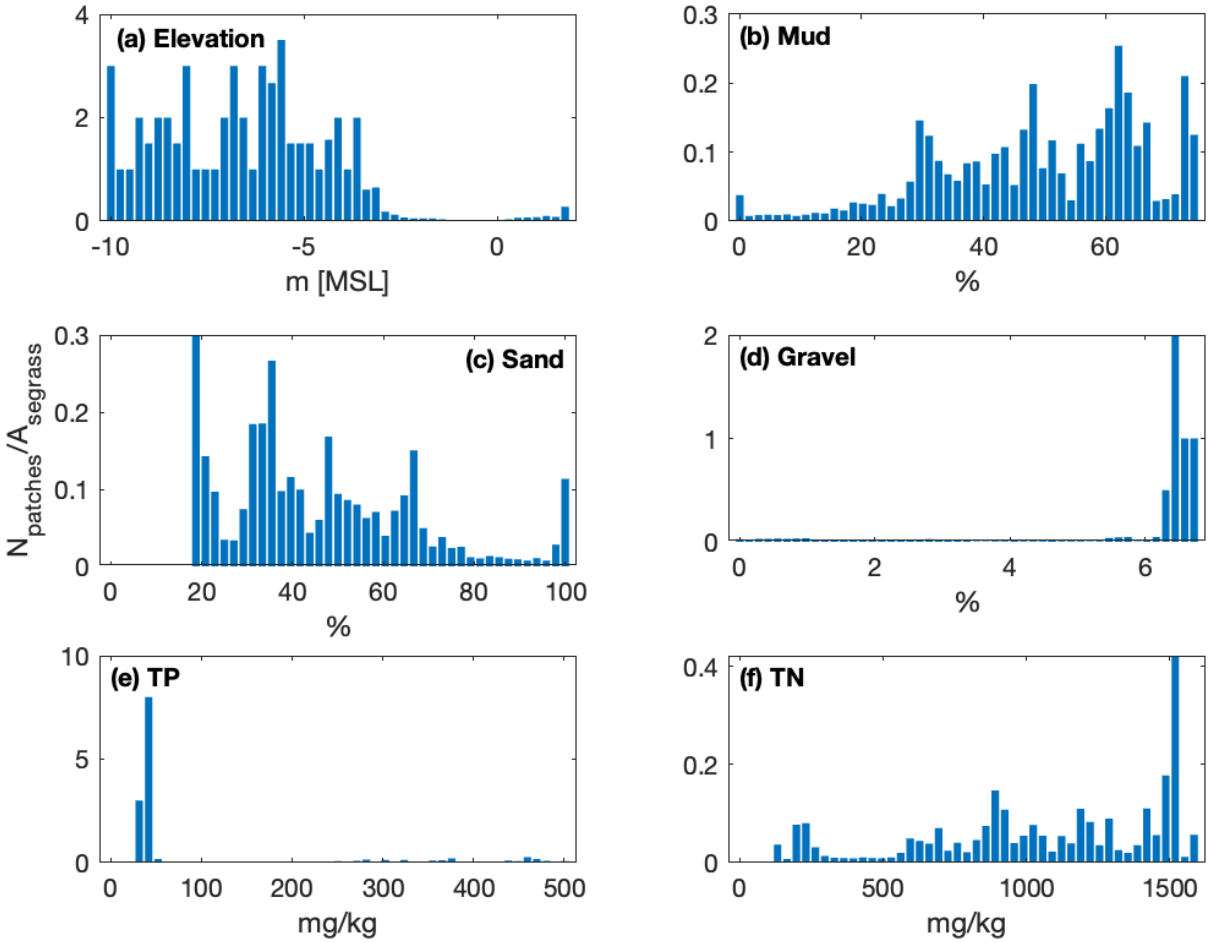

Figure 4.8: Influence of elevation and sediment properties on patch density, represented as the ratio of the number of patches to the total seagrass area within 50 specified bins. Each panel shows the relationship for different environmental variables: (a) Elevation relative to mean sea level (MSL), (b) Mud content (%), (c) Sand content (%), (d) Gravel content (mg/kg), (e) Total phosphorus (TP) concentration (mg/kg), and (f) Total nitrogen (TN) concentration (mg/kg).

4.4 Discussion

The machine-learning models developed in this study showed that topographical and sediment characteristics accurately predicted the distribution of seagrass habitat in Tauranga Harbour, achieving a mean AUC score of 0.84. These results confirm that physical environmental variables, specifically topography and sediment properties, can effectively indicate the suitability of seagrass habitats. Elevation emerged as the most influential predictor, consistent with findings from other coastal systems (Bertelli et al., 2022), while sediment properties such as mud and sand content were also significant factors. The optimal elevation range for seagrass was found to be between -0.5 and 0.6 meters relative to mean sea level (MSL). This optimal

range is primarily governed by light availability, which is crucial for photosynthesis. In deeper waters, reduced light penetration due to absorption and scattering limits seagrass growth (Adams et al., 2016; Ralph et al., 2007). In Tauranga Harbour, insufficient light conditions, lower than the critical threshold required for seagrass survival, have been reported in subtidal channels and are associated with increased concentrations of suspended particles (Cussioli et al., 2019). At the upper elevation limit, seagrass growth is constrained by the ability of seagrass to withstand desiccation and temperature fluctuations due to sunlight exposure during low tides, as well as the impact of local wind waves (Shafer et al., 2007; Wang et al., 2024).

Sediment properties were identified as the second most influential group of variables affecting the spatial distribution of seagrass in the study area (De Falco et al., 2000). The models suggest that sandy substrates with low mud content are the most suitable for *Zostera muelleri* habitats, as they provide a stable substrate for rooting and anchoring seagrass rhizomes. High mud content, however, negatively impacts seagrass by reducing sediment permeability and altering key physicochemical properties such as redox potential, phytotoxin retention, and solute exchange capacity (Glud, 2008; Huettel et al., 2014; Terrados et al., 1999). These conditions create an increased irradiance demand in seagrass colonizing muddy areas due to an oxygenation compensation mechanism for adverse conditions in the rhizomes (Zabarte-Maeztu et al., 2021). While seagrass can stabilize sediments by trapping fine particles after establishment, this benefit is only evident in dense seagrass beds, indicating that moderate mud levels (5-20%) can be tolerated, but excessive mud content (>39%) leads to habitat degradation and loss (Flowers et al., 2024; Van Katwijk et al., 2010).

The models showed a smaller influence of secondary terrain attributes such as small-scale bathymetric position indices (BPIs), slope, gradient of slope, roughness, terrain ruggedness index, and aspect. These attributes contribute less critically to habitat conditions at the estuary scale compared to elevation and sediment composition, although they still influence

microhabitat conditions and localised habitat suitability, particularly in areas with greater physical variability. In more uniform environments, their influence diminishes. Recognising the primary role of elevation and sediment properties can help prioritize conservation and management efforts, while still considering the contributions of these secondary factors.

Extending previous research, this study demonstrates that specific combinations of environmental conditions, such as depth and substrate type, exert influence broad-scale patchiness in seagrass habitats. Patchiness was found to be greater in subtidal regions with higher gravel content, where seagrass beds are more likely to be fragmented due to light limitations and hydrodynamic forces (Green & Coco, 2014), and areas with lower hydrodynamic dominance with mud content greater than 20%, where increased sediment loads further inhibit seagrass growth and induce patchiness. The innovative combination of supervised classification for seagrass detection and species distribution modelling provided new perspectives on the drivers of seagrass patchiness, showing that seagrass patch density increases in response to unfavourable conditions. By forming in patches, seagrass create microenvironments that buffer against physical stressors such as strong currents and sediment resuspension, improve local light conditions, and stabilize sediments, thus enhancing survival in areas that are otherwise suboptimal for seagrass growth (Fonseca & Bell, 1998; Koehl et al., 2007). Broad-scale patches in areas of lower habitat suitability, characterised by a higher prevalence of bare gaps, may be more susceptible to gap-induced flow alterations. Bare gaps intensify horizontal flow and enhance turbulence within the surrounding vegetation, further influencing the local hydrodynamics and potentially exacerbating the vulnerability of these patches to environmental stressors (da Silva et al., 2024).

Potential limitations to this study arise from the relatively coarse spatial resolution of the Sentinel-2 imagery, bathymetry and sediment variables, which may not fully capture fine-scale spatial heterogeneity and patch dynamics within seagrass beds. The minimum patch size

considered (0.1 ha) could lead to an underestimation of smaller or more fragmented patches, potentially overlooking subtle variations in sediment composition and microhabitat conditions. Future research could benefit from higher-resolution data to better capture finer-scale environmental gradients and to incorporate additional dynamic variables, such as turbidity, nutrient loading, and temporal changes in hydrodynamic conditions. Expanding the temporal scope to include seasonal and interannual variations in seagrass cover and environmental conditions could further improve the understanding of habitat suitability and inform adaptive management strategies (Green & Coco, 2014; Syvitski et al., 2005a). While seasonal variations in seagrass cover might influence patch dynamics, these changes are typically less than 10% (Shao et al., 2024), suggesting limited impact on the broader findings of this study.

The predictive relationships identified in this study between seagrass distribution and environmental drivers such as elevation and sediment composition have direct relevance to climate change scenarios. Sea-level rise may alter the spatial extent of elevation bands currently associated with optimal conditions, particularly in estuarine systems where both light availability and hydrodynamic exposure are depth-dependent. In Tauranga Harbour, seagrass was found to be less patchy in shallow zones and increasingly fragmented in deeper areas, where light limitation and intensified hydrodynamic stress constrain growth. As sea levels rise, zones that currently support continuous seagrass may transition into deeper, less favourable conditions, promoting fragmentation and loss (Short & Neckles, 1999). While newly intertidal areas could offer potential for colonization, this possibility is often constrained by shoreline hardening, which restricts landward migration. An increasing proportion of developed coastlines are lined with protective structures such as seawalls, revetments, and breakwaters, which prevent the landward migration of intertidal and shallow subtidal habitats (Capistrant-Fossa & Dunton, 2024). This restriction on spatial adjustment in response to sea-level rise limits the potential expansion of seagrass into newly submerged areas and contributes to a net

reduction in suitable habitat. These changes, combined with projected increases in storm intensity, precipitation, and catchment runoff, are expected to elevate turbidity and sediment loads (Syvitski et al., 2005b), further reducing light penetration and reinforcing patchiness. Alterations in sediment composition due to shifting hydrodynamics or land-use pressures may also reduce the availability of sandy substrates, which were associated with higher habitat suitability in this study. Taken together, these drivers are likely to intensify existing patterns of spatial fragmentation and increase the vulnerability of seagrass meadows to environmental stress.

The findings of this study have practical applications for seagrass restoration and management. Understanding the key environmental drivers, such as depth and sediment composition, provides a basis for targeted restoration efforts. Areas identified as suitable but currently lacking seagrass cover, particularly those with sandy substrates and depths within the optimal range should be prioritised for restoration. Focusing on bare gaps within smaller patches where established vegetation may provide protective effects against environmental stressors could enhance the success of restoration initiatives. Restoring these areas may create conditions conducive to natural seagrass expansion and long-term habitat sustainability by leveraging natural feedback mechanisms, such as the ability of seagrass to trap fine particles and stabilise sediments (Van Katwijk et al., 2010).

4.5 Conclusions

This study highlights the effectiveness of machine-learning models in predicting seagrass habitat suitability in Tauranga Harbour, New Zealand, based on topographical and sediment characteristics. Elevation was the most critical factor, with *Zostera muelleri* occurring between -0.5 and 0.6 meters relative to mean sea level, influenced by light availability and exposure. Sandy substrates with low mud content were also significant in determining suitable habitats. Model results show that successful colonization of *Zostera muelleri* depends on optimal depth

and sediment composition. Depth and substrate not only affect seagrass distribution but also broader patterns of patchiness, with less suitable areas displaying more fragmented patches and bare gaps. Areas identified as suitable but lacking seagrass present opportunities for restoration efforts. However, further studies with higher-resolution data and dynamic environmental variables are needed to refine predictions. These findings offer a framework to guide targeted conservation and management strategies in temperate seagrass ecosystems.

Chapter 5: General conclusions

This thesis aimed to enhance the understanding of the impacts of patchiness on plant-flow interactions, and the consequences of this spatial heterogeneity for the suitability of seagrass habitats from a multiscale perspective. The introduction outlined three primary research questions that guide this investigation.

5.1 Review of key findings

1. **What are the temporal and spatial variations in flow and turbulence within and surrounding bare gaps in shortleaf seagrass meadows, and how do these variations connect to the spatial distribution of seagrass?**

In Chapter 2 of this thesis, high-resolution, small-scale, concurrent measurements of flow and turbulence within and around a bare gap in a shortleaf seagrass meadow were conducted and integrated with vegetation mapping data. These measurements revealed complex temporal and spatial variations closely linked to the spatial distribution of seagrass. These variations influenced not only the immediate environment around the gaps but also extend across the broader meadow, affecting seagrass distribution and growth dynamics. The flow dynamics within fragmented seagrass meadows are shaped by a combination of larger-scale processes, such as tidal asymmetry, and smaller-scale plant-flow interactions, which together determine the spatial arrangement of seagrass patches. In the flood-dominant estuary of Tauranga Harbour, New Zealand, temporal variations in flow and turbulence over vegetated and unvegetated patches is primarily driven by tidal asymmetry. During the faster incoming flood currents, the differential drag between vegetated and bare patches become sufficient to divert flow toward the bare patches. Over the adjacent seagrass, this diversion is accompanied by downward-directed turbulence, including down-deceleration and sweeps, which are known to enhance nutrient and oxygen inputs, supporting the growth and health of the seagrass. In

contrast, during ebb tides, when flow speeds are slower, the vegetation exerts minimal drag on flow, resulting in negligible differences in flow speeds between vegetated and bare patches. These findings illustrate how the interplay between flow speed, tidal asymmetry, and vegetation structure governs the small-scale ($O(10^0$ m)) flow dynamics within patchy seagrass meadows. Areas of higher turbulence and flow speeds, particularly at the edges of bare gaps, create conditions that may enhance or inhibit seagrass growth. The observations indicate that the attenuation of near-canopy currents, especially on the sides of gaps perpendicular to the dominant flow direction, can promote denser vegetation, suggesting that flow conditions within bare gaps contribute to shaping the spatial configuration of seagrass meadows. The similarity between tidal and continuity ellipses observed at a broader scale ($O(10^2$ m)) further supports the connection between tidal variability and flow patterns around the gaps. The spatial arrangement of seagrass patches is influenced not only by hydrodynamic forces but also by internal structural factors, such as canopy density and shoot growth direction. Under conditions of unidirectional flow, the patterns of seagrass beds align perpendicularly to the dominant flow axis, which minimizes disturbances at patch edges. This pattern of alignment contrasts with riverine systems, where vegetation tends to orient parallel to the flow. Temporal and spatial variations in flow and turbulence, shaped by both tidal dynamics and local plant-flow interactions, are critical determinants of the spatial distribution of seagrass in fragmented meadows.

2. **How do bare gaps of varying sizes and different spatial configurations interact to collectively affect horizontal flow within meadows of emergent aquatic vegetation?**

Chapter 2 quantified the influence of a single bare gap on flow structure, demonstrating that localized flow acceleration and elevated turbulence occur in response to gap-induced disruption of the vegetative canopy. Although these results provide important insights into gap-scale dynamics, the findings do not capture how accelerated flows redistribute or interact when

multiple gaps are present. To address this knowledge gap, Chapter 3 revealed that the impacts of multiple bare gaps on horizontal flows within emergent vegetation are controlled by the total bare area, the distances between the gaps, and their spatial configuration. Simulations in a meadow-scale test channel detailed how bare gaps reroute and concentrate horizontal flows, creating wakes of accelerated flow within emergent canopies. As the area of a single gap increases, horizontal flow speeds within the canopy also rise, although the increase levels off beyond a certain gap size. Simulations involving pairs of gaps indicated that when a second gap is present in the meadow, the wakes of accelerated flow only interact at relatively short (less than or equal to two times the gap diameter) gap separation distances, irrespective of gap size. The vegetation between the bare gaps confines the enhanced flow to the immediate vicinity of the gaps, thereby limiting the distances at which hydraulic interactions occur. Gaps aligned with the flow direction produce the greatest change in flow speeds, as the wake generated by the upstream gap merges with and reinforces the wake of the downstream gap. In contrast, gaps arranged side by side induce minimal changes in horizontal flow speeds, as the upstream flow is partitioned between the two gaps. Simulations with varying numbers and sizes of gaps (while maintaining a constant total bare area) revealed that flow changes within emergent vegetation are influenced not only by the ratio of bare to vegetated substrate, but also by the degree of fragmentation, defined by the number and size of gaps. Larger and fewer gaps tended to produce a more pronounced impact on in-canopy flow speeds than smaller, more numerous gaps. The differences in flow between scenarios with many smaller gaps and those with fewer, larger gaps became more pronounced as the bare bed coverage increased. While moderate increases in flow within aquatic vegetation can be beneficial, enhancing nutrient replenishment and facilitating the breakdown of boundary layers, flow beyond certain thresholds may act as a stressor. The simulations suggest that fewer, interspersed gaps in less degraded beds (i.e., lower bare bed coverage) are more likely to provide these beneficial

effects, in contrast to larger or more closely spaced gaps, which tend to function as hydrodynamic stressors, potentially creating conditions that could lead to sediment resuspension and redistribution. The loss of aquatic plants that results in large, concentrated bare gaps, rather than smaller, scattered ones, therefore may increase the likelihood of negative feedback on plant-flow interactions. This feedback can intensify erosion, promote sediment resuspension, and undermine habitat stability.

3. **How effectively do topographic variables predict habitat suitability of shortleaf temperate seagrass, and what are the connections of these variables to patchiness patterns?**

The hydrodynamic interactions associated with patchiness, investigated in Chapters 2 and 3, are addressed at a broader spatial scale in Chapter 4 through the use of topographic and sediment variables as indirect proxies of hydrodynamic forcing. While previous chapters focused on how gap size and configuration alter flow and sediment dynamics at the patch and meadow scales, Chapter 4 evaluates how the cumulative imprint of these processes influences seagrass habitat suitability and patch structure across the estuary. Topographic and sediment composition variables were highly effective in predicting the habitat suitability of *Zostera muelleri*, a temperate shortleaf seagrass, in Tauranga Harbour. The seagrass distribution models based on random forests identified elevation as the primary predictor of habitat suitability, with seagrass habitats concentrated near mean sea level, within a relatively narrow elevation range. Similar to other seagrass species inhabiting other systems, elevation is the primary driver of seagrass distribution in the study area, as depth regulates light availability, a critical factor for seagrass survival. While colonising a narrow elevation range provides the advantage of increased light availability, occupying areas near mean sea level requires seagrass to withstand exposure and desiccation during low tides. Sediment composition had the second most important role in determining the habitat suitability for seagrass in the study area, with

sandy substrates associated with higher suitability compared to muddy areas. Sandy sediments provide a stable foundation for seagrass rooting and minimise sediment erosion during tidal movements, which is essential for maintaining seagrass bed structure. Conversely, areas with higher mud content exhibited lower suitability, as muddy sediments can impede seagrass establishment by reducing sediment permeability and altering key physicochemical properties. Additionally, muddy areas often have higher turbidity, which limits light penetration, further hindering seagrass growth. Muddy conditions make it more challenging for seagrass to establish robust root systems, leading to diminished growth and stability. Together, elevation and sediment composition are closely linked to photosynthesis and nutrient uptake, positioning these variables as key determinants of suitability in *Zostera muelleri* habitat. The results of the species distribution models indicated that areas with lower habitat suitability, driven by suboptimal elevation or sediment conditions, exhibited increased fragmentation and a greater number of bare gaps. In the higher intertidal areas seagrass patches were larger and more uniform, as a result of more suitable habitats. Intertidal areas were more commonly associated with continuous patches. In contrast, the lower end of the elevation gradient, especially in subtidal areas with less suitable conditions exhibited increased patchiness, with more bare gaps. Also, shallower, muddier areas showed to increase fragmentation of seagrass. These patterns indicate the environmental challenges facing by seagrass in these areas experiences environmental challenges such as reduced light penetration and sediment instability. However, despite these stressors, seagrass demonstrated resilience, likely due to its ability to tolerate exposure and desiccation during low tides. In the subtidal areas, harsh conditions, including low light and hydrodynamic stress, also contributed to patchy formations. These fragmented patches help reduce stress by buffering against hydrodynamic forces, enabling seagrass to thrive even under challenging environmental pressures in both intertidal and subtidal regions.

5.2 Recommendations for future work

Chapter 3 focused on the transition between relatively uniform vegetation (with consistent density) and bare patches, while the meadows examined in Chapter 2 and Chapter 4 exhibit intra-meadow gradients in vegetation density. Further research should investigate how different vegetation densities influence interactions between gaps in seagrass meadows. Variations in density may alter flow dynamics around gaps, impacting flow mediation of plants, turbulence, and sediment transport. Understanding these effects could help to further refine strategies for seagrass restoration and conservation, ensuring that planting densities promote stability and resilience within the meadow.

It is also important to explore whether the links between tidal flow asymmetry, flow transience, and gap dynamics found in Chapter 2 are consistent across other meadows in the region and in different aquatic ecosystems. Comparative analyses across multiple sites could clarify whether these patterns are unique to certain environmental conditions or are more widely applicable. This suggested future work could involve a combination of fieldwork, remote sensing, and numerical modelling to understand how different tidal regimes and flow conditions interact with seagrass structure. Expanding the scope of study could provide a wider basis for effective habitat management.

Moreover, although Chapter 4 examined the estuary system as a whole, additional research into site-specific controls is needed. Future work should explore the potential role of microtopographic variables in seagrass habitat suitability across multiple sites with varying physical environmental conditions. A multi-site investigation would allow for a wider assessment of how differing physical settings, such as hydrodynamics, sediment composition, and bathymetry, interact with microtopographic features to affect seagrass distribution.

The findings of this study also provide a basis for future modelling efforts that integrate processes across spatial scales. The relationships established between hydrodynamic forcing,

gap-induced patchiness, and habitat suitability can inform spatially explicit models that simulate seagrass dynamics. While Chapters 2 and 3 focused on flow redistribution and sediment transport at the patch and meadow scales, Chapter 4 demonstrates that topographic and sediment variables (proxies of long-term hydrodynamic influence) effectively predict habitat suitability at the estuary scale. These results support a scaling framework in which small-scale processes are embedded through process-based parametrizations. For example, the relationship between gap size and flow acceleration, as quantified in Chapter 2, can be incorporated into spatially explicit models using simplified functional representations. Such parametrizations enable the influence of local-scale interactions to be captured within broader-scale models without the need to explicitly resolve all small-scale dynamics in broader spatial gradients. Future work could formalize this framework into a model that links canopy-scale hydrodynamic interactions with estuarine-scale distribution patterns, enabling scenario testing under varying environmental or anthropogenic conditions. A key step toward this goal is to couple fine-scale flow and sediment transport processes with broader-scale habitat suitability models, in order to assess how spatial heterogeneity in physical conditions drives the development and persistence of patchiness across scales.

5.1 Implications for management and conservation

Based on the findings of this thesis, effective management of seagrass ecosystems should prioritize maintaining meadow continuity and minimizing fragmentation, particularly in areas identified as highly suitable for seagrass growth. The formation of large or numerous bare gaps, which were shown to alter flow dynamics, should also be minimized. Additionally, management strategies should address external pressures such as anchoring and mooring, by controlling the number of boats and limiting the spatial extent of designated mooring areas, which often overlap with vulnerable seagrass habitats. Consideration should also be given to ecological stressors like waterfowl grazing, as some bird species exhibit strong spatial

preferences that may compound habitat degradation in specific zones. In deeper areas of the estuary, where the seabed is less suitable and seagrass was found to be naturally more fragmented, restoration should avoid planting isolated or sparsely distributed seedlings. Instead, transplanting seagrass in dense patches may enhance positive feedbacks that support plant establishment and expansion such as flow attenuation, sediment stabilization, and improved light conditions. Integrating these elements with the predictive habitat suitability models developed in this study can help identify and prioritize areas for conservation or restoration, increasing the long-term resilience and functionality of seagrass meadows.

5.2 Summary

This thesis investigates how spatial patchiness in seagrass meadows influences flow dynamics and habitat suitability. The work combines field observations, numerical modelling, and machine learning to understand both the mechanisms driving hydrodynamic variability across fragmented canopies and the environmental conditions associated with seagrass persistence and distribution. Chapter 2 focuses on the flow structure within and around a single bare gap in a shortleaf seagrass meadow. High-resolution velocity measurements reveal that tidal asymmetry drives horizontal flow acceleration across the gap, increasing turbulence and mixing near its edges. These dynamics have implications for nutrient input, and microhabitat conditions, all of which affect seagrass growth and survival near gap margins. Expanding the spatial scale, Chapter 3 explores how multiple gaps influence flow redistribution across entire meadows. Numerical simulations demonstrate that the effects of fragmentation does not simply scale linearly from single-gap effects. Instead, gap configuration and spacing govern how momentum is redistributed within the canopy. Under the same total bare area, meadows with more numerous, smaller gaps generate stronger intra-canopy flow than those with fewer, larger gaps, even. These findings address the influence of gap structure on flow heterogeneity within aquatic canopies. Chapter 4 shifts to the estuary scale, using a data-driven approach to identify

physical predictors of seagrass distribution. Elevation and sediment composition emerge as dominant variables, reflecting the long-term effects of tidal exposure, light availability, and substrate conditions. Persistent seagrass is associated with sandy substrates and intermediate elevations, while fragmented meadows are more common in muddier or less optimal zones.

Together, the results show that patchiness both results from and contributes to hydrodynamic variability. The spatial configuration of vegetation influences flow, and in turn, physical processes shape habitat structure. These findings support the development of predictive models that account for fragmentation and environmental stress.

Appendix A: Fieldwork dates and details

Table A.1 presents the dates and details of the fieldwork carried out in the Chapter 2, encompassing the survey type, vertical measurement position, and the sampling methodology for flow and turbulence measurements.

Table A.1: Summary of fieldwork conducted, and data gathered. The terms "static" and "sliding" sampling strategies for flow and turbulence denote measurements where instruments were respectively stationary for the full tidal cycle or moved horizontally across the gap and seagrass to provide measurements at few locations.

Dates	Type of survey	Vertical position (height above bed [m])	Sampling strategy for flow and turbulence	Instruments
10/03/2020	Flow and turbulence - Tidal cycle 1	0.13 – 0.16	static	Vectrino profilers
	Water levels		-	RBR CTD
11/03/2020	Flow and turbulence - Tidal cycle 2	0.13 – 0.16	sliding	Vectrino profilers
	Water levels	0.17	-	RBR CTD
	Seagrass biomass (above and below ground vegetation density)	3	-	PVC sediment core
12/03/2020	Flow and turbulence - Tidal cycle 3	0.05 – 0.08	static	Vectrino profilers
	Water levels	0.17	-	RBR CTD
13/03/2020	Flow and turbulence - Tidal cycle 4	0.05 – 0.08	sliding	Vectrino profilers
	Water levels	0.17	-	RBR CTD
	Bed elevation	3	-	RTK-GNSS
	Photographic survey (gap scale)	3	-	Wide-angle mini camera
	Vegetation cover (gap scale)	3	-	NDVI mini camera
30/03/2020	Vegetation cover (meadow scale)	-	-	PlanetScope 4Band Sattelite

Appendix B: Comparison of PlanetScope NDVI and seagrass biomass

Panel a of Figure B.1 presents the normalised difference vegetation index (NDVI) and the sample collection sites for seagrass biomass, which were used to assess correlation with NDVI, as displayed in panel b. The analysis revealed a moderate correlation between NDVI and above-ground biomass, alongside a weaker yet statistically significant correlation between NDVI and below-ground biomass ($p < 0.05$).

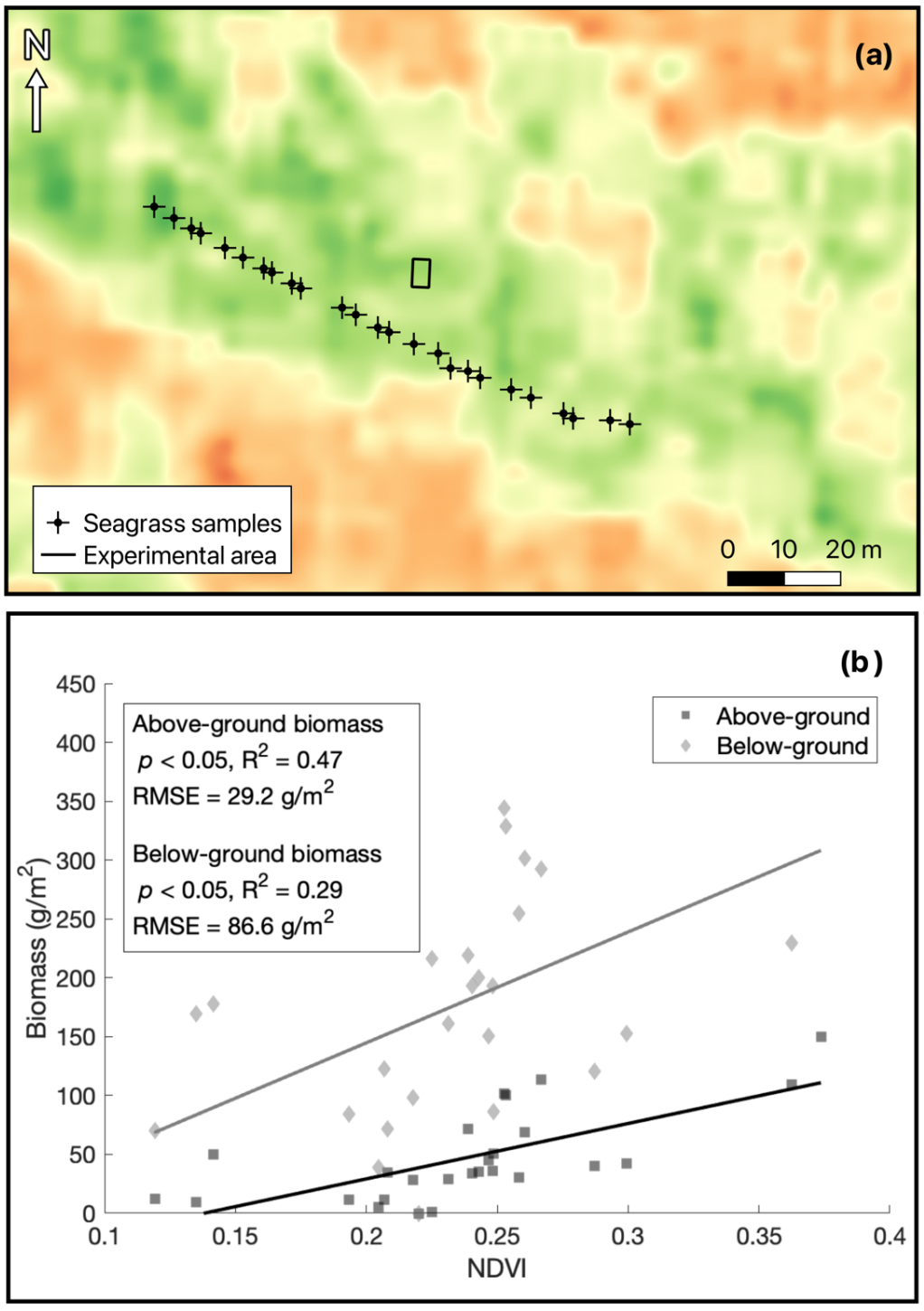

Figure B.1: (a) spatial distribution of seagrass biomass samples, overlapped by the normalised difference vegetation index (NDVI) from PlanetScope imagery, and (b) scatter plots depicting the relationship between NDVI and both above-ground biomass and below-ground biomass, with linear fits represented by grey and black lines, respectively.

Appendix C: Flow measurements at different locations and heights above the bed

To check the consistency of the data used in the analysis in Chapter 2, we compared the data measured at the fixed locations with the measurements taken at other locations within and around the gap. During tides 2 and 4, the outer instruments (seagrass and gap edge) were moved to collect data at different locations within and around the gap, with the instrument in the centre remained fixed. For each location the instruments were slide through, the data was captured for between 10 and 20 min (Figure C.1, Table C.1). The time series of the entire dataset can be seen in Figure C.2.

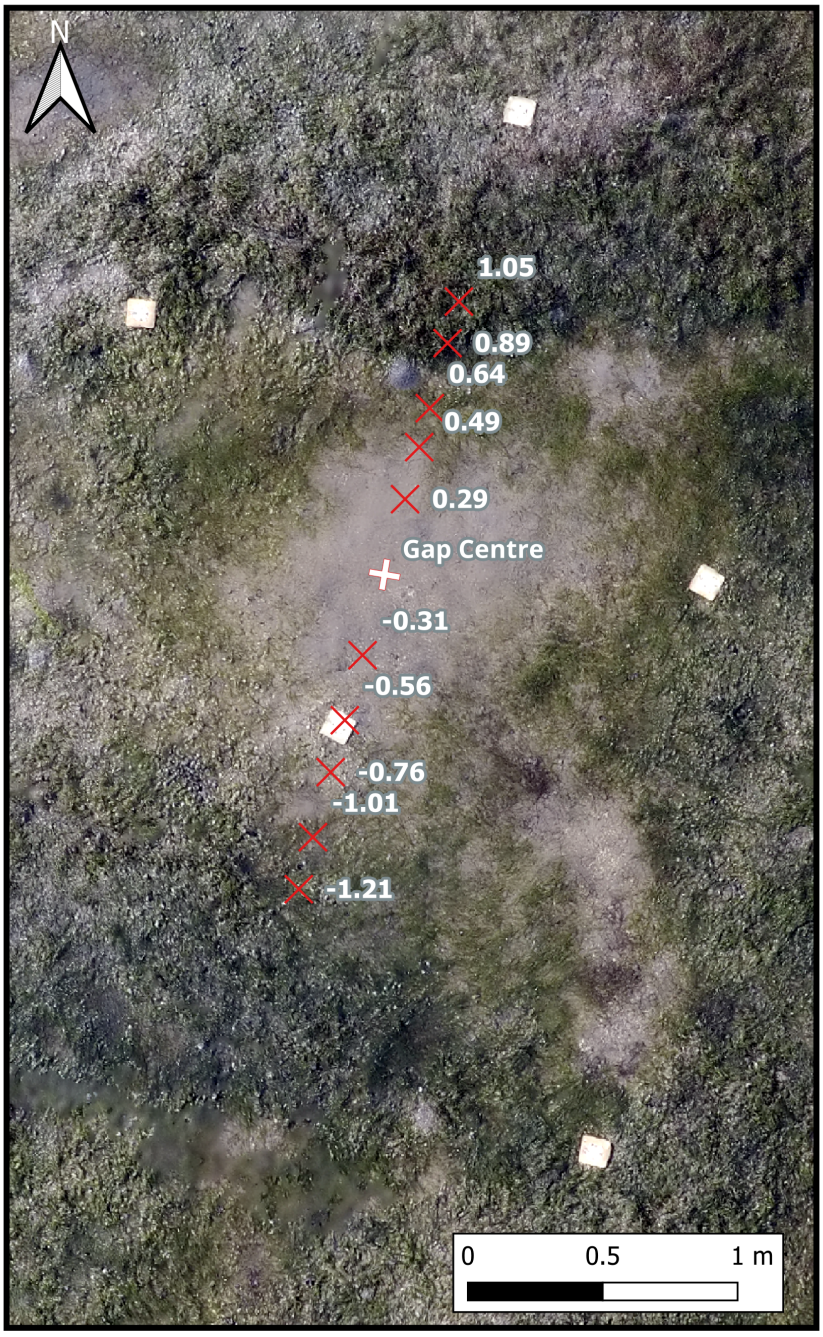

Figure C.1: Locations of the dynamic measurements within and around the gap. The instrument at the Gap Centre was kept in a fixed location throughout. The outer instruments, ('seagrass', positive coordinates and 'gap Edge', negative coordinates) were moved during the several tides. Data was captured over windows of 10-20 min at each location. The coordinates are expressed in meters.

Table C.1: Horizontal locations of each measurement taken during the dynamic measurements on tidal cycles 2 and 4. The numbers refer to the measurements over each tidal cycle, indicated in the time-series in Figure A1. The centre of the gap is set to 0 m in the transect. Heights are measured with respect to the bed.

Measurement #	Cycle 2 (Z = 0.13 – 0.16 m)		Cycle 4 (Z = 0.05 – 0.08 m)	
	Seagrass	Gap Edge	Seagrass	Gap Edge
1	1.05	-1.21	0.89	-1.01
2	0.89	-1.01	0.64	-0.76
3	0.64	-0.76	0.49	-0.56
4	0.49	-0.56	0.29	-0.31
5	0.29	-0.31	1.05	-1.21
6	1.05	-1.21	0.89	-1.01
7	0.64	-0.76	0.64	-0.76
8	0.49	-0.56	0.49	-0.56
9	0.29	-0.31	0.29	-0.31
10	0.49	-0.56	0.49	-0.56
11	0.64	-0.76	0.64	-0.76
12	0.89	-1.01	0.89	-1.01
13	1.05	-1.21	-	-
14	0.89	-1.01	-	-

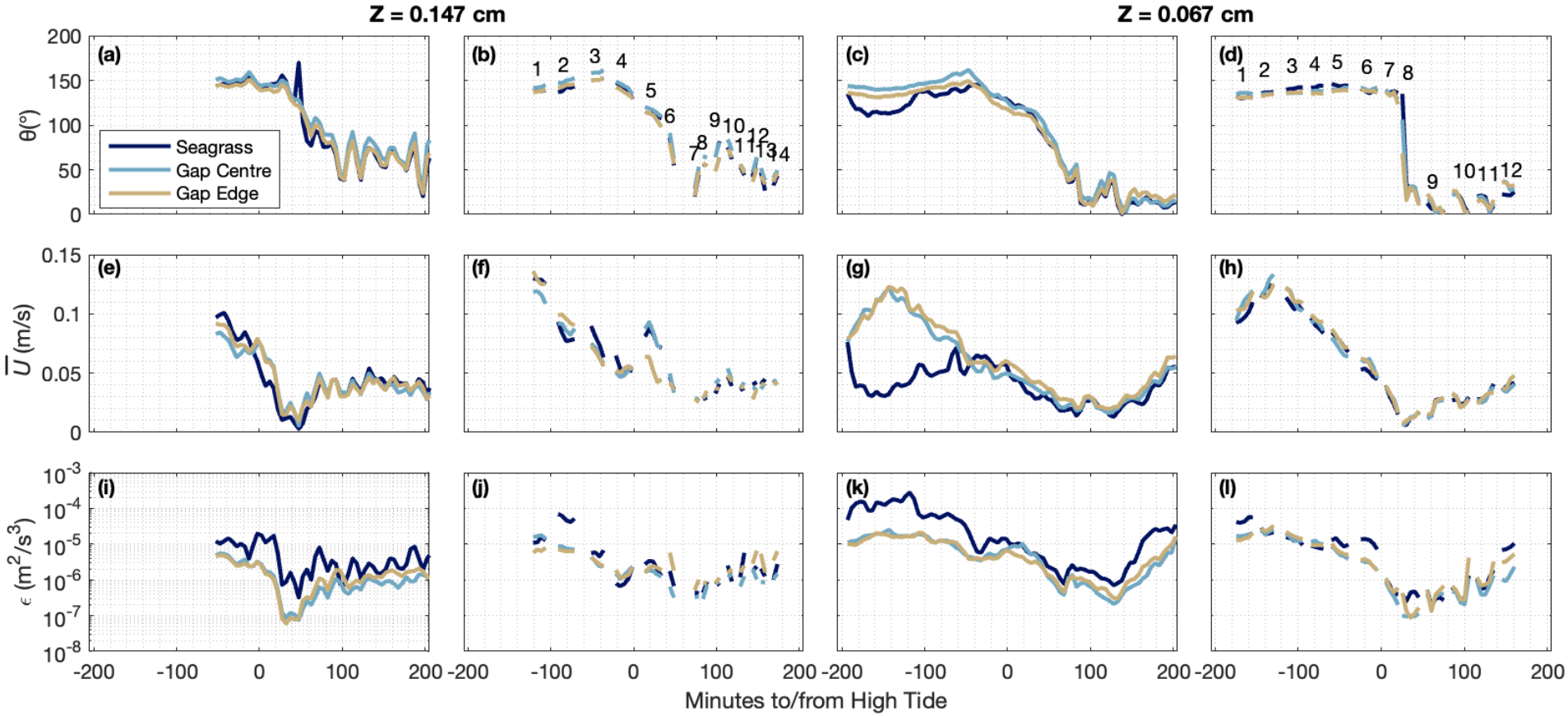

Figure C.2: Time-series of horizontal flow directions (θ, a-d) and speeds ($\overline{U}$, e to h), and rates of turbulent dissipation (ε, i to l) within and around the gap. Each of the four columns represents the data collected during a single tidal. The first two columns show the data collected at 0.147 m above the bed (tidal cycles 1 and 2) and the last two columns the data collected with at 0.067 m above the bed (tidal cycles 3 and 4). The flow direction is given relative to true north.

Appendix D: Determination of turbulent dissipation rates using the structure function

The structure function method has been successfully used in measurements derived by Vectrino Profilers in very shallow coastal environments (e.g., Norris et al., 2019). By employing this approach, turbulence estimates can be obtained by comparing velocities measured at multiple closely spaced locations, along the sampled profile. This method offers the advantage of effectively eliminating large-scale variations in the velocity field, such as wave oscillations, enabling the analysis of smaller-scale turbulent eddies. The second-order structure function, $D(z, r)$, at height (z)and r representing a separation distance between two different velocity cells in the profile is defined as

$$D(z, r) = \overline{(w'(z) - w'(z + r))^2}, \quad \text{(D.1)}$$

where overbars denote a time average. The structure function relies on the fact that the primary cause of velocity variation between two points separated by distance r is the presence of eddies that have a length scale similar to r, and a corresponding velocity scale of w', which is dependent on both r and z. From Kolmogorov's theory, in the inertial subrange and at the length scales of the separation distances r, the dissipation rate of turbulent kinetic energy can be estimated as

$$D(z, r) = C_v \varepsilon^{2/3} r^{2/3}, \quad \text{(D.2)}$$

in which $C_v = 1.41$ is determined empirically (Pope, 2000). Following Wiles et al. (2006), we use

$$D(z, r) = 2\sigma^2 + A\, r^{2/3}, \quad \text{(D.3)}$$

in which σ is the adjusted offset and is associated with errors in the estimates of ε resulting from instrument noise and A is the fitted slope. An analysis was conducted on various separation distances (which are not illustrated), and it was revealed that the smallest errors ($2\sigma^2$) were obtained with separation distances of 7 bins (i.e., over 7 mm).

Appendix E: Validation of the rigid vegetation model (RVM)

We validated the RVM model implemented in Delft3D (see section 2.1) by simulating the laboratory experiments of Vandenbruwaene et al. (2011). In their experiments, patches of emergent saltmarsh *Spartina* with uniform density of different dimensions were used. The average stem diameter and density of the patches were 0.035 m and 658 stems/m^2, respectively. The stem diameter and density lead to a frontal area per canopy volume of 19.74 m^{-1} and a Solid Plant Fraction (SPF) of 0.47, where the frontal area per bed area is defined as $a = nd$. Flow measurements were taken around, inside, and between the patches at a depth which aimed to be close to the depth-averaged flow velocity (for more details see Vandenbruwaene et al. 2011).

To validate the model, we simulated depth-averaged flows speeds in a domain of 26 m x 16 m with a grid resolution of 5 cm in both x and y directions. Emergent vegetation was used in the experiments ($h_v > H$, where $h_v$is vegetation height and H is water depth). As information about the roughness of the channel bed was not available, a uniform standard Chèzy coefficient of 65 $m^{1/2}s^{-1}$ was applied in unvegetated areas.

The results were sensitive to the horizontal eddy viscosity (ν_H) and the cylindrical resistance coefficient (C_d). We compared the depth-averaged flow speeds predicted by the model $\mathbf{U}_{i_p}$ to the observed velocities $\mathbf{U}_{i_o}$ form the laboratory experiments, where the index i denotes each location of measurement at different points around, inside and between the patches of vegetation (Figure A.1). The model performance was quantitatively assessed by the Root Mean-Square-Error (RMSE) and the Relative Mean Absolute Error (RMAE), which is less prone to be influenced by outliers than RMSE (C. Willmott & Matsuura, 2005), the Index of

Agreement (IA) (C. J. Willmott, 1981), and the Correlation Index (r^2, Table A.1). These are defined as

$$\mathrm{RMSE} = \sqrt{\frac{\sum_{i=1}^{N}\left(\left|\mathbf{U}_{i_p}\right| - \left|\mathbf{U}_{i_o}\right|\right)^2}{N}} \tag{A.1}$$

$$\mathrm{RMAE} = \frac{1}{N}\sum_{i=1}^{N}\frac{\left|\left|\mathbf{U}_{i_p}\right| - \left|\mathbf{U}_{i_o}\right|\right|}{\left|\mathbf{U}_{i_o}\right|} \tag{A.2}$$

$$\mathrm{IA} = 1 - \frac{\sum_{i=1}^{N}\left(\left|\mathbf{U}_{i_p}\right| - \left|\mathbf{U}_{i_o}\right|\right)^2}{\sum_{i=1}^{N}\left(\left|\mathbf{U}_{i_p} - \overline{\mathbf{U}_{i_o}}\right| + \left|\mathbf{U}_{i_o} - \overline{\mathbf{U}_{i_o}}\right|\right)^2} \tag{A.3}$$

and

$$r = \frac{N\sum_{i=1}^{N}\left|u_{i_p}\right|\left|u_{i_o}\right| - \sum_{i=1}^{N}\left|u_{i_p}\right|\sum_{i=1}^{N}\left|u_{i_o}\right|}{\left[N\sum_{i=1}^{N}\left|u_{i_p}\right|^2 - \left(\sum_{i=1}^{N}\left|u_{i_p}\right|\right)^2\right]^{1/2}\left[N\sum_{i=1}^{N}\left|u_{i_o}\right|^2 - \left(\sum_{i=1}^{N}\left|u_{i_o}\right|\right)^2\right]^{1/2}} \tag{A.4}$$

We varied ν_H and C_d and the best results were obtained with ν_H = 0.002 m^2/s^2 and C_d = 1.0. The performance parameters calculated with these values are shown in Table E.1.

The model performed well, with RMSE smaller than 0.07 cm/s in all simulations. The RMAE of modelled velocities were in general below 15% the measured velocities and model performance is classified as ‘Good’ according to (Van Rijn et al., 2003). The IA are all above 0.9, which is classified by (Sutherland et al., 2004) as an ‘excellent’ result. Moreover, the modelled velocities showed a very strong correlation with the measured velocities, with correlation coefficients greater than 0.93.

Table E.1: Model performance statistics for validation simulations. According to van Rijn et al. (2003), model performance based on RMAE can be classified as: Excellent (<0.1), Good (0.1–0.3), Reasonable (0.3–0.5), Poor (0.5–0.7), and Bad (>0.7). Similarly, following Sutherland et al. (2004), performance based on the Index of Agreement (IA) is classified as: Excellent (0.8–1.0), Good (0.6–0.8), Reasonable (0.3–0.6), Poor (0.0–0.3), and Bad (<0.0).

Experiment	Patch Size (m)	Interpatch distance (m)	Inlet Flow Speed (m/s)	RMSE (m/s)	RMAE (%)	Index of Agreement (IA)	Correlation Coefficient (R)
A	1	2.3	0.3	0.05	16.09	0.92	0.93
B	2	1.3		0.05	11.1	0.96	0.95
C	3	0.3		0.04	12.4	0.99	0.98
D	1			0.04	11.62	0.97	0.99
E	2			0.05	15.19	0.97	0.96
F	2	3		0.07	15.25	0.91	0.9
G	2		0.1	0.01	7.68	0.98	0.97
H	2		0.2	0.02	8.63	0.98	0.98
I	2	0	0.3	0.04	13.31	0.99	1
J	2	single patch		0.04	13.43	0.98	0.99
Mean				**0.04**	**12.47**	**0.97**	**0.97**

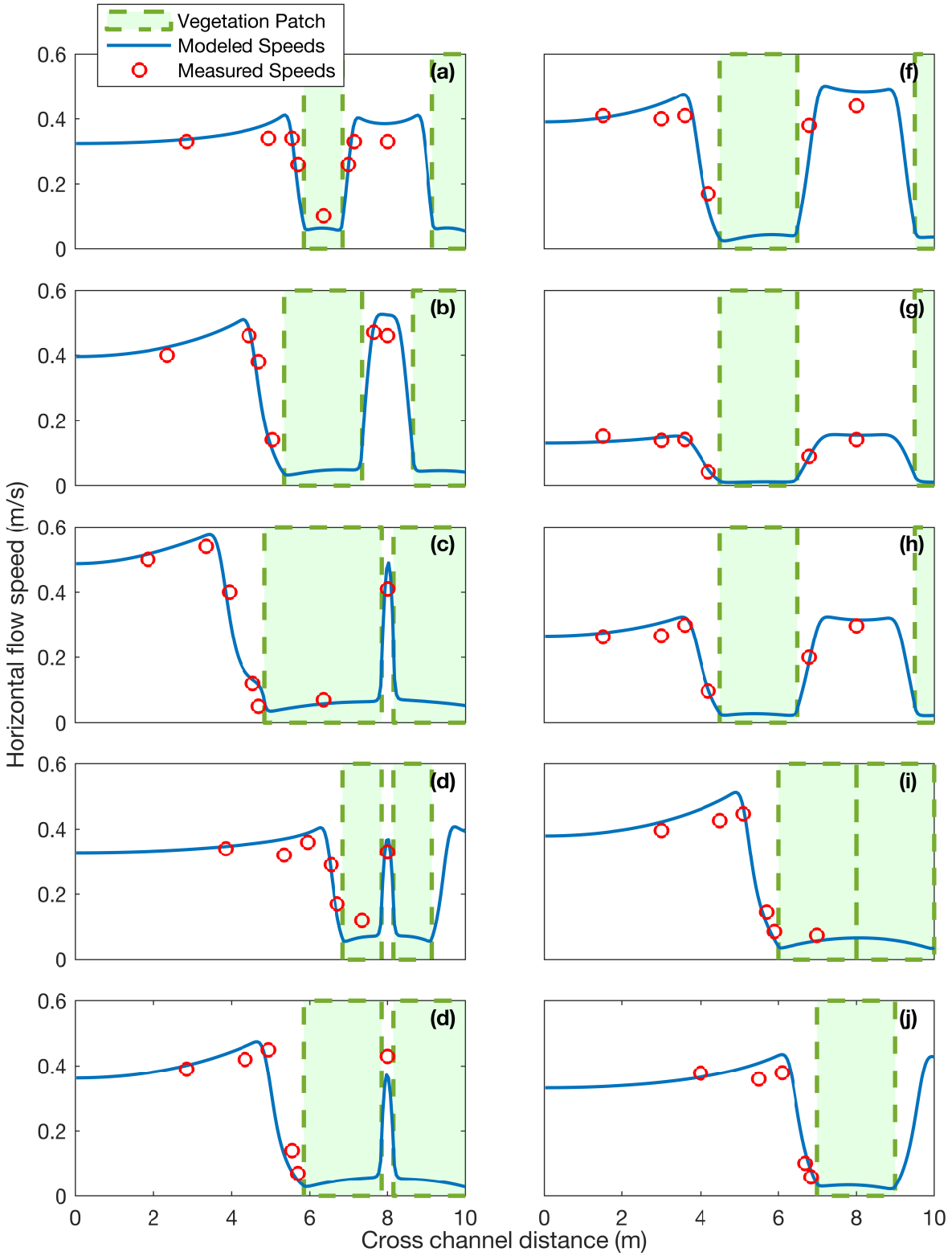

Figure E.1: Transverse (T) profiles of depth-averaged speeds from numerical simulations, ($\mathbf{U}_{i_p}$, blue lines), compared with laboratory observations ($\mathbf{U}_{i_o}$, red lines), from Vanderbruwaene et al. (2011). Each panel (a–j) represents a different experimental configuration, with corresponding patch sizes, interpatch distances, and inlet flow speeds detailed in **Error! Reference source not found.** E.1.

Appendix F: Colourmaps of topographic variables used as predictors for habitat suitability modelling

Figure F.1 presents colourmaps of the variables used as predictors in the species distribution model outlined in Chapter 4.

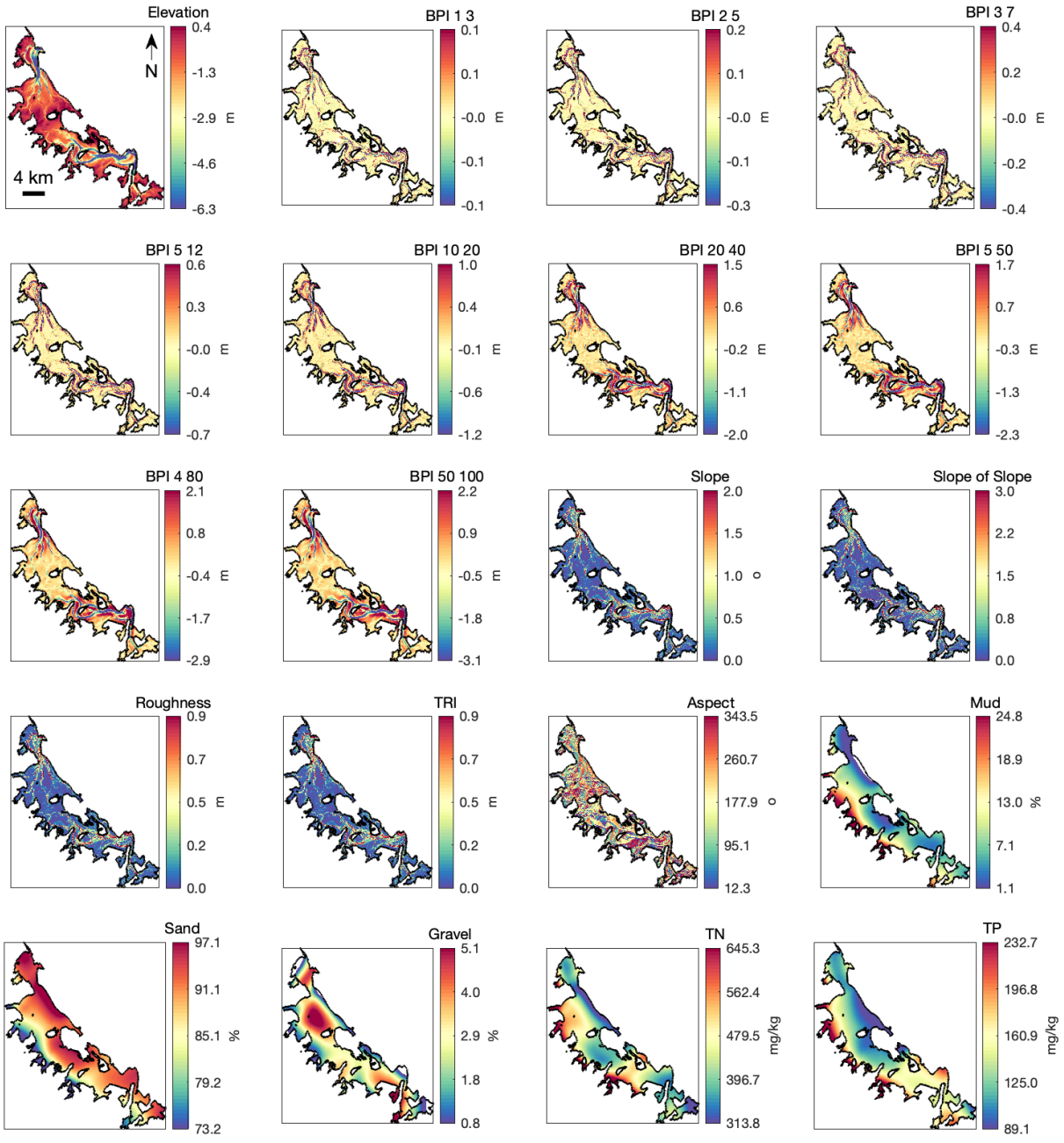

Figure F.1: Colourmaps of variables considered as predictor variables for seagrass habitat suitability. BPI = Bathymetric Position Index; TRI = Terrain Ruggedness Index; TN = Total Nitrogen; TP = Total Phosphorus.

References

Abadie, A., Gobert, S., Bonacorsi, M., Lejeune, P., Pergent, G., & Pergent-Martini, C. (2015). Marine space ecology and seagrasses. Does patch type matter in *Posidonia oceanica* seascapes? *Ecological Indicators*, *57*, 435–446. https://doi.org/10.1016/j.ecolind.2015.05.020

Ackerman, J. D. (2006). Sexual Reproduction of Seagrasses: Pollination in the Marine Context. In *Seagrasses: Biology, ecology and conservation* (pp. 89–109). Springer Netherlands. https://doi.org/10.1007/978-1-4020-2983-7_4

Adams, M. P., Hovey, R. K., Hipsey, M. R., Bruce, L. C., Ghisalberti, M., Lowe, R. J., Gruber, R. K., Ruiz-Montoya, L., Maxwell, P. S., Callaghan, D. P., Kendrick, G. A., & O'Brien, K. R. (2016). Feedback between sediment and light for seagrass: Where is it important? *Limnology and Oceanography*, *61*(6), 1937–1955. https://doi.org/10.1002/lno.10319

Adhitya, A., Bouma, T. J., Folkard, A. M., Van Katwijk, M. M., Callaghan, D. P., De Iongh, H. H., & Herman, P. M. J. (2014). Comparison of the influence of patch-scale and meadow-scale characteristics on flow within seagrass meadows: A flume study. *Marine Ecology Progress Series*, *516*, 49–59. https://doi.org/10.3354/meps10873

Adhitya, A., Folkard, A. M., Govers, L. L., Van Katwijk, M. M., De Iongh, H. H., Herman, P. M. J., & Bouma, T. J. (2016). The exchange of dissolved nutrients between the water column and substrate pore-water due to hydrodynamic adjustment at seagrass meadow edges: A flume study. *Limnology and Oceanography*, *61*(6), 2286–2295. https://doi.org/10.1002/lno.10376

Andrews, E. L., Irving, A. D., Sherman, C. D. H., & Jackson, E. L. (2023). Spatio-temporal analysis of the environmental ranges and phenotypic traits of *Zostera muelleri* subpopulations in Central Queensland. *Estuarine, Coastal and Shelf Science*, *281*, 108191. https://doi.org/10.1016/j.ecss.2022.108191

Aranda, M., Peralta, G., Montes, J., Gracia, F. J., Fivash, G. S., Bouma, T. J., & Van Der Wal, D. (2022). Salt marsh fragmentation in a mesotidal estuary: Implications for medium to long-term management. *Science of The Total Environment*, *846*, 157410. https://doi.org/10.1016/j.scitotenv.2022.157410

Banerjee, T., Katul, G., Fontan, S., Poggi, D., & Kumar, M. (2013). Mean flow near edges and within cavities situated inside dense canopies. *Boundary-Layer Meteorology*, *149*(1), 19–41. https://doi.org/10.1007/s10546-013-9826-x

Barcelona, A., Colomer, J., Soler, M., Gracias, N., & Serra, T. (2021). Meadow fragmentation influences *Posidonia oceanica* density at the edge of nearby gaps. *Estuarine, Coastal and Shelf Science*, *249*, 107106. https://doi.org/10.1016/j.ecss.2020.107106

Bell, S. S. (1999). Gap Dynamics in a Seagrass Landscape. *Ecosystems*, *2*(6), 493–504. https://doi.org/10.1007/s100219900097

Berkenbusch, K., & Rowden, A. A. (2007). An examination of the spatial and temporal generality of the influence of ecosystem engineers on the composition of associated assemblages. *Aquatic Ecology*, *41*(1), 129–147. https://doi.org/10.1007/s10452-006-9053-3

Bertelli, C. M., Stokes, H. J., Bull, J. C., & Unsworth, R. K. F. (2022). The use of habitat suitability modelling for seagrass: A review. *Frontiers in Marine Science*, *9*, 997831. https://doi.org/10.3389/fmars.2022.997831

Boon, J. D., & Byrne, R. J. (1981). On basin hypsometry and the morphodynamic response of coastal inlet systems. *Marine Geology*, *40*(1–2), 27–48. https://doi.org/10.1016/0025-3227(81)90041-4

Bos, A. R., Bouma, T. J., De Kort, G. L. J., & Van Katwijk, M. M. (2007). Ecosystem engineering by annual intertidal seagrass beds: Sediment accretion and modification. *Estuarine, Coastal and Shelf Science*, *74*(1–2), 344–348. https://doi.org/10.1016/j.ecss.2007.04.006

Boström, C., Jackson, E. L., & Simenstad, C. A. (2006). Seagrass landscapes and their effects on associated fauna: A review. *Estuarine, Coastal and Shelf Science*, *68*(3–4), 383–403. https://doi.org/10.1016/j.ecss.2006.01.026

Boudouresque, C. F., Bernard, G., Pergent, G., Shili, A., & Verlaque, M. (2009). Regression of Mediterranean seagrasses caused by natural processes and anthropogenic disturbances and stress: A critical review. *Botm*, *52*(5), 395–418. https://doi.org/10.1515/BOT.2009.057

Bouma, T. J., Olenin, S., Reise, K., & Ysebaert, T. (2009). Ecosystem engineering and biodiversity in coastal sediments: Posing hypotheses. *Helgoland Marine Research*, *63*(1), 95–106. https://doi.org/10.1007/s10152-009-0146-y

Bouma, T. J., Temmerman, S., Van Duren, L. A., Martini, E., Vandenbruwaene, W., Callaghan, D. P., Balke, T., Biermans, G., Klaassen, P. C., Van Steeg, P., Dekker, F., Van De Koppel, J., De Vries, M. B., & Herman, P. M. J. (2013). Organism traits determine the strength of scale-dependent bio-geomorphic feedbacks: A flume study on three intertidal plant species. *Geomorphology*, *180–181*, 57–65. https://doi.org/10.1016/j.geomorph.2012.09.005

Bouma, T. J., Van Duren, L. A., Temmerman, S., Claverie, T., Blanco-Garcia, A., Ysebaert, T., & Herman, P. M. J. (2007). Spatial flow and sedimentation patterns within patches of epibenthic structures: Combining field, flume and modelling experiments. *Continental Shelf Research*, *27*(8), 1020–1045. https://doi.org/10.1016/j.csr.2005.12.019

Bradley, K., & Houser, C. (2009). Relative velocity of seagrass blades: Implications for wave attenuation in low-energy environments. *Journal of Geophysical Research: Earth Surface*, *114*(F1), 2007JF000951. https://doi.org/10.1029/2007JF000951

Breiman, L. (2001). Random forests. *Machine Learning*, *45*(1), 5–32. https://doi.org/10.1023/A:1010933404324

Bryan, K. R., Pilditch, C. A., Tay, H., & Lundquist, C. (2007). The effects of seagrass (*Zostera muelleri*) on boundary-layer hydrodynamics in Whangapoua Estuary, New Zealand. *Journal of Coastal Research*, 668–672. https://doi.org/10.2112/JCR-SI50-126.1

Burnett, N. P., & Gaylord, B. (2022). Flow, form, and force: Methods and frameworks for field studies of macroalgal biomechanics. *Journal of Experimental Botany*, *73*(4), 1122–1138. https://doi.org/10.1093/jxb/erab498

Burrough, P. A., & McDonnell, R. A. (1998). *Principles of Geographical Information Systems*. Oxford University Press.

Capistrant-Fossa, K. A., & Dunton, K. H. (2024). Rapid sea level rise causes loss of seagrass meadows. *Communications Earth & Environment*, *5*(1), 87. https://doi.org/10.1038/s43247-024-01236-7

Carr, J. A., D'Odorico, P., McGlathery, K. J., & Wiberg, P. L. (2016). Spatially explicit feedbacks between seagrass meadow structure, sediment and light: Habitat suitability for seagrass growth. *Advances in Water Resources*, *93*, 315–325. https://doi.org/10.1016/j.advwatres.2015.09.001

Chapman, J. A., Gulliver, J. S., & Wilson, B. N. (2014). Flume instrumentation for measurement of drag on flexible elements under waves. *Experiments in Fluids*, *55*(4), 1715. https://doi.org/10.1007/s00348-014-1715-7

Chen, S.-N., Sanford, L. P., Koch, E. W., Shi, F., & North, E. W. (2007). A nearshore model to investigate the effects of seagrass bed geometry on wave attenuation and suspended sediment transport. *Estuaries and Coasts*, *30*(2), 296–310. https://doi.org/10.1007/BF02700172

Chung, H., & Koseff, J. (2021). Turbulence structure and scales in canopy-wake reattachment. *Physical Review Fluids*, *6*(11), 114605. https://doi.org/10.1103/PhysRevFluids.6.114605

Chung, H., Mandel, T., Zarama, F., & Koseff, J. R. (2021). Local and nonlocal impacts of gaps on submerged canopy flow. *Water Resources Research*, *57*(2). https://doi.org/10.1029/2019WR026915

Clark, D., Taiapa, C., Sinner, J., Taikato, V. R., Culliford, D., Battershill, C. N., & Patterson, M. (2018). *2016 subtidal ecological survey of Tauranga Harbour and development of benthic health models*. Cawthron Institute.

Colomer, J., & Serra, T. (2021). The world of edges in submerged vegetated marine canopies: From patch to canopy scale. *Water*, *13*(17), 2430. https://doi.org/10.3390/w13172430

Colomer, J., Soler, M., Serra, T., Casamitjana, X., & Oldham, C. (2017). Impact of anthropogenically created canopy gaps on wave attenuation in a *Posidonia oceanica* seagrass meadow. *Marine Ecology Progress Series*, *569*, 103–116. https://doi.org/10.3354/meps12090

Contti Neto, N., Pomeroy, A., Lowe, R., & Ghisalberti, M. (2022). Seagrass meadows reduce wind-wave driven sediment resuspension in sheltered environment. *Frontiers in Marine Science*, *8*, 733542. https://doi.org/10.3389/fmars.2021.733542

Cornacchia, L., Davies, G., Grabowski, R., van der Wal, D., van de Koppel, J., Wharton, G., & Bouma, T. (2016). *Biophysical interactions in fluvial ecosystems: Effects of submerged aquatic macrophytes on hydro-morphological processes and ecosystem functioning*. EPSC2016-8454. https://ui.adsabs.harvard.edu/abs/2016EGUGA..18.8454C

Cornacchia, L., Van De Koppel, J., Van Der Wal, D., Wharton, G., Puijalon, S., & Bouma, T. J. (2018). Landscapes of facilitation: How self-organized patchiness of aquatic macrophytes promotes diversity in streams. *Ecology*, *99*(4), 832–847. https://doi.org/10.1002/ecy.2177

Crawshaw, J. (2020). *Seagrass health monitoring in Tauranga Harbour* [Enviromental Publication]. Bay of Plenty Regional Council.

Cussioli, M. C., Bryan, K. R., Pilditch, C. A., De Lange, W. P., & Bischof, K. (2019). Light penetration in a temperate meso-tidal lagoon: Implications for seagrass growth and dredging in Tauranga Harbour, New Zealand. *Ocean & Coastal Management*, *174*, 25–37. https://doi.org/10.1016/j.ocecoaman.2019.01.014

da Silva, T. D., Mullarney, J. C., Pilditch, C. A., & Coco, G. (2024). The interaction between vegetation patchiness and tidal flows in a shortleaf seagrass meadow. *Limnology and Oceanography*, 1–14. https://doi.org/10.1002/lno.12679

De Boer, W. F. (2007). Seagrass–sediment interactions, positive feedbacks and critical thresholds for occurrence: A review. *Hydrobiologia*, *591*(1), 5–24. https://doi.org/10.1007/s10750-007-0780-9

De Falco, G., Ferrari, S., Cancemi, G., & Baroli, M. (2000). Relationship between sediment distribution and *Posidonia oceanica* seagrass. *Geo-Marine Letters*, *20*(1), 50–57. https://doi.org/10.1007/s003670000030

de Lima, P. H. S., Janzen, J. G., & Nepf, H. M. (2015). Flow patterns around two neighboring patches of emergent vegetation and possible implications for deposition and vegetation growth. *Environmental Fluid Mechanics*, *15*(4), 881–898. https://doi.org/10.1007/s10652-015-9395-2

de Ruiter, P. J., Mullarney, J. C., Bryan, K. R., & Winter, C. (2019). The links between entrance geometry, hypsometry and hydrodynamics in shallow tidally dominated basins. *Earth Surface Processes and Landforms*, *44*(10), 1957–1972. https://doi.org/10.1002/esp.4622

Deltares. (2024). *Delft3D-FLOW simulation of multidimensional hydrodynamic flows and transport phenomena, including sediment: User manual hydrodynamics*. https://oss.deltares.nl/web/delft3d/manuals

Dos Santos, V. M., Matheson, F. E., Pilditch, C. A., & Elger, A. (2013). Seagrass resilience to waterfowl grazing in a temperate estuary: A multi-site experimental study. *Journal of*

Experimental Marine Biology and Ecology, *446*, 194–201. https://doi.org/10.1016/j.jembe.2013.05.030

Dronkers, J. (1986). Tidal asymmetry and estuarine morphology. *Netherlands Journal of Sea Research*, *20*(2–3), 117–131. https://doi.org/10.1016/0077-7579(86)90036-0

Duarte, C. M. (2002). The future of seagrass meadows. *Environmental Conservation*, *29*(2), 192–206. https://doi.org/10.1017/S0376892902000127

Duarte, C. M., Fourqurean, J. W., Krause-Jensen, D., & Olesen, B. (2006). Dynamics of seagrass stability and change. In *Seagrasses: Biology, Ecology and Conservation* (pp. 271–294). Springer Netherlands. https://doi.org/10.1007/1-4020-2983-7_11

Duarte, C. M., Kennedy, H., Marbà, N., & Hendriks, I. (2013). Assessing the capacity of seagrass meadows for carbon burial: Current limitations and future strategies. *Ocean & Coastal Management*, *83*, 32–38. https://doi.org/10.1016/j.ocecoaman.2011.09.001

Dubos, N., Préau, C., Lenormand, M., Papuga, G., Monsarrat, S., Denelle, P., Louarn, M. L., Heremans, S., May, R., Roche, P., & Luque, S. (2022). Assessing the effect of sample bias correction in species distribution models. *Ecological Indicators*, *145*, 109487. https://doi.org/10.1016/j.ecolind.2022.109487

El Allaoui, N., Serra, T., Colomer, J., Soler, M., Casamitjana, X., & Oldham, C. (2016). Interactions between Fragmented Seagrass Canopies and the Local Hydrodynamics. *PLOS ONE*, *11*(5), e0156264. https://doi.org/10.1371/journal.pone.0156264

Ellis, J. I., Clark, D., Hewitt, J. E., Taiapa, C., Sinner, J., & Patterson, M. (2017). *Ecological survey of Tauranga Harbour*. Cawthron Institute.

Escapa, M., Perillo, G. M. E., & Iribarne, O. (2015). Biogeomorphically driven salt pan formation in Sarcocornia-dominated salt-marshes. *Geomorphology*, *228*, 147–157. https://doi.org/10.1016/j.geomorph.2014.08.032

Flowers, G. J. L., Needham, H. R., Bulmer, R. H., Lohrer, A. M., & Pilditch, C. A. (2024). The effect of sediment mud content on primary production in seagrass and unvegetated intertidal flats. *Estuaries and Coasts*. https://doi.org/10.1007/s12237-024-01403-1

Folkard, A. M. (2019). Biophysical interactions in fragmented marine canopies: Fundamental processes, consequences, and upscaling. *Frontiers in Marine Science*, *6*, 279. https://doi.org/10.3389/fmars.2019.00279

Fonseca, M., & Fisher, J. (1986). A comparison of canopy friction and sediment movement between four species of seagrass with reference to their ecology and restoration. *Marine Ecology Progress Series*, *29*, 15–22. https://doi.org/10.3354/meps029015

Fonseca, M. S., & Bell, S. S. (1998). Influence of physical setting on seagrass landscapes near Beaufort, North Carolina, USA. *Marine Ecology Progress Series*, *171*, 109–121. https://doi.org/10.3354/meps171109

Fonseca, M. S., Fourqurean, J. W., & Koehl, M. A. R. (2019). Effect of seagrass on current Speed: Importance of flexibility vs. shoot density. *Frontiers in Marine Science*, *6*, 376. https://doi.org/10.3389/fmars.2019.00376

Fonseca, M. S., Koehl, M. A. R., & Kopp, B. S. (2007a). Biomechanical factors contributing to self-organization in seagrass landscapes. *Journal of Experimental Marine Biology and Ecology*, *340*(2), 227–246. https://doi.org/10.1016/j.jembe.2006.09.015

Fonseca, M. S., Koehl, M. A. R., & Kopp, B. S. (2007b). Biomechanical factors contributing to self-organization in seagrass landscapes. *Journal of Experimental Marine Biology and Ecology*, *340*(2), 227–246. https://doi.org/10.1016/j.jembe.2006.09.015

Forrester, J., Leonardi, N., Cooper, J. R., & Kumar, P. (2024). Seagrass as a nature-based solution for coastal protection. *Ecological Engineering*, *206*, 107316. https://doi.org/10.1016/j.ecoleng.2024.107316

Friedrichs, C. T., & Aubrey, D. G. (1988). Non-linear tidal distortion in shallow well-mixed estuaries: A synthesis. *Estuarine, Coastal and Shelf Science*, *27*(5), 521–545. https://doi.org/10.1016/0272-7714(88)90082-0

Gambi, M. C., Nowell, A. R., & Jumars, P. A. (1990). Flume observations on flow dynamics in *Zostera marina* (eelgrass) beds. *Marine Ecology Progress Series*, *61*, 159–169. https://doi.org/10.3354/meps061159

Ganthy, F., Soissons, L., Sauriau, P., Verney, R., & Sottolichio, A. (2015). Effects of short flexible seagrass *Zostera noltei* on flow, erosion and deposition processes determined using flume experiments. *Sedimentology*, *62*(4), 997–1023. https://doi.org/10.1111/sed.12170

Gaylord, B., Reed, D. C., Raimondi, P. T., & Washburn, L. (2006). Macroalgal spore dispersal in coastal environment: Mechanistic insights revealed by theory and experiment. *Ecological Monographs*, *76*(4), 481–502. https://doi.org/10.1890/0012-9615(2006)076[0481:MSDICE]2.0.CO;2

Ghisalberti, M., & Nepf, H. (2005). Mass transport in vegetated shear flows. *Environmental Fluid Mechanics*, *5*(6), 527–551. https://doi.org/10.1007/s10652-005-0419-1

Ghisalberti, M., & Nepf, H. (2006). The structure of the shear layer in flows over rigid and flexible canopies. *Environmental Fluid Mechanics*, *6*(3), 277–301. https://doi.org/10.1007/s10652-006-0002-4

Glud, R. N. (2008). Oxygen dynamics of marine sediments. *Marine Biology Research*, *4*(4), 243–289. https://doi.org/10.1080/17451000801888726

Goring, D. G., & Nikora, V. I. (2002). Despiking Acoustic Doppler Velocimeter Data. *Journal of Hydraulic Engineering*, *128*(1), 117–126. https://doi.org/10.1061/(ASCE)0733-9429(2002)128:1(117)

Granata, T., Serra, T., Colomer, J., Casamitjana, X., Duarte, C., & Gacia, E. (2001). Flow and particle distributions in a nearshore seagrass meadow before and after a storm. *Marine Ecology Progress Series*, *218*, 95–106. https://doi.org/10.3354/meps218095

Green, M. O., & Coco, G. (2014). Review of wave-driven sediment resuspension and transport in estuaries: Wave-driven sediment transport. *Reviews of Geophysics*, *52*(1), 77–117. https://doi.org/10.1002/2013RG000437

Grew, M., Gaston, T. F., Griffin, A. S., Duce, S. J., & Raoult, V. (2024). Ray bioturbation rates suggest they shape estuary processes. *Remote Sensing in Ecology and Conservation*, rse2.411. https://doi.org/10.1002/rse2.411

Grinnell, J. (1917). The miche-relationships of the California thrasher. *The Auk*, *34*(4), 427–433. https://doi.org/10.2307/4072271

Guisan, A., & Thuiller, W. (2005). Predicting species distribution: Offering more than simple habitat models. *Ecology Letters*, *8*(9), 993–1009. https://doi.org/10.1111/j.1461-0248.2005.00792.x

Ha, N. T., Manley-Harris, M., Pham, T. D., & Hawes, I. (2021). Detecting multi-decadal changes in seagrass cover in Tauranga Harbour, New Zealand, using Landsat imagery and boosting ensemble classification techniques. *ISPRS International Journal of Geo-Information*, *10*(6), 371. https://doi.org/10.3390/ijgi10060371

Hamed, A. M., Peterlein, A. M., & Speck, I. (2020). Characteristics of the turbulent flow within short canopy gaps. *Physical Review Fluids*, *5*(12), 123801. https://doi.org/10.1103/PhysRevFluids.5.123801

Hansen, J. C. R., & Reidenbach, M. A. (2013). Seasonal growth and senescence of a *Zostera marina* seagrass meadow alters wave-dominated flow and sediment suspension within a coastal bay. *Estuaries and Coasts*, *36*(6), 1099–1114. https://doi.org/10.1007/s12237-013-9620-5

Hansen, J. C. R., & Reidenbach, M. A. (2017). Turbulent mixing and fluid transport within Florida Bay seagrass meadows. *Advances in Water Resources*, *108*, 205–215. https://doi.org/10.1016/j.advwatres.2017.08.001

Hargis, C. D., Bissonette, J. A., & David, J. L. (1998). The behavior of landscape metrics commonly used in the study of habitat fragmentation. *Landscape Ecology*, *13*(3), 167–186. https://doi.org/10.1023/A:1007965018633

Hartog, C. D., & Kuo, J. (2006). Taxonomy and biogeography of seagrasses. In *Seagrasses: Biology, ecology and conservation* (pp. 1–23). Springer Netherlands. https://doi.org/10.1007/978-1-4020-2983-7_1

Heath, R. A. (1976). Broad classification of New Zealand inlets with emphasis on residence times. *New Zealand Journal of Marine and Freshwater Research*, *10*(3), 429–444. https://doi.org/10.1080/00288330.1976.9515628

Heath, R. A. (1985). A review of the physical oceanography of the seas around New Zealand—1982. *New Zealand Journal of Marine and Freshwater Research*, *19*(1), 79–124. https://doi.org/10.1080/00288330.1985.9516077

Hemminga, M. A., & Duarte, C. M. (2000). *Seagrass ecology*. Cambridge University Press.

Horstman, E., Dohmen-Janssen, M., & Hulscher, S. J. M. H. (2013). Modeling tidal dynamics in a mangrove creek catchment in Delft3D. *Coastal Dynamics*, *2013*, 833–844.

Hovel, K. A., Fonseca, M. S., Myer, D. I., Kenworthy, W. J., & Whitfield, P. E. (2002). Effects of seagrass landscape structure, structural complexity and hydrodynamic regime on macrofaunal densities in North Carolina seagrass beds. *Marine Ecology Progress Series*, *243*, 11–24. https://doi.org/10.3354/meps243011

Hu, Z., Lei, J., Liu, C., & Nepf, H. (2018). Wake structure and sediment deposition behind models of submerged vegetation with and without flexible leaves. *Advances in Water Resources*, *118*, 28–38. https://doi.org/10.1016/j.advwatres.2018.06.001

Huettel, M., Berg, P., & Kostka, J. E. (2014). Benthic Exchange and Biogeochemical Cycling in Permeable Sediments. *Annual Review of Marine Science*, *6*(1), 23–51. https://doi.org/10.1146/annurev-marine-051413-012706

Hume, T. M., Snelder, T., Weatherhead, M., & Liefting, R. (2007). A controlling factor approach to estuary classification. *Ocean & Coastal Management*, *50*(11–12), 905–929. https://doi.org/10.1016/j.ocecoaman.2007.05.009

Hurd, C. L. (2000). Water motion, marine macroalgal physiology and production. *Journal of Phycology*, *36*(3), 453–472. https://doi.org/10.1046/j.1529-8817.2000.99139.x

Igaz, D., Šinka, K., Varga, P., Vrbičanová, G., Aydın, E., & Tárník, A. (2021). The Evaluation of the Accuracy of Interpolation Methods in Crafting Maps of Physical and Hydro-Physical Soil Properties. *Water*, *13*(2), 212. https://doi.org/10.3390/w13020212

Infantes, E., Orfila, A., Simarro, G., Terrados, J., Luhar, M., & Nepf, H. (2012). Effect of a seagrass (*Posidonia oceanica*) meadow on wave propagation. *Marine Ecology Progress Series*, *456*, 63–72. https://doi.org/10.3354/meps09754

Inglis, G. J., Gust, N., Fitridge, I., Floerl, O., Hayden, B. J., & Fenwick, G. D. (2006). *Port of Tauranga: Second baseline survey for non-indigenous marine species*. NIWA.

Irving, A. D., Connell, S. D., & Russell, B. D. (2011). Restoring coastal plants to improve global carbon storage: Reaping what we sow. *PLoS ONE*, *6*(3), e18311. https://doi.org/10.1371/journal.pone.0018311

Jones, C. G., Lawton, J. H., & Shachak, M. (1994a). Organisms as ecosystem engineers. In F. B. Samson & F. L. Knopf, *Ecosystem Management* (pp. 130–147). Springer New York. https://doi.org/10.1007/978-1-4612-4018-1_14

Jones, C. G., Lawton, J. H., & Shachak, M. (1994b). *Organisms as Ecosystem Engineers*. 15.

Kaller, M. D., Keim, R. F., Edwards, B. L., Raynie Harlan, A., Pasco, T. E., Kelso, W. E., & Allen Rutherford, D. (2015). Aquatic vegetation mediates the relationship between hydrologic connectivity and water quality in a managed floodplain. *Hydrobiologia*, *760*(1), 29–41. https://doi.org/10.1007/s10750-015-2300-7

Kline, S. J., Reynolds, W. C., Schraub, F. A., & Runstadler, P. W. (1967). The structure of turbulent boundary layers. *Journal of Fluid Mechanics*, *30*(4), 741–773. https://doi.org/10.1017/S0022112067001740

Koch, E. W., Ackerman, J. D., Verduin, J., & Keulen, M. V. (2006). Fluid dynamics in seagrass ecology—From molecules to ecosystems. In *Seagrasses: Biology, ecology and conservation* (pp. 193–225). Springer Netherlands. https://doi.org/10.1007/978-1-4020-2983-7_8

Koehl, M. A. R. (2022a). Ecological biomechanics of marine macrophytes. *Journal of Experimental Botany*, *73*(4), 1104–1121. https://doi.org/10.1093/jxb/erab536

Koehl, M. A. R. (2022b). Ecological biomechanics of marine macrophytes. *Journal of Experimental Botany*, *73*(4), 1104–1121. https://doi.org/10.1093/jxb/erab536

Kramer, O. (2016). Scikit-Learn. In O. Kramer, *Machine learning for evolution strategies* (Vol. 20, pp. 45–53). Springer International Publishing. https://doi.org/10.1007/978-3-319-33383-0_5

Lai, S., Yaakub, S. M., Poh, T. S. M., Bouma, T. J., & Todd, P. A. (2018). Unlikely nomads: Settlement, establishment, and dislodgement processes of vegetative seagrass fragments. *Frontiers in Plant Science*, *9*, 160. https://doi.org/10.3389/fpls.2018.00160

Lampietro, P. J., Kvitek, R. G., & Morris, E. (2005). Recent advances in automated genus-specific marine Habitat mapping enabled by high-resolution multibeam bathymetry. *Marine Technology Society Journal*, *39*(3), 83–93. https://doi.org/10.4031/002533205787442495

Larsen, L. G., & Harvey, J. W. (2011). Modeling of hydroecological feedbacks predicts distinct classes of landscape pattern, process, and restoration potential in shallow aquatic ecosystems. *Geomorphology*, *126*(3–4), 279–296. https://doi.org/10.1016/j.geomorph.2010.03.015

Lee, H., Golicz, A. A., Bayer, P. E., Jiao, Y., Tang, H., Paterson, A. H., Sablok, G., Krishnaraj, R. R., Chan, C.-K. K., Batley, J., Kendrick, G. A., Larkum, A. W. D., Ralph, P. J., & Edwards, D. (2016). The genome of a southern hemisphere seagrass species (*Zostera muelleri*). *Plant Physiology*, *172*(1), 272–283. https://doi.org/10.1104/pp.16.00868

Lefebvre, A., Thompson, C. E. L., & Amos, C. L. (2010). Influence of *Zostera marina* canopies on unidirectional flow, hydraulic roughness and sediment movement. *Continental Shelf Research*, *30*(16), 1783–1794. https://doi.org/10.1016/j.csr.2010.08.006

Licci, S., Marmonier, P., Wharton, G., Delolme, C., Mermillod-Blondin, F., Simon, L., Vallier, F., Bouma, T. J., & Puijalon, S. (2022). Scale-dependent effects of vegetation on flow velocity and biogeochemical conditions in aquatic systems. *Science of The Total Environment*, *833*, 155123. https://doi.org/10.1016/j.scitotenv.2022.155123

Lightbody, A. F., Avener, M. E., & Nepf, H. M. (2008). Observations of short-circuiting flow paths within a free-surface wetland in Augusta, Georgia, U.S.A. *Limnology and Oceanography*, *53*(3), 1040–1053. https://doi.org/10.4319/lo.2008.53.3.1040

Loidi, J. (2017). Dynamism in vegetation: Vegetation changes on a short time scale. In J. Loidi (Ed.), *The Vegetation of the Iberian Peninsula* (Vol. 12, pp. 81–99). Springer International Publishing. https://doi.org/10.1007/978-3-319-54784-8_3

Lowe, R. J., Koseff, J. R., & Monismith, S. G. (2005). Oscillatory flow through submerged canopies: 1. Velocity structure. *Journal of Geophysical Research: Oceans*, *110*(C10), 2004JC002788. https://doi.org/10.1029/2004JC002788

Luhar, M., Coutu, S., Infantes, E., Fox, S., & Nepf, H. (2010). Wave-induced velocities inside a model seagrass bed. *Journal of Geophysical Research: Oceans*, *115*(C12), 2010JC006345. https://doi.org/10.1029/2010JC006345

Luhar, M., Rominger, J., & Nepf, H. (2008). Interaction between flow, transport and vegetation spatial structure. *Environmental Fluid Mechanics*, *8*(5–6), 423–439. https://doi.org/10.1007/s10652-008-9080-9

Madsen, J. D., Chambers, P. A., James, W. F., Koch, E. W., & Westlake, D. F. (2001). The interaction between water movement, sediment dynamics and submersed macrophytes. *Hydrobiologia*, *444*(1/3), 71–84. https://doi.org/10.1023/A:1017520800568

Maji, S., Hanmaiahgari, P., Balachandar, R., Pu, J., Ricardo, A., & Ferreira, R. (2020). A Review on hydrodynamics of free surface flows in emergent vegetated channels. *Water*, *12*(4), 1218. https://doi.org/10.3390/w12041218

Mariotti, G., Spivak, A. C., Luk, S. Y., Ceccherini, G., Tyrrell, M., & Gonneea, M. E. (2020). Modeling the spatial dynamics of marsh ponds in New England salt marshes. *Geomorphology*, *365*, 107262. https://doi.org/10.1016/j.geomorph.2020.107262

Matheson, F. E. (2009). *New Zealand seagrass: General information guide*. NIWA.

Matheson, F. E., & Schwarz, A.-M. (2007). Growth responses of *Zostera capricorni* to estuarine sediment conditions. *Aquatic Botany*, *87*(4), 299–306. https://doi.org/10.1016/j.aquabot.2007.07.002

Maxwell, P. S., Eklöf, J. S., Van Katwijk, M. M., O'Brien, K. R., De La Torre-Castro, M., Boström, C., Bouma, T. J., Krause-Jensen, D., Unsworth, R. K. F., Van Tussenbroek, B. I., & Van Der Heide, T. (2017). The fundamental role of ecological feedback mechanisms for the adaptive management of seagrass ecosystems – a review. *Biological Reviews*, *92*(3), 1521–1538. https://doi.org/10.1111/brv.12294

Meire, D. W. S. A., Kondziolka, J. M., & Nepf, H. M. (2014). Interaction between neighboring vegetation patches: Impact on flow and deposition. *Water Resources Research*, *50*(5), 3809–3825. https://doi.org/10.1002/2013WR015070

Mena, A., & Fernández-Salas, L. M. (2024). Optimizing bathymetric position index (BPI) calculation: An analysis of parameters and recommendations for the selection of their optimal values. *Applied Computing and Geosciences*, *23*, 100168. https://doi.org/10.1016/j.acags.2024.100168

Meysick, L., Infantes, E., & Boström, C. (2019). The influence of hydrodynamics and ecosystem engineers on eelgrass seed trapping. *PLOS ONE*, *14*(9), e0222020. https://doi.org/10.1371/journal.pone.0222020

Mills, V. S., & Berkenbusch, K. (2009). Seagrass (*Zostera muelleri*) patch size and spatial location influence infaunal macroinvertebrate assemblages. *Estuarine, Coastal and Shelf Science*, *81*(1), 123–129. https://doi.org/10.1016/j.ecss.2008.10.005

Möller, I., Kudella, M., Rupprecht, F., Spencer, T., Paul, M., Van Wesenbeeck, B. K., Wolters, G., Jensen, K., Bouma, T. J., Miranda-Lange, M., & Schimmels, S. (2014). Wave attenuation over coastal salt marshes under storm surge conditions. *Nature Geoscience*, *7*(10), 727–731. https://doi.org/10.1038/ngeo2251

Montefalcone, M., Parravicini, V., Vacchi, M., Albertelli, G., Ferrari, M., Morri, C., & Bianchi, C. N. (2010). Human influence on seagrass habitat fragmentation in NW Mediterranean Sea. *Estuarine, Coastal and Shelf Science*, *86*(2), 292–298. https://doi.org/10.1016/j.ecss.2009.11.018

Mullarney, J. C., & Henderson, S. M. (2018). Flows within marine vegetation canopies. In *Advances In Coastal Hydraulics* (pp. 1–46). https://doi.org/10.1142/9789813231283_0001

Nepf, H., & Ghisalberti, M. (2008). Flow and transport in channels with submerged vegetation. *Acta Geophysica*, *56*(3), 753–777. https://doi.org/10.2478/s11600-008-0017-y

Nepf, H. M. (2012a). Flow and Transport in Regions with Aquatic Vegetation. *Annual Review of Fluid Mechanics*, *44*(1), 123–142. https://doi.org/10.1146/annurev-fluid-120710-101048

Nepf, H. M. (2012b). Hydrodynamics of vegetated channels. *Journal of Hydraulic Research*, *50*(3), 262–279. https://doi.org/10.1080/00221686.2012.696559

Nikora, V. (2010). Hydrodynamics of aquatic ecosystems: An interface between ecology, biomechanics and environmental fluid mechanics. *River Research and Applications*, *26*(4), 367–384. https://doi.org/10.1002/rra.1291

Norris, B. K., Mullarney, J. C., Bryan, K. R., & Henderson, S. M. (2019). Turbulence Within Natural Mangrove Pneumatophore Canopies. *Journal of Geophysical Research: Oceans*, *124*(4), 2263–2288. https://doi.org/10.1029/2018JC014562

Norris, B. K., Mullarney, J. C., Bryan, K. R., & Henderson, S. M. (2021). Relating millimeter-scale turbulence to meter-scale subtidal erosion and accretion across the fringe of a coastal mangrove forest. *Earth Surface Processes and Landforms*, *46*(3), 573–592. https://doi.org/10.1002/esp.5047

Nurdin, N., Amri, K., Mashoreng, S., & Komatsu, T. (2022). Estimation of Seagrass Biomass by In Situ Measurement and Remote Sensing Technology on Small Islands, Indonesia. *Ocean Science Journal*, *57*(1), 118–129. https://doi.org/10.1007/s12601-022-00054-2

Ogden, J. (2006). Seagrasses: Biology, ecology and conservation. *Marine Ecology*, *27*(4), 431–432. https://doi.org/10.1111/j.1439-0485.2006.00138.x

Ondiviela, B., Losada, I., J., Lara, J. L., Maza, M., Galván, C., Bouma, T. J., & Van Belzen, J. (2014). The role of seagrasses in coastal protection in a changing climate. *Coastal Engineering*, *87*, 158–168. https://doi.org/10.1016/j.coastaleng.2013.11.005

Ooi, J. L. S., Van Niel, K. P., Kendrick, G. A., & Holmes, K. W. (2014). Spatial structure of seagrass suggests that size-dependent plant traits have a strong influence on the distribution and maintenance of tropical multispecies meadows. *PLoS ONE*, *9*(1), e86782. https://doi.org/10.1371/journal.pone.0086782

Orth, R. J., Carruthers, T. J. B., Dennison, W. C., Duarte, C. M., Fourqurean, J. W., Heck, K. L., Hughes, A. R., Kendrick, G. A., Kenworthy, W. J., Olyarnik, S., Short, F. T., Waycott, M., & Williams, S. L. (2006). A global crisis for seagrass ecosystems. *BioScience*, *56*(12), 987. https://doi.org/10.1641/0006-3568(2006)56[987:AGCFSE]2.0.CO;2

Park, S. G. (2016). *Extent of seagrass in the Bay of Plenty in 2011*. Bay of Plenty Regional Council.

Peterson, C., Luettich, R., Micheli, F., & Skilleter, G. (2004). Attenuation of water flow inside seagrass canopies of differing structure. *Marine Ecology Progress Series*, *268*, 81–92. https://doi.org/10.3354/meps268081

Phillips, S. J., Anderson, R. P., & Schapire, R. E. (2006). Maximum entropy modeling of species geographic distributions. *Ecological Modelling*, *190*(3–4), 231–259. https://doi.org/10.1016/j.ecolmodel.2005.03.026

Pope, S. B. (2000). *Turbulent Flows* (1st ed.). Cambridge University Press. https://doi.org/10.1017/CBO9780511840531

Ralph, P. J., Durako, M. J., Enríquez, S., Collier, C. J., & Doblin, M. A. (2007). Impact of light limitation on seagrasses. *Journal of Experimental Marine Biology and Ecology*, *350*(1–2), 176–193. https://doi.org/10.1016/j.jembe.2007.06.017

Ramage, D., & Schiel, D. (1999). Patch dynamics and response to disturbance of the seagrass *Zostera novazelandica* on intertidal platforms in southern New Zealand. *Marine Ecology Progress Series*, *189*, 275–288. https://doi.org/10.3354/meps189275

Ranjan, P., Mittal, K., Chamorro, L. P., & Tinoco, R. O. (2022). Impact of gaps on the flow statistics in an emergent rigid canopy. *Physics of Fluids*, *34*(6), 066601. https://doi.org/10.1063/5.0088527

Rao, R., Alcoverro, T., Kongari, P., Yoayela, S., Arthur, R., & D'Souza, E. (2023). Tolerance to aerial exposure influences distributional patterns in multi-species intertidal seagrass meadows. *Marine Environmental Research*, *191*, 106146. https://doi.org/10.1016/j.marenvres.2023.106146

Reidenbach, M. A., & Thomas, E. L. (2018). Influence of the seagrass, *Zostera marina*, on wave attenuation and bed shear stress within a shallow coastal bay. *Frontiers in Marine Science*, *5*, 397. https://doi.org/10.3389/fmars.2018.00397

Reidenbaugh, T. G., & Banta, W. C. (1980). Origins and effects of Spartina wrack in a Virginia salt marsh. *Gulf Research Reports*, *6*. https://doi.org/10.18785/grr.0604.07

Rietkerk, M., & Van De Koppel, J. (2008). Regular pattern formation in real ecosystems. *Trends in Ecology & Evolution*, *23*(3), 169–175. https://doi.org/10.1016/j.tree.2007.10.013

Riffe, K. C., Henderson, S. M., & Mullarney, J. C. (2011). Wave dissipation by flexible vegetation. *Geophysical Research Letters*, *38*(18). https://doi.org/10.1029/2011GL048773

Riley, S. J., DeGloria, S. D., & Elliot, R. (1999). A terrain ruggedness index that quantifies topographic heterogeneneity. *Intermountain Journal of Sciences*, *5*, 1–4.

Roca, G., Alcoverro, T., Krause-Jensen, D., Balsby, T. J. S., Van Katwijk, M. M., Marbà, N., Santos, R., Arthur, R., Mascaró, O., Fernández-Torquemada, Y., Pérez, M., Duarte, C. M., & Romero, J. (2016). Response of seagrass indicators to shifts in environmental stressors: A global review and management synthesis. *Ecological Indicators*, *63*, 310–323. https://doi.org/10.1016/j.ecolind.2015.12.007

Ruiz-Reynés, D., Gomila, D., Sintes, T., Hernández-García, E., Marbà, N., & Duarte, C. M. (2017). Fairy circle landscapes under the sea. *Science Advances*, *3*(8), e1603262. https://doi.org/10.1126/sciadv.1603262

Sagerman, J., Hansen, J. P., & Wikström, S. A. (2020). Effects of boat traffic and mooring infrastructure on aquatic vegetation: A systematic review and meta-analysis. *Ambio*, *49*(2), 517–530. https://doi.org/10.1007/s13280-019-01215-9

Santamaría, L. (2002). Why are most aquatic plants widely distributed? Dispersal, clonal growth and small-scale heterogeneity in a stressful environment. *Acta Oecologica*, *23*(3), 137–154. https://doi.org/10.1016/S1146-609X(02)01146-3

Schanz, A., & Asmus, H. (2003). Impact of hydrodynamics on development and morphology of intertidal seagrasses in the Wadden Sea. *Marine Ecology Progress Series*, *261*, 123–134. https://doi.org/10.3354/meps261123

Schepers, L., Kirwan, M., Guntenspergen, G., & Temmerman, S. (2017). Spatio-temporal development of vegetation die-off in a submerging coastal marsh. *Limnology and Oceanography*, *62*(1), 137–150. https://doi.org/10.1002/lno.10381

Schepers, L., Van Braeckel, A., Bouma, T. J., & Temmerman, S. (2020). How progressive vegetation die-off in a tidal marsh would affect flow and sedimentation patterns: A field demonstration. *Limnology and Oceanography*, *65*(2), 401–412. https://doi.org/10.1002/lno.11308

Schoelynck, J., De Groote, T., Bal, K., Vandenbruwaene, W., Meire, P., & Temmerman, S. (2012). Self-organised patchiness and scale-dependent bio-geomorphic feedbacks in aquatic river vegetation. *Ecography*, *35*(8), 760–768. https://doi.org/10.1111/j.1600-0587.2011.07177.x

Shafer, D. J., Sherman, T. D., & Wyllie-Echeverria, S. (2007). Do desiccation tolerances control the vertical distribution of intertidal seagrasses? *Aquatic Botany*, *87*(2), 161–166. https://doi.org/10.1016/j.aquabot.2007.04.003

Shao, Z., Bryan, K. R., Lehmann, M. K., Flowers, G. J. L., & Pilditch, C. A. (2024). Scaling up benthic primary productivity estimates in a large intertidal estuary using remote sensing. *Science of The Total Environment*, *906*, 167389. https://doi.org/10.1016/j.scitotenv.2023.167389

Short, F. T., & Neckles, H. A. (1999). The effects of global climate change on seagrasses. *Aquatic Botany*, *63*(3–4), 169–196. https://doi.org/10.1016/S0304-3770(98)00117-X

Short, F. T., Polidoro, B., Livingstone, S. R., Carpenter, K. E., Bandeira, S., Bujang, J. S., Calumpong, H. P., Carruthers, T. J. B., Coles, R. G., Dennison, W. C., Erftemeijer, P. L. A., Fortes, M. D., Freeman, A. S., Jagtap, T. G., Kamal, A. H. M., Kendrick, G. A., Judson Kenworthy, W., La Nafie, Y. A., Nasution, I. M., … Zieman, J. C. (2011). Extinction risk assessment of the world's seagrass species. *Biological Conservation*, *144*(7), 1961–1971. https://doi.org/10.1016/j.biocon.2011.04.010

Silliman, B. R., Van De Koppel, J., Bertness, M. D., Stanton, L. E., & Mendelssohn, I. A. (2005). Drought, snails, and large-scale die-off of southern U.S. salt marshes. *Science*, *310*(5755), 1803–1806. https://doi.org/10.1126/science.1118229

Sullivan, J. C., Torres, R., Garrett, A., Blanton, J., Alexander, C., Robinson, M., Moore, T., Amft, J., & Hayes, D. (2015). Complexity in salt marsh circulation for a semienclosed basin. *Journal of Geophysical Research: Earth Surface*, *120*(10), 1973–1989. https://doi.org/10.1002/2014JF003365

Sutherland, J., Peet, A. H., & Soulsby, R. L. (2004). Evaluating the performance of morphological models. *Coastal Engineering*, *51*(8–9), 917–939. https://doi.org/10.1016/j.coastaleng.2004.07.015

Swadling, D. S., West, G. J., Gibson, P. T., Laird, R. J., & Glasby, T. M. (2023). Don't go breaking apart: Anthropogenic disturbances predict meadow fragmentation of an endangered seagrass. *Aquatic Conservation: Marine and Freshwater Ecosystems*, *33*(1), 56–69. https://doi.org/10.1002/aqc.3905

Swets, J. A. (1988). Measuring the accuracy of diagnostic systems. *Science*, *240*(4857), 1285–1293. https://doi.org/10.1126/science.3287615

Syvitski, J. P. M., Vörösmarty, C. J., Kettner, A. J., & Green, P. (2005a). Impact of humans on the flux of terrestrial sediment to the global coastal ocean. *Science*, *308*(5720), 376–380. https://doi.org/10.1126/science.1109454

Syvitski, J. P. M., Vörösmarty, C. J., Kettner, A. J., & Green, P. (2005b). Impact of Humans on the Flux of Terrestrial Sediment to the Global Coastal Ocean. *Science*, *308*(5720), 376–380. https://doi.org/10.1126/science.1109454

Temmerman, S., Bouma, T. J., Govers, G., Wang, Z. B., De Vries, M. B., & Herman, P. M. J. (2005). Impact of vegetation on flow routing and sedimentation patterns: Three-dimensional modeling for a tidal marsh. *Journal of Geophysical Research: Earth Surface*, *110*(F4). https://doi.org/10.1029/2005JF000301

Temmerman, S., Horstman, E. M., Krauss, K. W., Mullarney, J. C., Pelckmans, I., & Schoutens, K. (2023). Marshes and mangroves as nature-based coastal storm buffers. *Annual Review of Marine Science*, *15*(1), 95–118. https://doi.org/10.1146/annurev-marine-040422-092951

Terrados, J., Duarte, C. M., Kamp-Nielsen, L., Agawin, N. S. R., Gacia, E., Lacap, D., Fortes, M. D., Borum, J., Lubanski, M., & Greve, T. (1999). Are seagrass growth and survival

constrained by the reducing conditions of the sediment? *Aquatic Botany*, *65*(1–4), 175–197. https://doi.org/10.1016/S0304-3770(99)00039-X

Thomas, R. E., Schindfessel, L., McLelland, S. J., Creëlle, S., & De Mulder, T. (2017). Bias in mean velocities and noise in variances and covariances measured using a multistatic acoustic profiler: The Nortek Vectrino Profiler. *Measurement Science and Technology*, *28*(7), 075302. https://doi.org/10.1088/1361-6501/aa7273

Thomaz, S. M., & Cunha, E. R. D. (2010). The role of macrophytes in habitat structuring in aquatic ecosystems: Methods of measurement, causes and consequences on animal assemblages' composition and biodiversity. *Acta Limnologica Brasiliensia*, *22*(02), 218–236. https://doi.org/10.4322/actalb.02202011

Tinoco, R. O., San Juan, J. E., & Mullarney, J. C. (2020). Simplification bias: Lessons from laboratory and field experiments on flow through aquatic vegetation. *Earth Surface Processes and Landforms*, *45*(1), 121–143. https://doi.org/10.1002/esp.4743

Townsend, E. C., & Fonseca, M. S. (1998). Bioturbation as a potential mechanism influencing spatial heterogeneity of North Carolina seagrass beds. *Marine Ecology Progress Series*, *169*, 123–132. https://doi.org/10.3354/meps169123

Uhrin, A. V., & Turner, M. G. (2018). Physical drivers of seagrass spatial configuration: The role of thresholds. *Landscape Ecology*, *33*(12), 2253–2272. https://doi.org/10.1007/s10980-018-0739-4

Uittenbogaard, R. E. (2003). *Modelling turbulence in vegetated aquatic flows*.

Vacchi, M., Montefalcone, M., Bianchi, C. N., Morri, C., & Ferrari, M. (2012). Hydrodynamic constraints to the seaward development of *Posidonia oceanica* meadows. *Estuarine, Coastal and Shelf Science*, *97*, 58–65. https://doi.org/10.1016/j.ecss.2011.11.024

Valavi, R., Elith, J., Lahoz-Monfort, J. J., & Guillera-Arroita, G. (2021). Modelling species presence-only data with random forests. *Ecography*, *44*(12), 1731–1742. https://doi.org/10.1111/ecog.05615

Van Der Heide, T., Eklöf, J. S., Van Nes, E. H., Van Der Zee, E. M., Donadi, S., Weerman, E. J., Olff, H., & Eriksson, B. K. (2012). Ecosystem engineering by seagrasses interacts with grazing to shape an intertidal landscape. *PLoS ONE*, *7*(8), e42060. https://doi.org/10.1371/journal.pone.0042060

Van Der Heide, T., Van Nes, E. H., Geerling, G. W., Smolders, A. J. P., Bouma, T. J., & Van Katwijk, M. M. (2007). Positive feedbacks in seagrass ecosystems: Implications for success in conservation and restoration. *Ecosystems*, *10*(8), 1311–1322. https://doi.org/10.1007/s10021-007-9099-7

Van Katwijk, M. M., Bos, A. R., Hermus, D. C. R., & Suykerbuyk, W. (2010). Sediment modification by seagrass beds: Muddification and sandification induced by plant cover and environmental conditions. *Estuarine, Coastal and Shelf Science*, *89*(2), 175–181. https://doi.org/10.1016/j.ecss.2010.06.008

Van Proosdij, D., Davidson-Arnott, R. G. D., & Ollerhead, J. (2006). Controls on spatial patterns of sediment deposition across a macro-tidal salt marsh surface over single tidal cycles. *Estuarine, Coastal and Shelf Science*, *69*(1–2), 64–86. https://doi.org/10.1016/j.ecss.2006.04.022

Van Rijn, L. C., Walstra, D. J. R., Grasmeijer, B., Sutherland, J., Pan, S., & Sierra, J. P. (2003). The predictability of cross-shore bed evolution of sandy beaches at the time scale of storms and seasons using process-based Profile models. *Coastal Engineering*, *47*(3), 295–327. https://doi.org/10.1016/S0378-3839(02)00120-5

Van Veelen, T. J., Nepf, H., Hulscher, S. J. M. H., & Borsje, B. W. (2025). The thresholds of sediment resuspension within emergent vegetation under combined wave-current conditions – A flume experiment. *Coastal Engineering*, *199*, 104727. https://doi.org/10.1016/j.coastaleng.2025.104727

Van Wesenbeeck, B., Van De Koppel, J., M. J. Herman, P., & J. Bouma, T. (2008). Does scale-dependent feedback explain spatial complexity in salt-marsh ecosystems? *Oikos*, *117*(1), 152–159. https://doi.org/10.1111/j.2007.0030-1299.16245.x

Vandenbruwaene, W., Temmerman, S., Bouma, T. J., Klaassen, P. C., De Vries, M. B., Callaghan, D. P., Van Steeg, P., Dekker, F., Van Duren, L. A., Martini, E., Balke, T., Biermans, G., Schoelynck, J., & Meire, P. (2011). Flow interaction with dynamic vegetation patches: Implications for biogeomorphic evolution of a tidal landscape. *Journal of Geophysical Research: Earth Surface*, *116*(F1). https://doi.org/10.1029/2010JF001788

Vanhellemont, Q., & Ruddick, K. (2018). Atmospheric correction of metre-scale optical satellite data for inland and coastal water applications. *Remote Sensing of Environment*, *216*, 586–597. https://doi.org/10.1016/j.rse.2018.07.015

Wackernagel, H. (2003). *Multivariate geostatistics: An introduction with applications*. Springer Science & Business Media.

Walbridge, S., Slocum, N., Pobuda, M., & Wright, D. (2018). Unified Geomorphological Analysis Workflows with Benthic Terrain Modeler. *Geosciences*, *8*(3), 94. https://doi.org/10.3390/geosciences8030094

Wang, X., Adams, M. P., & Shao, D. (2024). Trade-off between light deprivation and desiccation in intertidal seagrasses due to periodic tidal inundation and exposure: Insights from a data-calibrated model. *Journal of Geophysical Research: Biogeosciences*, *129*(4), e2024JG008000. https://doi.org/10.1029/2024JG008000

Waycott, M., Duarte, C. M., Carruthers, T. J. B., Orth, R. J., Dennison, W. C., Olyarnik, S., Calladine, A., Fourqurean, J. W., Heck, K. L., Hughes, A. R., Kendrick, G. A., Kenworthy, W. J., Short, F. T., & Williams, S. L. (2009). Accelerating loss of seagrasses across the globe threatens coastal ecosystems. *Proceedings of the National Academy of Sciences*, *106*(30), 12377–12381. https://doi.org/10.1073/pnas.0905620106

Weiss, A. (2001). *Topographic Position and Landform Analysis*. *200*.

Wiens, J. A., Stralberg, D., Jongsomjit, D., Howell, C. A., & Snyder, M. A. (2009). Niches, models, and climate change: Assessing the assumptions and uncertainties. *Proceedings of the National Academy of Sciences*, *106*(supplement 2), 19729–19736. https://doi.org/10.1073/pnas.0901639106

Wiles, P. J., Rippeth, T. P., Simpson, J. H., & Hendricks, P. J. (2006). A novel technique for measuring the rate of turbulent dissipation in the marine environment. *Geophysical Research Letters*, *33*(21), L21608. https://doi.org/10.1029/2006GL027050

Williams, J. A., Holt, G. J., Robillard, M. M. R., Holt, S. A., Hensgen, G., & Stunz, G. W. (2016). Seagrass fragmentation impacts recruitment dynamics of estuarine-dependent fish. *Journal of Experimental Marine Biology and Ecology*, *479*, 97–105. https://doi.org/10.1016/j.jembe.2016.03.008

Willmott, C. J. (1981). On the validation of models. *Physical Geography*, *2*(2), 184–194. https://doi.org/10.1080/02723646.1981.10642213

Willmott, C., & Matsuura, K. (2005). Advantages of the mean absolute error (MAE) over the root mean square error (RMSE) in assessing average model performance. *Climate Research*, *30*, 79–82. https://doi.org/10.3354/cr030079

Xu, J., Lightsom, F., Noble, M. A., & Denham, C. (2002). *CMGTool user's manual* (Report Nos. 2002–19; Open-File Report). U.S. Geological Survey. https://doi.org/10.3133/ofr0219

Yamasaki, T. N., De Lima, P. H. S., Silva, D. F., Preza, C. G. de A., Janzen, J. G., & Nepf, H. M. (2019). From patch to channel scale: The evolution of emergent vegetation in a channel. *Advances in Water Resources*, *129*, 131–145. https://doi.org/10.1016/j.advwatres.2019.05.009

Zabarte-Maeztu, I., Matheson, F. E., Manley-Harris, M., Davies-Colley, R. J., & Hawes, I. (2021). Interaction of substrate muddiness and low irradiance on seagrass: A mesocosm study of *Zostera muelleri*. *Aquatic Botany*, *175*, 103435. https://doi.org/10.1016/j.aquabot.2021.103435

Zhang, Y., Lai, X., Ma, J., Zhang, Q., Yu, R., Yao, X., & Deng, H. (2021). Field study on flow structures within aquatic vegetation under combined currents and small-scale waves. *Hydrological Processes*, *35*(4). https://doi.org/10.1002/hyp.14121

Zoffoli, M. L., Gernez, P., Oiry, S., Godet, L., Dalloyau, S., Davies, B. F. R., & Barillé, L. (2022). Remote sensing in seagrass ecology: Coupled dynamics between migratory herbivorous birds and intertidal meadows observed by satellite during four decades. *Remote Sensing in Ecology and Conservation*, rse2.319. https://doi.org/10.1002/rse2.319